47

# THE SOLID PARTICLE EROSION OF WC-Co ALLOYS



by

R.C. PENNEFATHER

A thesis submitted to the Faculty of Engineering, University of Cape Town in fulfilment of the degree of Master of Science in Applied Science

Department of Materials Engineering
University of Cape Town

JUNE 1986

## ACKNOWLEDGEMENTS

I would like to thank the following people who assisted me in producing this thesis.

Dr R. Hutchings, my supervisor, for his patience, support and guidance.

Professor A. Ball for his help and advice.

Mr N. Dreze and Mr A. Rapley for their technical assistance.

Mr B. Greeves for the photographic work.

Miss T. Leveton, Mrs H. Böhm and Mrs S. Betz for their help in the preparation of the manuscript.

Staff and fellow students for their support and encouragement.

Professor L.P. Adams for making available the teletronix 4055-summagraphic digitizer system and Ann Tregidga for assistance with parallax bar and mirror stereoscope.

Boart International Industrial Division for financial support of this project, and Mr R.J. Hosking, of that company, for his valued advice.

The CSIR for provision of a research bursary.

## ABSTRACT

An investigation involving the erosion of WC-Co alloys by solid particle impact erosion was undertaken to determine the mechanism by which material is removed. For this purpose a simple particle-gas stream erosion apparatus was employed.

The nineteen different WC-Co alloys studied were initially characterised according to microstructural and mechanical properties. An investigation of the influence of various parameters on erosion was conducted to establish the manner by which the WC-Co alloys were eroded. A limit in erosion rate occurred with increasing particle size for all samples, which is associated with ductile erosion. The variation of erosion rate with the angle of impact was found to be dependent on the binder content. A maximum in erosion occurred at a 90° angle of incidence for the low cobalt content alloys and in the region of a 50° angle of incidence for high cobalt content alloys. Thus suggesting a predominantly brittle mode of erosion, with a ductile mode becoming more important with increasing binder content.

The erosion rate was found to increase with decreasing hardness. For impact angles of 45° and greater, the hardness effect was masked by microstructural influences. Examination of the steady state eroded surface and the single particle impact event, using the scanning electron microscope revealed three modes of material removal. These may occur simultaneously, the predominant mode, however, changes with binder content. For WC-Co alloys containing less than 10 wt-% cobalt, cobalt extrusion was observed as being the controlling mode of material removal. Maximum carbide grain cracking was associated with a cobalt content of 10 wt-%. Above this binder level ductile cutting of the matrix became an increasingly important mode of material removal.

## LIST OF SYMBOLS

$a$ : half indent diagonal length

$a_w$ : erosion value of pure WC

$b_{90}$ : erosion value of the cobalt phase due to the normal component of velocity

$b-b_{90}$ : erosion of the cobalt phase due to the glancing component of velocity

$C$ : contiguity

$c$ : half-penny crack length

$d$ : grain size

$E$ : Young's modulus

$E_R$ : erosion rate

$F$ : area of wear

$f_{co}$ : cobalt volume fraction

$H$ : hardness

$G$ : mass of impacting particles

$G_{IC}$ : energy release rate

$K_{IC}$ : fracture toughness

$L$ : distance separating the two discs

$l$ : Palmqvist crack length

$m$ : particle exponent

$n$ : velocity exponent

$p$ : flow stress of the target material

$R$ : particle size

$r$ : radius from the disc centre

$t$ : time

$v$ : particle velocity

$V_c$ : mean volume per crater of the resulting craters

$u$ : rotational frequency of the disc

$W$ : Palmqvist toughness

$\alpha$ : angle of incidence

$\eta$ : double carbide phase

$\theta$ : linear separation of the erosion lines

$\lambda$ : mean free path

$\mu$ : mean

$\rho$ : particle density

$\sigma$ : standard deviation

$\psi$ : particle concentration

# CONTENTS

PAGE

PAGE

# CHAPTER 1

## INTRODUCTION

Erosion has been defined by the American Society for Testing and Materials (ASTM, 1980) as "progressive loss of original material from a solid surface due to the mechanical interactions between the surface and a fluid, a multicomponent fluid or impinging liquid or solid particles".

The degradation of material due to solid particle impact erosion poses a serious financial problem to industry. The occurrence of impact erosion has been reported in cases as diverse as the transportation of airborne solid particles through pipes (Bitter, 1963), rocket motor tail nozzles (Nielson and Gilchrist, 1968), gas turbines and boiler units (Uuemôis and Kleis, 1975) and helicopter engines operating in dusty environments (Goodwin et al, 1969).

In coal conversion plants (Conrad et al, 1982) and coal gasification systems (Hansen et al, 1979) WC-Co alloys have been found to be the best material for combating solid particle erosion. The success of these alloys in such applications is due to the combination of the hard, wear resistant carbide phase with the ductile binder, which provides the toughness. However, only little is known of the mechanism of the erosion of the alloy and the microstructural effect thereon. The following objectives were therefore pursued in this investigation:

i) Since a variety of WC-Co alloys were the target materials considered in this research, it was first necessary to microstructually characterize these alloys before investigating the effect of solid particle impact erosion on the WC-Co alloy.

ii) The influence of various parameters on the erosion of WC-Co alloys was investigated using a simple particle-gas stream erosion apparatus. The velocity was maintained at a constant 40 $ms^{-1}$. This is an easily obtainable velocity which produces a measurable erosion rate. The velocity was not varied, as the parameter is considered to reveal little information regarding the mechanism of erosion.

iii) Both the steady state erosion surfaces and single impact events were studied in an attempt to determine the mechanism by which material is removed during solid particle impact erosion.

# CHAPTER 2

## A REVIEW OF THE PROPERTIES OF THE WC-Co ALLOYS

WC-Co is a sintered two-phase alloy. The major constituent is the hard but brittle carbide phase. The toughness is given by the more ductile binder phase. The appropriate combination of hardness and strength for a particular application may be controlled by varying the WC grain size and the percentage cobalt present (Murray, (1977)).

## 2.1 CHEMICAL COMPOSITION AND CRYSTALLOGRAPHIC STRUCTURE

### 2.1.1 Tungsten Carbide

Tungsten combines with carbon to form two hexagonal carbides, the monocarbide WC and the subcarbide $W_2C$. At a temperature of 1575 K, the eutectoid reaction $W_2C \longrightarrow WC + W$ is believed to occur. However, Exner (1979) notes that $W_2C$ is obtained far below this temperature, suggesting that the eutectoid reaction does not take place.

The crystal structure of tungsten carbide is a simple hexagonal, as shown in Figure 2.1, with lattice constants a = 2,91 Å and c = 2,84 Å (Luyckx, 1970; Gurland and Exner, 1970; Exner, 1979). The crystal is anisotropic in most properties. French and Thomas (1965) found the knoop hardness on the basal plane (0001) of the WC crystal to vary. In the [1120] direction the knoop hardness was 2200, but an an angle of 30° to the direction with threefold symmetry it was 2500. On the prism plane $(10\bar{1}0)$ the knoop hardness varied from 1000 in the $\{0001\}$ direction to 2400 at 90° to this direction with two fold symmetry. The anisotropic nature of the crystal, however, does not affect the alloy where there is random orientation of the WC grains.

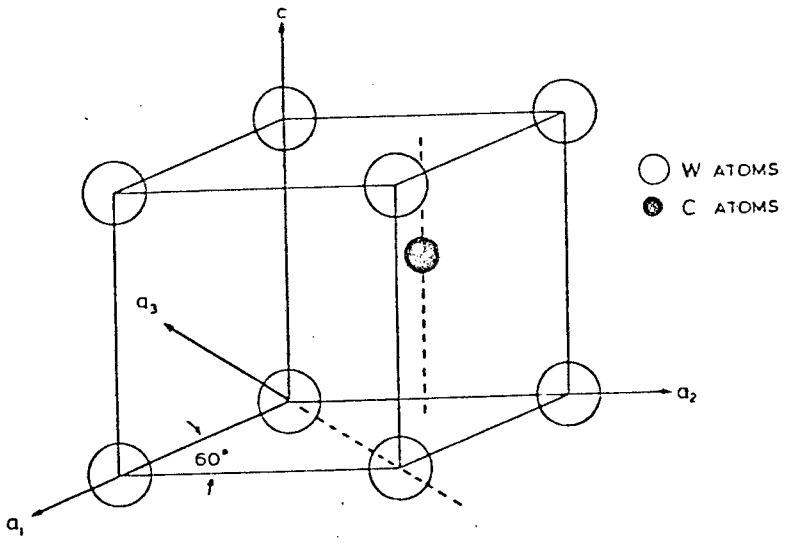


FIGURE 2.1 : Crystal structure of tungsten carbide

In the past WC crystals were believed to deform by brittle means. Luyckx (1970), however, noted plastic deformation in the form of slip lines when the WC crystal was subjected to bending and microindentation. Greenwood et al (1982), in more recent work, have observed dislocations in the hard carbide phase while analysing deformed WC-Co alloys using the TEM. The strength of individual tungsten particles is size dependent; strength decreases with increasing particle size (Gurland and Exner, 1970).

### 2.1.2 Cobalt Binder

Due to cobalt's excellent wetting, adhesion and adequate mechanical properties, it is the most common binder metal. At room temperature, the equilibrium crystal structure is close-packed hexagonal, which, above a temperature of 700 K, modifies to face centred cubic (f.c.c.).

The occurrence of retained f.c.c. phase in sintered WC-Co is well documented. Almond and Roebuck (1982) examined diffraction patterns from electron microscope specimens and discovered the binder was predominantly f.c.c.. The amount present is determined by the plastic strain introduced after cooling, the mean free path (see Section 2.2 for definition), the cooling rate and the amount of WC disolved in the binder (Roebuck et al, 1984).

At equilibrium, cobalt contains $\simeq$ 10% WC in solid solution at a temperature of approximately 1523 K. According to Pfau and Rix (in Dawihl and Frisch, 1964), the solid solution tungsten atoms substitute for cobalt atoms, while the carbon atoms fill the octahedral interstices in the cobalt matrix. The cobalt, however, does not dissolve in the WC phase.

### 2.1.3 Carbon Content

The carbon content in a WC-Co alloy is critical, as the range in which the two phase WC-Co structure occurs is very small. A carbon deficiency causes the precipitation of double carbides of variable composition (eg. $W_3Co_3C$), while excess carbon leads to the formation of free graphite.

The $\eta$ phase (eg $W_3Co_3C$) occurs as hard brittle particles within the matrix. As the $\eta$ phase reacts with cobalt from the binder, the region around the $\eta$ phase is denuded of binder, creating areas of structural weakness (Peters and Cooper, 1978).

## 2.2 MICROSTRUCTURAL FEATURES

Microstructural features are dictated by the nature of the starting powder, and are developed during sintering (Almond and Roebuck, 1982). Each feature can be described by a given parameter and hence evaluated quantitatively. Figure 2.2 illustrates schematically the microstructural parameters of the WC-Co alloy.

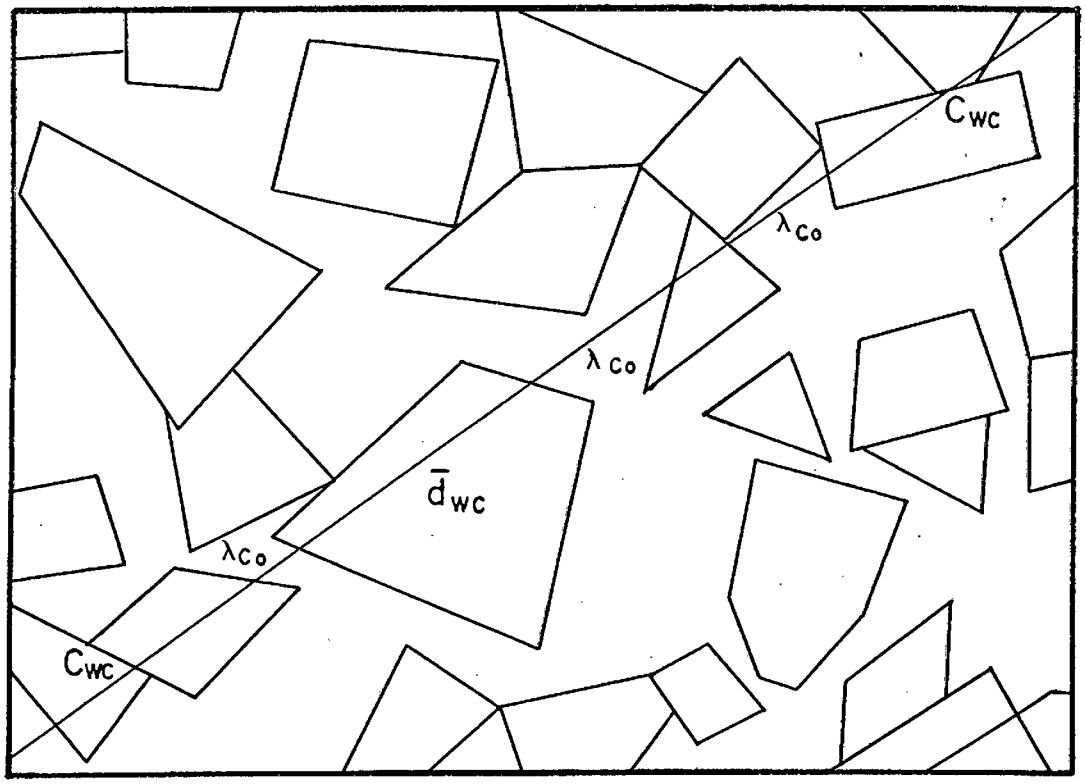


FIGURE 2.2 : A schematic representation of the WC-Co alloy illustrating the microstructural parameters, where $\lambda$ is mean free path of the binder phase, $\bar{d}_{WC}$ is the WC grain size and C is contiguity

Gurland (Lee and Gurland, 1978) defines contiguity as the fraction of the total internal surface area of a phase that is shared by particles of the same phase. The obvious difficulty in calculating the number of WC-WC grain contacts is in distinguishing whether a thin cobalt film is present. Many researchers (Luyckx, 1968; Chemant et al, 1975; Lee and Gurland, 1978) assume a continuous carbide 'skeleton' exists in WC-Co alloys containing up to approximately 15 vol-% cobalt. Exner (1979), however, believes that continguity decreases with increasing cobalt content, but is still present in grades containing greater than 30 vol-% cobalt. There has been no direct evidence of carbide grain contact, but Laugier (1985 b) studied the WC powder and found that some aggregate consists of crystallographically well aligned WC grains which are very stable. These are believed to be a source of contiguity in sintered WC-Co alloys.

Porosity is generally caused by insufficient milling and entrapped gases. It is also often associated with a low carbon content. Isostatic hot pressing has reduced the occurrence of high porosity. Uniformally distributed residual porosity may still occur, this however, is commonly accepted as not being detrimental to the mechanical properties (Exner and Gurland, 1970).

## 2.3 PHYSICAL PROPERTIES

### 2.3.1 Youngs Modulus

For WC-Co alloys the Youngs modulus is found to decrease with increasing binder content. However, for a small size distribution the influence of grain size on the value of Youngs modulus seems to be minimal (Chermant et al, 1975).

Chermant et al (1975) obtained theoretical values for the Youngs data modulus of the WC phase. These were in agreement with the published WC values. The theoretical values for cobalt were, however, greater than published results. This was attributed to the stress state of the cobalt phase as well as the dissolution of WC in the cobalt. These results suggest the law of mixtures to be an oversimplified theory for the Youngs modulus of the WC-Co alloy. The law, however, can still be used to account greatly for the variation of Youngs modulus as a function of binder content (Chermant et al, 1975).

### 2.3.2 Residual Stresses

#### 2.3.2.1 Thermal Stresses

Thermally induced stresses are introduced on cooling of the WC-Co alloy from the sintering temperature. The thermal expansion coefficient of cobalt is approximately three times that of WC, resulting in continual compressive stress of the WC phase (Exner and Gurland, 1970; Exner, 1979). Exner (1979) notes that the thermal stresses are compressive in the carbide phase at all

compositions, while the tensile stresses in the cobalt phase decrease slightly with increased cobalt (Figure 2.3).

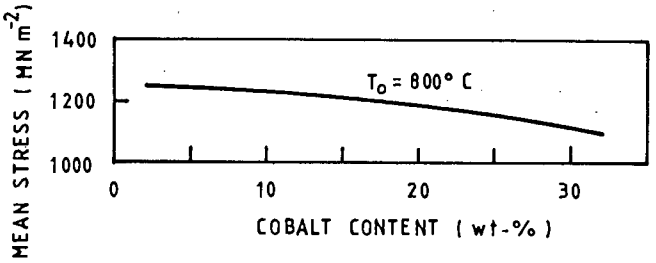


FIGURE 2.3 : Thermal stresses in the cobalt phase as a function of cobalt content (after Exner, 1979)

2.3.2.2 Mechanically Introduced Stresses

Thermally induced stress patterns can be modified by grinding. Compressive stresses are introduced in regions near the surface which are dependent upon cobalt content and severity of grinding (Exner, 1979). These compressive stresses reduce or convert the tensile stress in the cobalt phase to a compressive stress. Exner (1979) observed that higher compressive stresses were introduced into the cobalt phase after SiC-grinding than after diamond wheel grinding.

## 2.4 MECHANICAL PROPERTIES

Toughness and hardness are believed to be the important mechanical properties controlling erosion of the target material. Both are strongly dependent upon the microstructural parameters of the WC-Co alloy.

### 2.4.1 Hardness

Hardness decreases with increasing cobalt content and grain size as illustrated in Figure 2.4(a). Exner and Gurland (1970)

observed an apparently simple function between hardness and the mean free path (Figure 2.4(b)). However, on closer analysis of the scatter band it was found that additional independent parameters, such as particle size and composition are necessary to describe the relationship precisely. Peters & Cooper (1978) noted that a small increase in hardness was associated with $\eta$ phase precipitate.

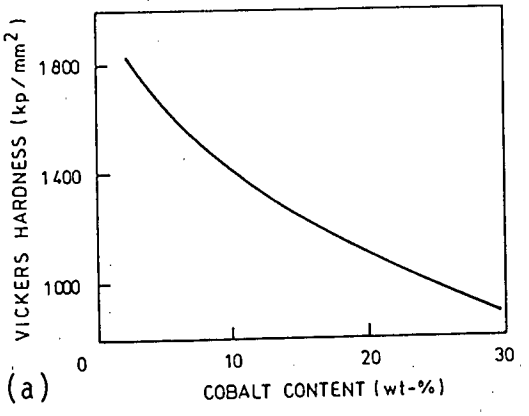


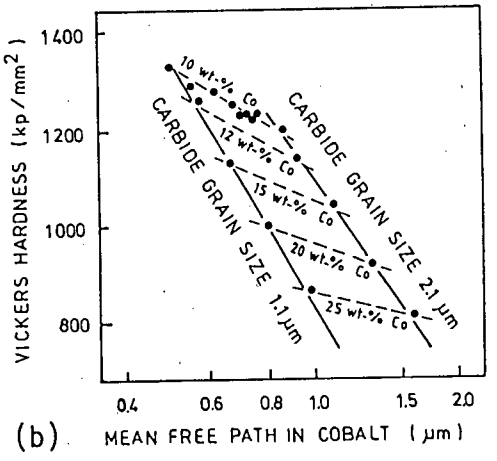


FIGURE 2.4 : Effect of (a) cobalt content (b) mean free path on the hardness (after Exner and Gurland, 1970)

## 2.4.2 Transverse Rupture Strength

Transverse rupture strength is a measure of WC-Co alloy resistance to fracture. When plotted against the mean free path (Figure 2.5), transverse rupture strength exhibits a peak, which is dependent upon the cobalt content.

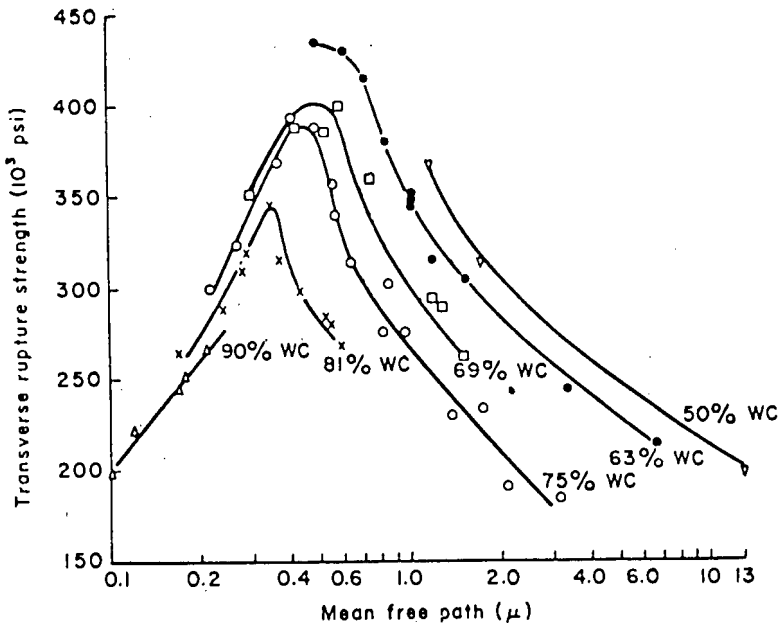


FIGURE 2.5 : Transverse rupture strength as a function of mean free path (after Gurland and Parikh, 1972)

Various authors (Exner and Gurland, 1970; Gurland and Parikh, 1972; Peters & Cooper, 1978) have explained the shape of the curve in Figure 2.5 by considering a change in fracture mode. A gradual transition is brought about by a change of the alloy structure from 'skeleton' to 'embedded'. The initial increase in transverse rupture strength is caused by the reduction of plastic constraint, due to an increase in mean free path. The increase in plastic flow relaxes the stress concentrations, thus allowing higher stress levels to be obtained without premature failure. The decrease in transverse rupture strength can be explained by the dispersion hardening model, where the increase in free mean path reduces the flow strength.

Transverse rupture strength is also dependent upon carbon content: as the carbon content is reduced, the strength is reduced. Peters and Cooper (1978) attributed this to the role of the $\eta$ phase as stress raisers.

### 2.4.3 Fracture Toughness

As WC-Co alloys generally fail by brittle fracture at normal temperature, toughness is a measure of their resistance to fracture. This results in the loss of distinction between strength and toughness. However, their dependence on mean free path differs; fracture toughness varies smoothly with mean free path. Larsen-Basse (1974) suggested that the fracture toughness measurements may give added information which cannot be given by other strength measurement methods.

Fracture toughness has been determined by various methods and there is, as yet, no standard method of measuring the fracture toughness of WC-Co alloys. Table 2.1 summarizes the more frequent methods employed, most of which show that the mean free path of the binder bears a strong influence on fracture toughness.

#### 2.4.3.1 Palmqvist Test

Palmqvist initiated and developed the idea of testing the toughness of cemented carbides using the cracks formed at the corners of a Vickers hardness indentation (see Figure 2.6) (Shetty et al, 1985). It is widely accepted that the Palmqvist cracks propagate entirely within the plastically deformed region surrounding the indentation. The depth of the crack is approximately that of the indent (Ogilvy et al, 1977), while the length can be longer than the lengths of the diagonals of the indent (Perrott, 1977). Ogilvy et al (1977) observed that crack growth occurs in roughly equal amounts during the loading and unloading of the indentor, with growth during unloading being more important for the harder alloys.

TABLE 2.1 : Summary of investigated fracture toughness methods

| AUTHOR | TEST METHOD | PRE-CRACKING TECHNIQUE | CONCLUSION |
|---|---|---|---|
| Chermant et al (1979) | 3-point bend | 'V' diamond wheel and spark erosion | KIC varies linearly with mean free path ($\lambda$) |
| Cutler & Virkar (1985) | Short rod, double cantilever beam | Diamond saw | Binder thickness and residual stresses important factors affecting KIC |
| Ingelstrom & Nordberg (1974) | 3-point bend<br>4-point bend<br>Compact tension | Knoop diamond indentation<br>Wedge impact load | KIC decreases almost linearly with the hardness<br>KIC increases with increasing carbide grain size (therefore mean free path) |
| Kenny (1971) | 4-point bend | Knoop diamond indentation | KIC is affect by grain size variation |
| Leuth (1974) | Double cantilever beam | Wedge loaded | KIC increases with increasing binder thickness ($\lambda$) |
| Murray (1977) | Double torsion | | $KIC^2$ is linearly related to mean free path ($\lambda$) |
| Nakamura & Gurland (1980) | Single-edge notch beam | Electron discharge machining | For the temperature range tested, temperature had no effect on KIC |
| Nidikon & Davis (1980) | Double cantilever beam | Spark erosion | KIC is related to mean free path, carbide grain size and the stress to rupture value |
| Peters & Cooper (1978) | Palmqvist | | KIC decreased with decreasing carbon content |
| Pickens & Gurland (1978) | Single-edge notched beam | Electron discharge machining | Linear correlation exists between GIC (critical strain energy release), the in-situ yield strength of the binder phase and the mean free path |
| Viswanadham et al (1981) | Short rod | Diamond saw | Binder mean free path, the area fraction of binder on the fracture surface, and the in-situ yield behaviour of the binder are the principle factors determing KIC |
| Wright et al (1983) | Palmqvist | | KIC varied inversely with hardness |

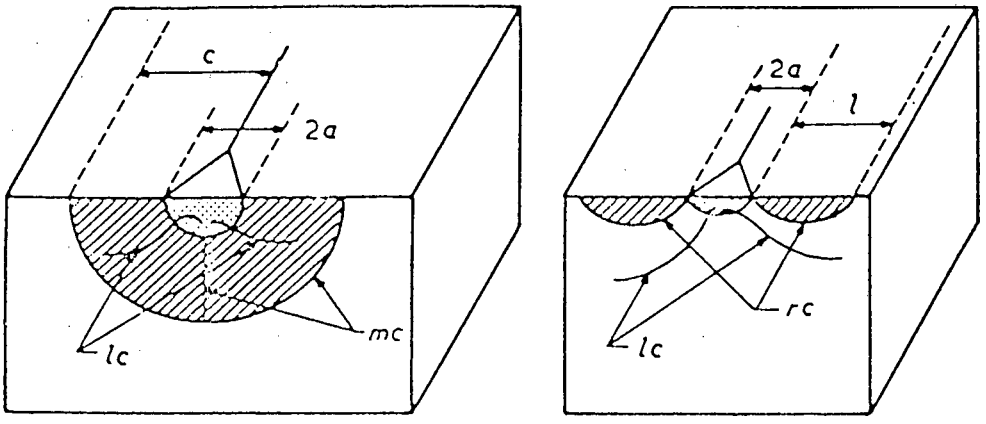


FIGURE 2.6 : Indentation showing (a) half-penny cracking and (b) Palmqvist cracking, where 'a' is half the indent diagonal length, 'c' is the crack length for a half-penny crack and 'l' is the Palmqvist crack length (after Niihara et al, 1982)

The Palmqvist toughness (w) is defined by the following relationship:

$$w = P/L \qquad (2.1)$$

where P is the load and L is the sum of the four crack lengths measured at the indentation corners (Peters, 1979). Various attempts have been made to relate Palmqvist toughness with the energy release rate ($G_{IC}$) and fracture toughness ($K_{IC}$).

Exner et al (1978) and Peters (1979) have empirically found a linear relationship between W and $G_{IC}$ which is valid for low-binder alloys.

More recently considerable interest has been shown in developing a relationship between $K_{IC}$ and W. Niihara et al (1982) suggested that the indentation fracture analysis for half-penny cracks by Evans and Charles (1976) (equation 2.2), should be modified to account for the change in crack geometry associated with Palmqvist cracks (equation 2.3).

$$\left(\frac{K_{IC}\phi}{H\ a^{\frac{1}{2}}}\right)\left(\frac{H}{E\phi}\right)^{0,4} = 0,129\ (c/a)^{-3/2} \qquad (2.2)$$

$$\left(\frac{K_{IC}\phi}{H\ a^{\frac{1}{2}}}\right)\left(\frac{H}{E\phi}\right)^{0,4} = 0,035\ (l/a)^{-1/2} \qquad (2.3)$$

where H is the hardness, E the Youngs modulus, $\phi$ is a constant factor and c, a and l are defined in Figure 2.6.

Lankford (1982) and Laugier (1985 a) both found equation 2.2 to give a better estimation of fracture toughness for WC-Co alloys. The opposite was found to be true by Wright and Shetty (1986), who, however, argued that the selection of a particular approach for analysis of indentation data should not be based purely on correlation of estimated and measured values. Instead, a correct fracture-mechanic interpretation of the Palmqvist crack is required, as the two available models are only approximations of the actual problem.

As of yet, fracture toughness measured by the Palmqvist method is not universally accepted, mainly as its basis is emperical, not theoretical. It is, however, argued that the method is a useful, simple, and inexpensive technique for evaluating and comparing commercial WC-Co alloys (Exner et al, 1978; Peters, 1979). The principal drawbacks to this technique are the method's sensitivity to surface finish, and its restriction to materials having a cobalt content of not higher than 15 wt-%.

# CHAPTER 3

## A REVIEW OF EROSION BY SOLID PARTICLE IMPACT

Identification and analysis of the mechanism of material removal is necessary for erosion to be understood. For this purpose, it is often convenient to divide materials into two categories - ductile and brittle. Though many materials fall between these two catgories, Finnie (1960) argues that is is necessary to understand the ductile and brittle mechanism of erosion, before it is possible to make a realistic analysis for the intermediate type of behaviour.

To date, a great number of parameters have been found to influence impact erosion. These include :

i) Properties of the target material
ii) Properties of the impacting particles
iii) Impact parameters

### 3.1 TARGET MATERIAL PROPERTIES

As mentioned previously (Section 2.4), hardness and strength are the frequently considered critical material properties governing erosion, although it is realised that other parameters frequently play a dominant role.

#### 3.1.1 Hardness

Hardness is a measure of a material's resistance to plastic flow. For the erosion of ductile materials where plastic deformation predominates, hardness is considered to be the most important parameter. Finnie et al (1967) showed the erosion rate of different ductile materials to decrease with the reciproval of hardness. Little change, however, was observed when the hardness of an individual alloy was varied through thermal treatments or by work hardening (Figure 3.1).

It has been proposed by Sheldon (1970) that the indentation hardness of a work-hardened surface would be a more appropriate measurement.

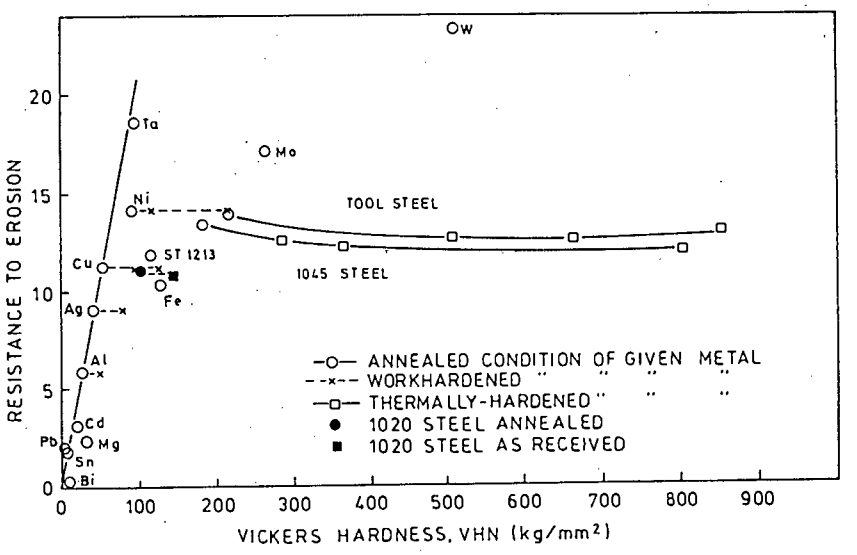


FIGURE 3.1 : Resistance to erosion as a function of hardness for erosion by 60 mesh SiC particles at an angle of 20° and a velocity of 250 ft/sec (after Finnie et al, 1967)

A similar relationship between hardness and erosion rate is predicted for brittle materials, if all other factors are equal. However, in practise toughness is the more important parameter.

### 3.1.2 Fracture Toughness

Fracture toughness is a measure of a material's resistance to fracture. In brittle materials, cracks are generated during impact, which results in chipping. Hence, the tougher the material, the less material removed, resulting in a decrease in erosion rate.

### 3.1.3 Microstructure

Various authors have reported a microstructural influence on erosion rate. Budinski and Chin (1983), however, observed that the correlation of erosion rate and microstructure disappeared when the impacting particle is above 50 μm in size and significantly harder than the target material.

Microstructure, as previously noted (Section 2.4) has an influence on the hardness and strength of a material. In brittle materials with a complex microstructure, phase interfaces or pores may cause a crack to be arrested (Routbort et al, 1980). These sites may, however, act as initiation sites for cracks and micromachining

chips. The latter was observed in Al-12 Si alloys by Hovis et al (1986).

## 3.2 PARTICLE PROPERTIES

### 3.2.1 Particle Size

It is generally accepted that the erosion rate, $E_R$, for brittle materials is governed by particle size, R, as expressed by the following equation:

$$E_R = \text{const } R^m \qquad (3.1)$$

The values of the particle exponent (m) lie in the range 2-5. In contrast, ductile materials show dependence on particle size over only a limited size range. Below a threshold size, 5 μm (Ruff and Wiederhorn, 1979), no significant erosion occurs. The initial particles are deflected by the sample, resulting in the incoming particles being deflected around the sample. Up to a particle size, 20 μm (Tabakoff et al, 1983; Tilly, 1979; Shewmon, 1981), particles are still affected by the curved airflow around the specimen, resulting in fewer particles impacting - or doing so at a modified velocity and angle.

Above a critical particle size, erosion is independent of particle size. Goodwin et al (1969) found the critical size to increase linearly with velocity (Figure 3.2).

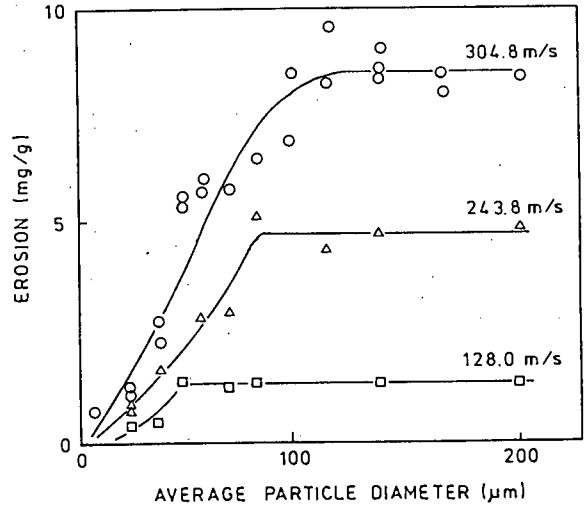


FIGURE 3.2 : Influence of particle size and velocity on erosion of an 11 per cent chromium steel (after Goodwin et al, 1969)

The size distribution of particles is another important consideration. Marshall et al (1981) observed that the erosion rate increased as the distribution range was expanded. Karlsen (1985) found the size distribution of the craters formed by the impacting particle is also important. The larger crater sites were found to be responsible for most of the material removal. For 240 grit SiC particles it was established that 10 percent of the sites were responsible for 50 percent of the volume of material removed.

Sheldon and Finnie (1966) observed that for nominally brittle materials, a transition from brittle to ductile behaviour occurs as the material is eroded by smaller and smaller particles.

### 3.2.2 Particle Shape

For both ductile and brittle materials, more effective erosion is generally found to be associated with angular particles (Finnie, 1960). Goodwin et al (1969) observed that hardness generally controls the sharpness of the particle, and erosion is dependant upon hardness. The sharpness of the hard particle may be due to the strong bonding of the atoms which is associated with hard material, a facetted crystal structure or brittle fracture. This is true if no fragmentation and hence no secondary erosion occurs.

For sharp angular particles, the orientation of the impacting particle will affect the impact process. For ductile materials, ploughing occurs for small rake angles, while cutting occurs at large rake angles (Winter and Hutchings, 1974).

### 3.2.3 Particle Concentration

Particle concentration has been defined by the American Society for Testing Material (ASTM, 1980) as "the mass of solid particles per unit volume of mixture in a solid impingement environment". However, Uuemôis and Kleis (1975) suggest that it is more accurate to describe concentration by the following relationship:

$$\psi = \frac{G}{Ft} \qquad (3.2)$$

where $\psi$ is particle concentration ($g.cm^2.s$); G is the mass of impacting particles (g); F is area of wear ($cm^2$) and t = the duration of the test.

Note that this relationship assumes a homogeneous distribution of particles across the surface. This may not be the case as shown later (see Section 7.1).

At high particle concentrations the erosion efficiency has been found to decrease (Smeltzer et al, 1970). Uuemôus and Kleis (1975) found this to be true for metals, alloys and ceramics, but not for rubber and some plastics (Figure 3.3).

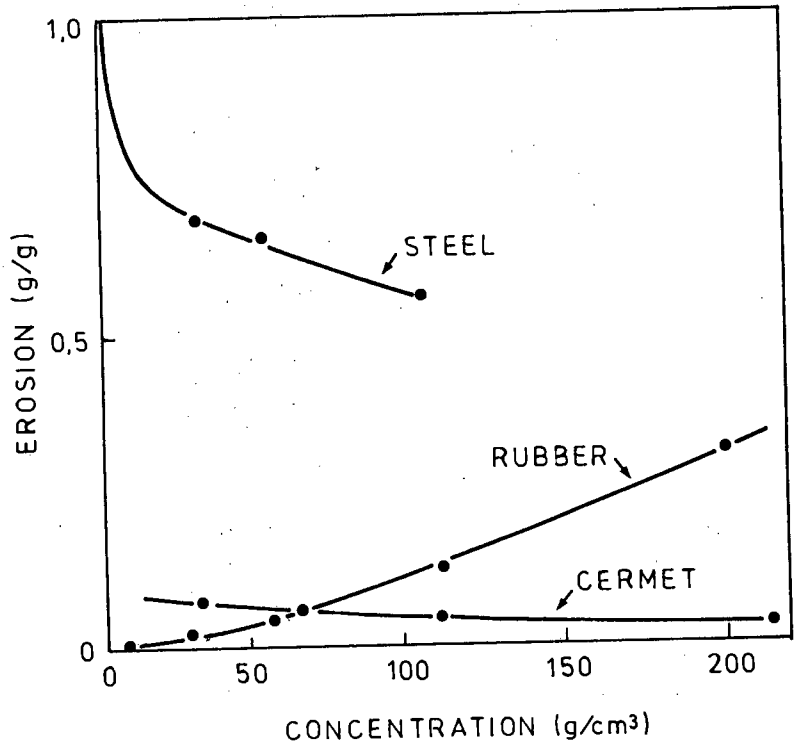


FIGURE 3.3 : The effect of particle concentration and erosion rate (v = 115 $m.s^{-1}$ and $\alpha$ = 90°) (after Uuemôus and Kleis, 1975)

The decrease in erosion is due to the reduction of the number of impacting particles by a 'cloud' of rebounding particles and debris. For rubber a 'cloud' is not formed, as the duration of impact and depth of penetration is much greater.

## 3.3 IMPACT PARAMETERS

### 3.3.1 Velocity

Numerous investigators have shown that erosion rate ($E_R$) increases with increasing particle velocity (V). This relationship is often expressed by the form:

$$E_R = \text{const } V^n \qquad (3.3)$$

For ductile materials the velocity exponent (n) lies typically in the range 2 - 3, while for brittle materials much higher exponents have been reported, for example an exponent of six for glass impacted with steel spheres (Finnie, 1960).

Ruff and Weiderhorn (1979) found that although particle velocity is the main parameter controlling erosion, the velocity exponent is insensitive to the microstructure of the material. Hence it is not a useful indicator for evaluating microstructural effects on erosion, nor for distinguishing between mechanisms of erosion.

### 3.3.2 Angle of Impact

Tilly (1979) defines angle of impact as the inclination between the target surface and the particle trajectory. The variation of erosion with angle is dependent upon the type of material - as illustrated in Figure 3.4. For ductile materials maximum erosion occurs at approximately 20°, while for brittle materials the maximum occurs at normal impact (90°).

Both Tilly (1979) and Ruff and Weiderhorn (1979) note that most materials exhibit a combination of brittle and ductile erosion. At low angles ductile erosion predominates, with the brittle mode becoming more important as the angle is increased.

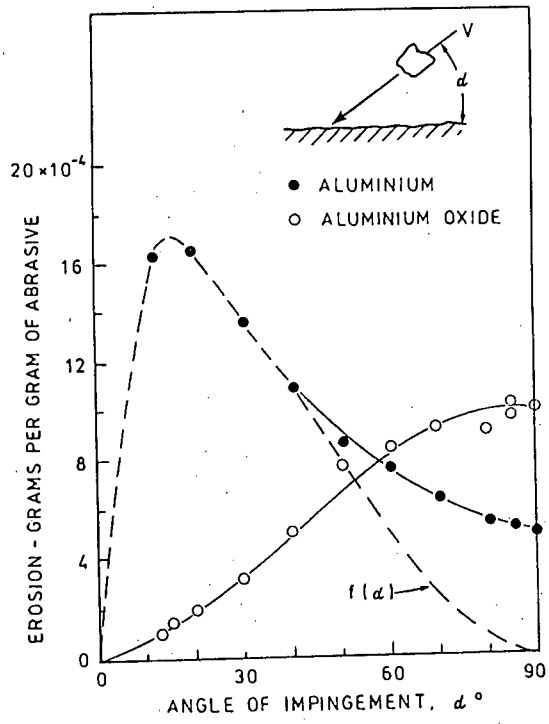


FIGURE 3.4 : The effect of impact on erosion rate for aluminium and aluminium oxide eroded by 100 μm SiC particles at 152 $ms^{-1}$ (after Finnie et al, 1967)

## 3.4 MECHANISMS OF EROSION

Various theories have been developed to explain erosion phenomena in terms of the mechanism of material removal. Tilly (1979) notes that although the theoretical models differ, there is general agreement that ductile and brittle erosion occur by very different mechanisms of material removal. A brief summary of the main theories of erosion follows:

### 3.4.1 Brittle Erosion

Until recently, brittle erosion was believed to occur entirely by crack propagation and chipping (Finnie, 1960; Bitter, 1963; Sheldon and Finnie, 1966). Hockey et al (1977), however, observed the presence of plastic deformation during the erosion of a variety of brittle materials. Consequently, more recent theories of brittle erosion have incorporated the concept of elastic-plastic deformation.

During impact by a sharp particle, stresses associated with the plastic zone are responsible for the nucleation and growth of radial-median cracks (Hockey and Weiderhorn, 1979). These cracks develop normal to the target surface (Figure 3.5) and are the main cause for strength degradation. As the particle leaves the surface, lateral cracks nucleate from the plastic zone. The cracks initially travel on a plane approximately parallel to the surface, but then grow towards the surface, resulting in chips of material being lost.

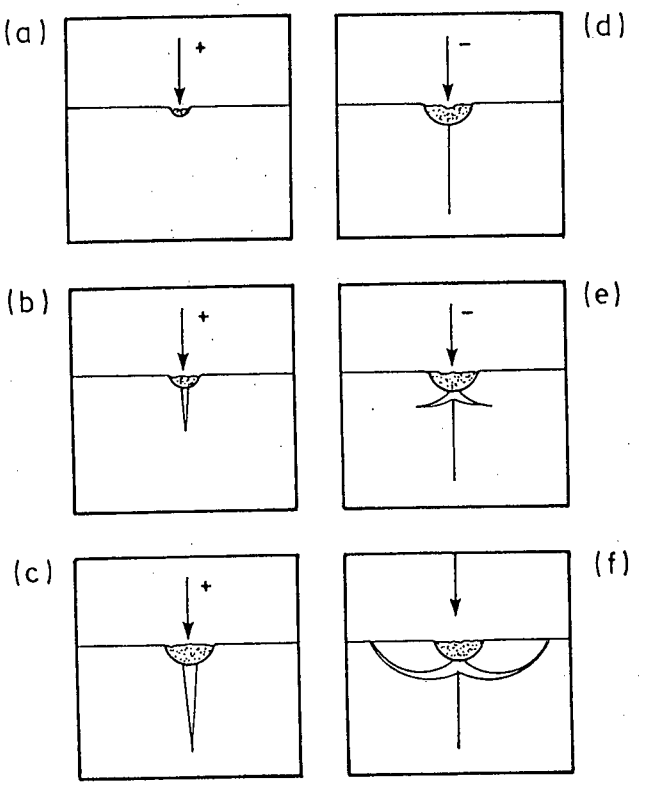


FIGURE 3.5 : Schematic diagram of crack growth during sharp particle impact. + sign indicates loading; - sign indicates unloading (after Hockey and Weiderhorn, 1979)

Two quantitative models have been developed for predicting the erosion rate ($E_R$) (volume loss per impact). Both models are based on the analysis of the volume removed from single particle impacts. Marshall et al (1981) presumed that the interactions between multiple impacts are negligible. The cumulative effect of multiple impacts is obtained by summing the volumes removed for individual impacts.

Weiderhorn and Lawn (1979) modelled the impact event on a quasi-static indentation and obtained the following expression:

$$E_R = V^{2.4}\, R^{3.7} \rho^{1.2}\, K_{IC}^{-1.3}\, H^{0.11} \qquad (3.4)$$

where V, R and $\rho$ are the projectile velocity, diameter and density respectively, and $K_{IC}$ and H are the target toughness and hardness.

Using a dynamic impact theory, Evan et al (1978) obtained the following expression, which differs only slightly from that of Weiderhorn and Lawn (1979).

$$E_R = V^{3.2}\, R^{3.7} \rho^{0.26}\, K_{IC}^{-1.3}\, H^{-0.25} \qquad (3.5)$$

At low angles of impingement, Tilly (1973) observed the primary mechanism of material removal for brittle materials is plastic ploughing, similar to that of ductile materials.

### 3.4.2 Ductile Erosion

Extensive plastic shear is considered necessary before ductile material removal occurs. Finnie (1960) proposed a model where the cutting action of the eroding particle is the only mode of material removal. The model is expressed by the following equation:

$$E_R = \frac{GV^2}{P} f(\alpha) \qquad (3.6)$$

where $E_R$ is the wear volume; G is the mass of the impinging particles; V is the particle velocity; P is the flow stress of the target material and $f(\alpha)$ is a function of the angle of particle impact, which has a cosine variation when the perpendicular velocity of the particle is greater than zero.

The above equation correlates with ductile erosion at glancing angles. It, however, underestimates the erosion at 90°, which is

predicted to be zero. Bitter (1963) explained the erosion at 90° by including ductile and brittle terms for the same material. Thus, the erosion at normal impact not accounted for by Finnie is due to the brittle components.

Other models of material removal from ductile cutting and brittle deformation have been proposed. Bellman and Levy (1981) consider the formation of an extruded lip, or platelet, and its subsequent fracture as the dominant mode of material removal. Figure 3.6 schematically illustrates the platelet formation sequence.

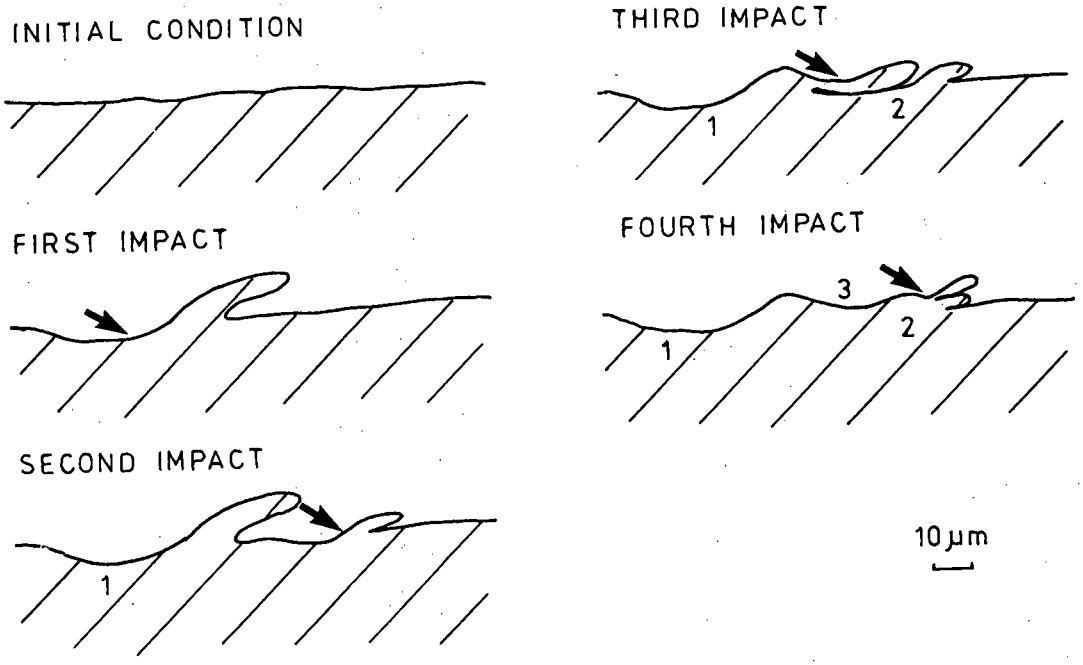


FIGURE 3.6 : A schematic representation of the platelet formation sequence (Levy, 1986)

Shewmon and Sundararajan (1983) note that during further impact a lip, or platelet, can fracture by either necking down or by separation along an adiabatic shear band formed at the base of the lip.

Other models have been developed where material loss is considered to occur only once a critical strain is reached. Ball (1985) notes that once initial strain accumulation has occurred material is lost by microfracture.

# CHAPTER 4

## REVIEW OF THE EROSION OF WC-CO

In Chapter 3 ductile and brittle erosion mechanisms were discussed as independent, alternative mechanisms. In many cases this assumption is an obvious oversimplification. Many materials exhibit a combination of ductile and brittle characteristics, depending upon the test conditions (Sheldon, 1970). Due to its two-phase nature, the WC-Co alloy, however, is considered to undergo a mixed mode of erosion. Both Ball and Paterson (1985) and Wright et al (1983) observed brittle fracture of the WC grains while the softer cobalt matrix was deformed by a ductile mode. Microstructural properties are thus an important consideration when studying the erosion of WC-Co alloys.

## 4.1 VARIABLES AFFECTING EROSION OF WC-Co Alloys

### 4.1.1 Target Materials

Hardness and toughness, which under normal circumstances work in opposition to each other, are considered to be important mechanical properties affecting erosion. Since both hardness and toughness are strongly dependent on binder content, it is of interest to study the erosion rate of an alloy as a function of binder content.

For solid particle impact erosion conditions, researchers have found in general that the erosion rate increases with increasing binder content (Conrad et al, 1982; Hanson et al, 1979; Uuémyis et al, 1974). Similar results were obtained by Shetty et al (1984) for slurry erosion tests. These slurry erosion results were found to give a reasonable fit to the following empirical power-law relationship:

$$V_c = V_o \, f_{co}^{2.32} \qquad (4.1)$$

where Vc is the mean volume per crater of the resulting craters, which is related to erosion rate; $V_o$ is an empirical parameter and $f_{co}$ is the cobalt volume fraction.

For solid impact erosion tests carried out at an attack angle of 45°, Ball and Paterson (1985) did not find the erosion rate to increase monotonically with increasing binder content. Instead, a peak in erosion rate was observed at 10 wt-% cobalt. The erosion rate was then found to decrease to an optimum condition of 20 wt-%, after which it increased. This curve was explained in terms of microtoughness and hardness, the optimum combination of which was proposed to occur at 20 wt-% cobalt. The Ball & Paterson model is explained in more detail in Section 4.3.2.

Slurry erosion tests carried out by Wright et al (1983) did not follow the trend of increasing erosion rate with increasing binder content either. Instead, a minimum erosion value was found to correspond with a binder level of 7,1 wt-%. The erosion of alloys with less than 7,1 wt-% cobalt was considered to be fracture-toughness controlled, similar to that of brittle materials. Above 7,1 wt-% cobalt the erosion rate is thought to be predominantly hardness controlled. No reason, however, was proposed to explain the transition.

The effect of WC grain size on erosion rate is not fully understood or agreed upon. Conrad et al (1982) observed that for WC-Co alloys containing 11.3 wt-% cobalt and less, the erosion rate appeared to pass through a maximum at a grain size of 1.5µm. These erosion tests were conducted at impact angles ranging from 20° to 90°. However, Uuémyis et al (1974) found that for 6 and 15 wt-% cobalt alloys, as the mean grain size was increased from 1.5 to 10.6 µm, the erosion rate increased by a factor of 30. No mention of the angle of impact employed was made.

### 4.1.2 Particle Size

The effect of the particle size of the erodent on the erosion rate of WC-Co alloy has not been extensively studied. For slurry erosion, where there is a wide range of particle size, Wright et al (1983) observed a mixed mode of the following effect of particle size on erosion. They postulated that larger particles in stream produce erosion of the tungsten carbide by chipping, while the smaller size particles erode by ductile cutting.

### 4.1.3 Velocity

The microstructural change in the WC-Co alloy, resulting from the change in cobalt, is expected to be reflected in the relative dependence of erosion rate on velocity (Wright et al, 1983). For solid particle impact erosion, the results of both Conrad et al (1982) and Uuémyis et al (1974) showed an increase in slope of the erosion rate - velocity curve with increasing binder content. Shetty et al (1984) calculated the slurry-jet velocity exponent to be 1,66 for the 5,1 wt-% cobalt alloy and 3.39 for the 36,9 wt-% cobalt alloy. It was, however, noted that although a velocity exponent of less than 2 is unusual for solid particle erosion, it has often been observed in slurry erosion.

### 4.1.4 Angle of Attack

As mentioned previously (Section 3.4), studying the effect of angle of attack on erosion is considered to be instructive with respect to determining the erosion mechanism. Solid particle impact erosion studies conducted by Conrad et al (1982) revealed that maximum erosion occurred at normal impact for all cobalt contents tested, as illustrated in Figure 4.1. This appears to indicate that a brittle mode of erosion occurs in WC-Co alloys. Note should be made of the fact that only low binder content alloys were tested. The highest cobalt content alloy tested was 11.3 wt-%.

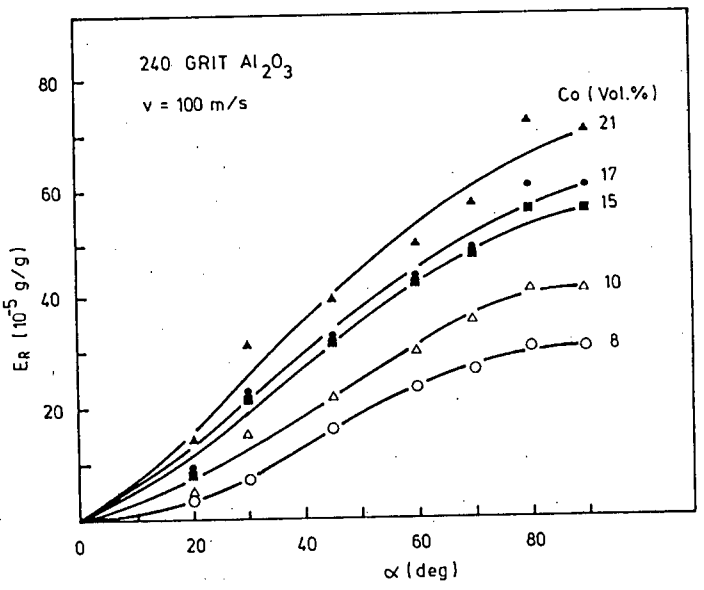


FIGURE 4.1 : Effect of impact angle of erosion rate as a function of cobalt content (after Conrad et al, 1982)

Slurry erosion tests carried out at a variety of angles corresponded neither to that expected for ductile erosion, nor to that expected for brittle erosion (Wright et al, 1983). Shetty et al (1984) observed maximum erosion rates in the attack angle range 50-90 degrees. This result is common for slurry erosion tests, and is believed to indicate that angular dependence tests tend to be independent of the material or mechanisms of erosion.

## 4.2 MODES OF MATERIAL REMOVAL

Various modes of material removal have been reported in literature. From Table 4.1, which summarizes these modes, it is apparent that cobalt removal is the initial and rate controlling step which precedes the fracture and removal of the brittle WC grains, in all proposed mechanisms.

TABLE 4.1 : Summary of the various modes of material removal reported in literature

| AUTHOR | COBALT MATRIX | WC GRAINS |
|---|---|---|
| Blombery et al (1974) | Preferential removal of cobalt (rate controlling step) | This leads to microfracture of the carbide skeleton |
| Hanson et al (1979) | Preferential removal of binder | |
| Conrad et al (1982) | Preferential removal of binder shadowing of the cobalt phase by the WC grains at small impingement angles | Cracking of carbides grains |
| Wright et al (1983) | Preferential removal of cobalt | Ductile erosion of WC grain. Brittle erosion of WC grain by chipping and/or fracture. Pull out of WC grains. |
| Shetty et al (1984) | Low cobalt content : Cobalt binder removed from triple point boundry junction<br><br>High cobalt content : Preferential removal of cobalt | Wear rate controlled by transgranular wear of contiguous network of WC grains. The grains are slightly rounded.<br><br>Grain pull out. Grains show evidence of cracking. |
| Ball & Paterson (1985) | Ductile removal at high cobalt contents | Brittle fracture of the WC grains at low cobalt contents |
| Larsen-Basse (1985) | Cobalt extrusion, possibly preceded by cracking of the brittle material | Relaxation of the residual stresses causes the fragmentation of the WC grains |

## 4.3 MODELS OF EROSION

### 4.3.1 The Conrad, Shin and Sargent Model

Conrad et al's (1982) model for the erosion of WC-Co considers seperate mechanisms for the erosion of the WC phase and the cobalt phase.

The erosion of pure WC is given by a constant ($a_w$), which is dependent on velocity and angle of impact. The additional erosion, due to cobalt is represented by b in equation 4.2, is angle dependent. For angles greater than 45°, the erosion rate is calculated by resolving the normal component of particle velocity. However, for impact angles less than 45° the extra contribution due to the glancing component of velocity, must be taken into account. Thus the overall erosion rate may be summarised by the form:

$$E_R^{WC-Co} = a_w + b_{90}\, f_{Co} + (b-b_{90})\, f_{Co} \qquad (4.2)$$

where $a_w$ is the erosion of WC, $b_{90}$ the erosion of cobalt due to the normal component of velocity, $(b-b_{90})$ is that due to the glancing component of velocity and $f_{Co}$ is the cobalt volume fraction.

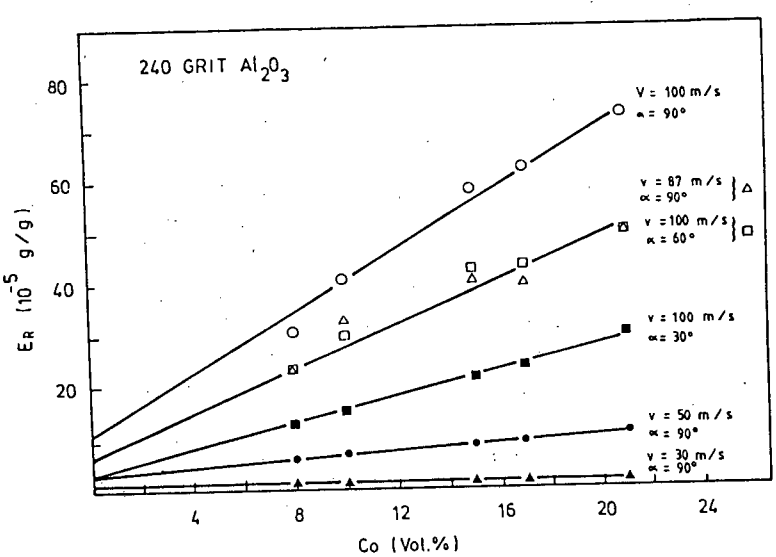


FIGURE 4.2 : Erosion rate versus cobalt content as a function of the particle velocity (after Conrad et al, 1982)

The velocity exponents of $a_W$, $b_{90}$ and $b-b_{90}$ were empirically found to be 2, 3.2 and 2 respectively. Thus, equation 4.2 takes the form:

$$E_R^{WC-Co} = A(V\sin\alpha)^2 + B(V\sin\alpha)^{3.2} f_{Co} + C(V\cos\alpha)^2 f_{Co} \quad (4.3)$$

where A, B and C are constants found to have the empirical values $1.0 \times 10^{-8}$, $1.3 \times 10^{-9}$ and $1.0 \times 10^{-6}$ respectively.

The exponent 2 for the WC term A $(V\sin\alpha)$ is in agreement with the Hertzian elastic fracture mechanism. The cobalt phase, however, erodes by a combination of cutting and deformation erosion mechanisms.

In this model consideration is given to a simple rule of mixtures, while microstructural influences are ignored. Thus, WC-Co alloys having the same binder level, but different mean free paths, are assumed to erode at the same rate.

### 4.3.2 The Ball and Paterson Model

Solid particle impact erosion tests carried out by Ball and Paterson (1985) included a larger range of WC-Co alloys than those used by Conrad et al (1982). For these tests, however, the velocity and angle of attack parameters were kept constant, at 40 $ms^{-1}$ and 45° respectively. As mentioned previously (Section 4.1.1), the erosion rate values did not increase with increasing cobalt content. Instead, the relationship found is illustrated in Figure 4.3. No quantitative equation was formulated, but a quantitative model of erosion was postulated.

The local maximum at 10 wt-% was explained in terms of a change in structure. Below 10 wt-% the erosion is controlled by the WC skeleton. As the amount of contiguity is increased, so the skeleton becomes more rigid, resulting in a decrease in erosion rate. However, a more rigid skeleton is usually associated with brittle erosion, causing an increase in erosion to be expected. This indicates that an underlying mechanism, which is not immediately apparent, must be responsible for the decrease in

erosion. Above this maximum, erosion is controlled by the strength and microtoughness of the binder. At 10 wt-% the cobalt has low toughness and the WC skeleton is fragile and discontinuous.

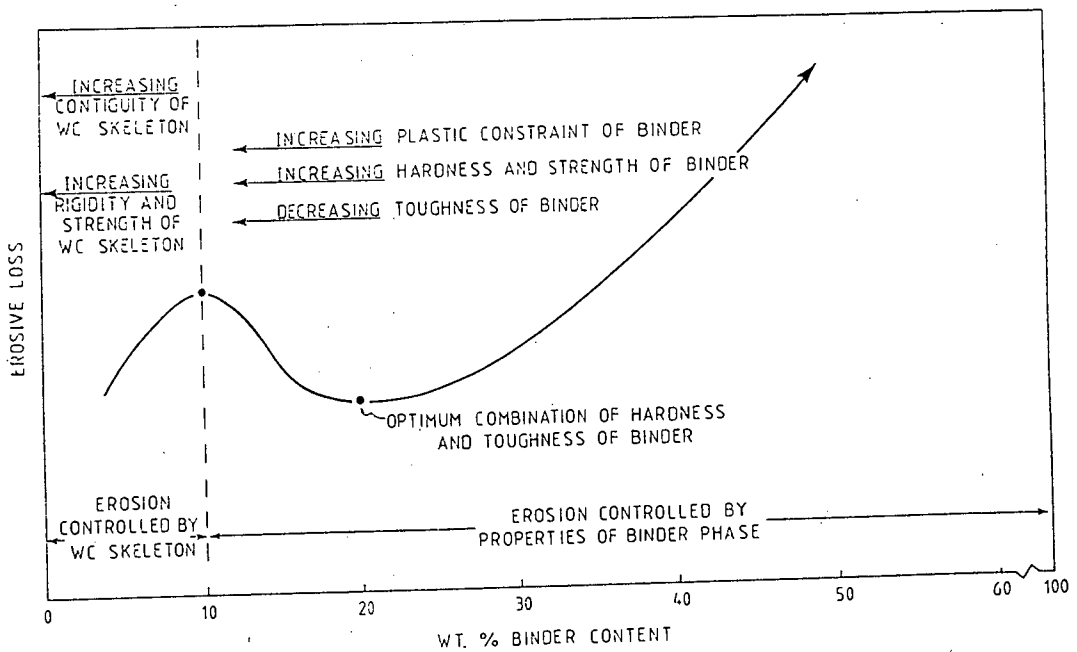


FIGURE 4.3 : A schematic representation of the erosion of WC-Co alloys as a function of binder content. The factors which are considered to control erosion are indicated (after Ball and Paterson, 1985)

A similar change of mechanism at approximately the same cobalt content, 15 vol-% (9 wt-%) cobalt, was observed by Shetty et al (1984) in slurry erosion studies. At low binder contents the erosion is controlled by the transgranular wear of the contiguous network of WC grains. However, at high binder levels erosion occurs by removal of the binder, undercutting of the WC particles, and the release of whole grains. This change in mechanism, did not, however, affect the linear dependence of erosion rate on binder content.

The minimum at 20 wt-% cobalt was explained as being the result of the optimum combination of hardness and toughness of the cobalt binder. However, once again no mechanism for the change in erosion rate was proposed by the model.

# CHAPTER 5

## EXPERIMENTAL TECHNIQUES

A series of WC-Co alloys, as supplied, were characterized and subjected to erosion testing using the following range of techniques.

### 5.1 MATERIAL

The WC-Co alloys used are all commercially available grades. Flat, circular disc specimens of the order to 14 mm diameter and 3 mm height were supplied in the ground state. The alloys were polished to a 1 $\mu$ m finish and then tested in the as received condition.

### 5.2 MICROSTRUCTURAL PROPERTIES

Lineal analysis measurements were performed on micrographs of flat, polished samples to determine the microstructural parameters. A semi-automatic image analysis system, developed for use on the Teletronix 4051 - Summagraphic digitizer system (Frith and Heckroodt, 1984), was used to quantitatively define parameters using the following equations:

Volume of Binder Phase $$V_B = \Sigma L_B$$

Tungsten Carbide Particle Size $$\bar{d} = \frac{2V_a}{2\,N_{aa} + N_{ab}}$$

Contiguity of Tungsten Carbide $$C = \frac{2\,N_{aa}}{2\,N_{aa} + N_{ab}}$$

Binder Mean Free Path $$\lambda = \bar{d}\,\frac{V_B}{(1-V_B)(1-C)}$$

where N is the average number of interfaces per unit length of test line with traces of a certain interface. $L_B$ is the length of cobalt phase per unit length of test line. The subscripts aa and ab refer to the carbide-carbide and carbide-cobalt interfaces respectively.

## 5.3 MECHANICAL PROPERTIES

Due to the importance of the hardness and fracture toughness on erosion, these two mechanical properties were the only ones tested.

### 5.3.1 Hardness

Hardness was tested using the Vickers diamond pyramid indentor. An average of five values was taken, using a load of 30 Kg.

### 5.3.2 Fracture Toughness

The sample size of the alloys was small (14 mm diameter), which meant the Palmqvist method was the only method available for measuring fracture toughness. (See Appendix A for a description of this method).

As mentioned previously (Section 2.4.3.1), the Palmqvist test is not universally accepted, but as a comparative method, it is considered to be adequate. Due to the method's sensitivity to surface finish, a special polishing routine had to be followed, which will be described in a later section (Section 6.2.2).

## 5.4 EROSION TESTING

A particle stream erosion tester was used to simulate impact erosion. The apparatus is schematically represented in Figure 5.1.

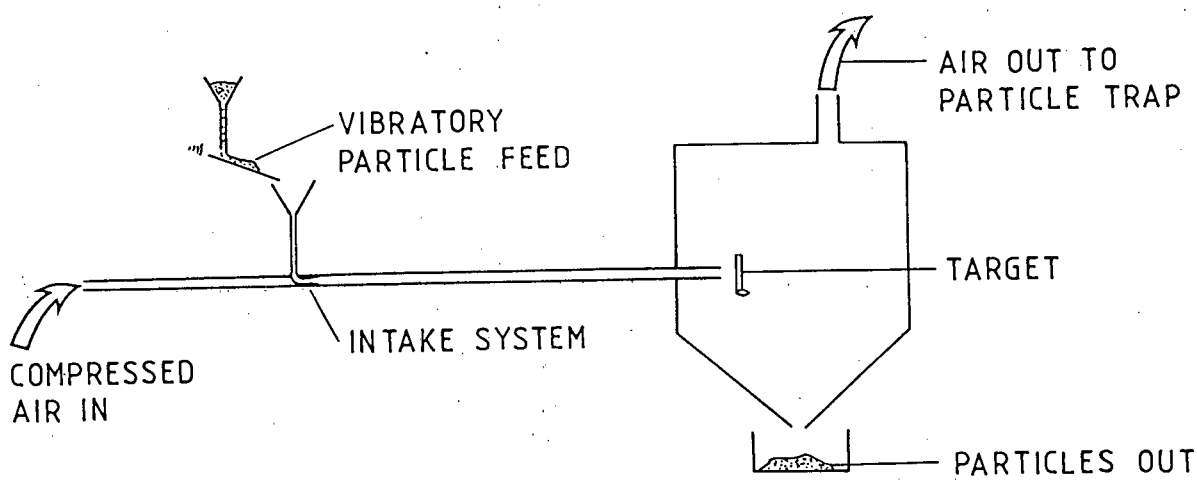


FIGURE 5.1 : Schematic diagram of apparatus

The basic operating parameters of the apparatus are summarized in Table 5.1.

TABLE 5.1 : Operating parameters of the particle stream erosion tester

| VARIABLE | RANGE |
|---|---|
| Particle velocity | 40 $ms^{-1}$ |
| Angle of attack | 15°, 30°, 45°, 60°, 90° |
| Operating temperature | Room temperature |
| Target material | WC-Co alloys |
| Erodent type | SiC |
| Erodent size | 100 $\mu$m, 50 $\mu$m, 30 $\mu$m |
| Particle feed rate | 0,166 $gs^{-1}$ |
| Particle concentration | 0,0166 $gs^{-1}$ $cm^{-1}$ |
| Distance between target and tube outlet | 30 mm |
| Inner diameter of tube | 10 mm |
| Length of tube | 3 m |

A predetermined amount of erodent was fed, via a vibratory particle feeder, into the airstream. The particle and carrier velocities were controlled by varying the pressure drop across the nozzle. The actual particle velocity was measured using the Ruff and Ives (1975) double rotating disc method. For a particle concentration of 0,016 $gcm^{-2}$ $s^{-1}$ it was calculated that no sheilding of particles should occur for any erodent size. To determine if shielding occurred, the probability of a collision occurring between an incoming and a rebounding particle was calculated using the mean free path lengths of the respective particles.

After each test the WC-Co alloy was cleaned ultrasonically in alcohol, dried and weighed on a 5 point balance. Tests were repeated until steady state erosion was obtained. The results of two separate runs, carried out on the same sample under the same conditions, are depicted in Figure 5.2.

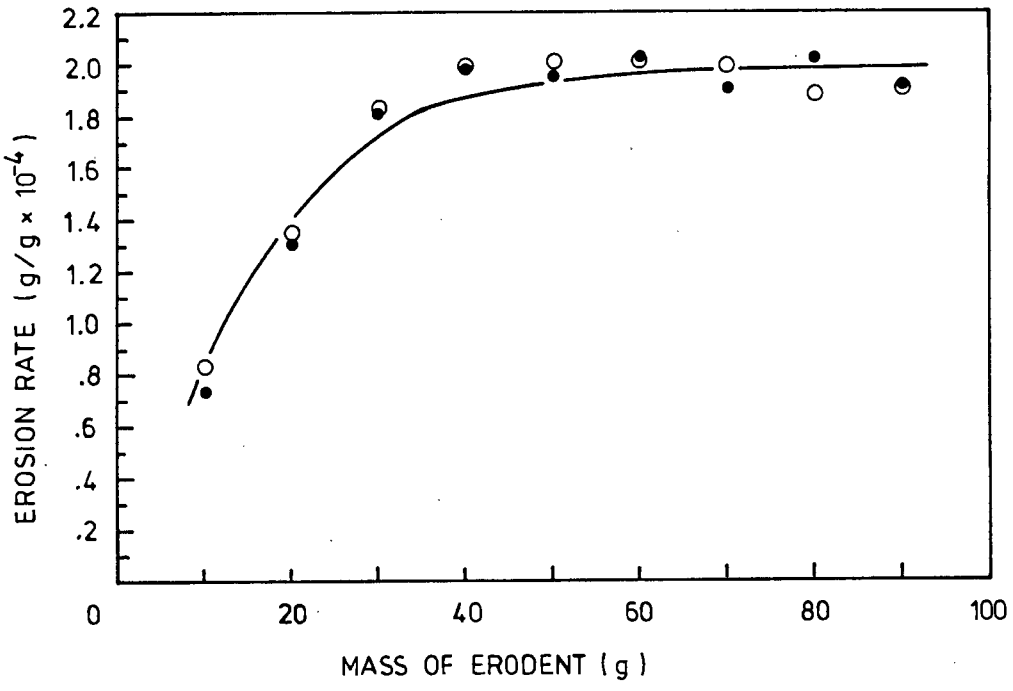


FIGURE 5.2 : Steady-state erosion of G1 (8 wt-%; 2.8 μm) for 120 grit SiC test at 90°. The symbol o represents the first run and ● represents the second run

The reproducibility of the two runs is seen to be satisfactory, indicating that this was an acceptable method of testing impact erosion.

## 5.5 ELECTRON MICROSCOPY

The alloys were eroded to steady state, and the eroded surfaces were examined using the scanning electron microscope.

Low concentration tests, for which the nominal amount of impacting particles was 0,1 g, were conducted. The resulting individual impact sites were then qualitatively analysed. Quantitative measurements were performed on the individual impact sites using stereo micrograph pairs.

# CHAPTER 6

## THE MICROSTRUCTURAL PARAMETERS AND MECHANICAL PROPERTIES OF THE WC-CO ALLOY

In this chapter results for experimentally determined microstructural parameters and mechanical properties will be presented. The correlation between these microstructural parameters and mechanical properties will then be discussed.

### 6.1 MICROSTRUCTURAL PARAMETERS

The microstructural parameters values obtained from lineal analysis, along with the supplier's specified cobalt content, are tabulated in Table 6.1. The correlation between experimental and supplier's value for cobalt content was considered acceptable, except for B3, where the experimental value was considered a little too high. Density tests (Hankey, 1986), have shown that the B3 density values lay inbetween the supplied and experimental values.

TABLE 6.1 : The binder content, nominal grain size, mean free path and contiguity of the WC-Co alloys

| MATERIAL | COBALT CONTENT (wt-%) | | NOMINAL GRAIN SIZE (μm) | MEAN FREE PATH (μm) | CONTIGUITY |
|---|---|---|---|---|---|
| | BOART | EXPERIMENTAL | | | |
| A1 | 5 | 5 | 1,46 | 0,642 | 0,790 |
| B1 | 6 | 7 | 1,85 | 0,810 | 0,773 |
| C1 | 6 | 5 | 2,42 | 0,823 | 0,728 |
| D1 | 6 | 6 | 1,28 | 0,510 | 0,660 |
| E1 | 6 | 6 | 0,56 | 0,330 | 0,831 |
| F1 | 6 | 7 | 2,98 | 1,317 | 0,715 |
| B2 | 7 | 8 | 1,88 | 0,927 | 0,670 |
| G1 | 7 | 7 | 2,80 | 1,425 | 0,710 |
| G2 | 8 | 9 | 2,64 | 1,581 | 0,694 |
| H1 | 8 | 8 | 3,31 | 1,714 | 0,680 |
| G3 | 9 | 10 | 2,82 | 1,740 | 0,673 |
| F2 | 10 | 12 | 2,83 | 1,729 | 0,604 |
| B3 | 10 | 14 | 1,78 | 1,024 | 0,510 |
| H2 | 10 | 12 | 3,00 | 1,986 | 0,550 |
| G4 | 12 | 14 | 2,58 | 1,637 | 0,556 |
| C2 | 12 | 13 | 2,00 | 1,435 | 0,630 |
| F3 | 15 | 15 | 2,85 | 1,950 | 0,540 |
| B4 | 20 | 20 | 1,76 | 1,436 | 0,475 |
| I1 | 30 | 30 | 2,17 | 2,69 | 0,392 |

The alphabetical letters not only refer to the nominal grain size, but also gives an indication of the grain size distribution. The supplied structures of the alloys are summarized in Table 6.2.

TABLE 6.2 : Summary of the grain size structure of the WC-Co alloys

| | GENERAL | SOME | SCATTERED | OCCASIONAL | ISOLATED |
|---|---|---|---|---|---|
| A | ½ - 1½ | 3 - 5 | 7 | 10 | 12 |
| B | ½ - 2 | 3 | 5 | 7 | 9 |
| C | ½ - 2½ | 3 - 5 | 5 - 7 | 7 - 9 | 9 - 12 |
| D | ½ - 2 | 3 | 5 | 5 | 9 |
| E | 1½ | | 2½ | | 8 |
| F | ½ - 2½ | 3 - 5 | 7 | 10 | 12 |
| G | ½ - 2½ | 3 - 5 | 7 | 9 | 11 - 14 |
| H | ½ - 2½ | 3 - 5 | 8 | 10 | 13 |
| I | ½ - 2½ | 3 | 5 | 7 | 9 |

The lineal analysis results suggested that the majority of materials could be divided into two groups according to grain size. The first group consisted of the A and B series, both of which had an approximate nominal grain size of 1,8 $\mu$m. The F, G and I series constituted the second group, where the approximate nominal grain size was 2,8 $\mu$m. Thus in various situations where the grain size effect is studied, only the materials in these two groups were considered.

As mean free path is a measure of the thickness of the cobalt layers, it is dependent on the cobalt content and WC grain size. The experimental data is summarised in Figure 6.1.

Figure 6.2 shows the effect of cobalt content and grain size on contiguity. The amount of contiguity present decreased with increasing cobalt content, as is to be expected from the equation defining contiguity (see Section 5.1). Contiguity, however, increases with increasing grain size, as noted by Lee and Gurland (1978).

## 6.2 MECHANICAL PROPERTIES

The experimentally determined values for hardness and toughness are tabulated in Table 6.3.

TABLE 6.3 : Hardness and fracture toughness values of the WC-Co grades

| MATERIAL | HARDNESS (HV30) | FRACTURE TOUGHNESS (MPa $m^{1/2}$) |
|---|---|---|
| A1 | 1652 | 5,43 |
| B1 | 1621 | 5,43 |
| C1 | 1516 | 6,00 |
| D1 | 1678 | 5,73 |
| E1 | 1800 | 5,00 |
| F1 | 1382 | 7,13 |
| B2 | 1566 | 5,87 |
| G1 | 1347 | 9,66 |
| G2 | 1326 | 10,42 |
| H1 | 1245 | 12,64 |
| G3 | 1232 | 12,05 |
| F2 | 1193 | 12,61 |
| B3 | 1270 | 8,51 |
| H2 | 1193 | 15,44 |
| G4 | 1175 | 16,29 |
| C2 | 1231 | 16,08 |
| F3 | 1146 | 18,31 |
| B4 | 1044 | 18,80 |
| I1 | 716 | - |

### 6.2.1 Hardness

The variation of hardness with cobalt content and grain size is shown in Figure 6.3. The observed data are in excellent agreement with the data available in the literature, as represented in Figure 2.4(a). The hardness of the WC-Co alloy is considered to be essentially controlled by the cobalt phase (M.T. Laugier, 1985 a ). The in-situ hardness of the binder phase was found by Lee and Gurland (1978) to vary with mean free path according to a Hall-Petch type relationship ($Hm = 304 + 12{,}7\,\lambda^{-1/2}$). Thus, due to the increase of mean free path with cobalt content, the hardness of the binder phase decreases with increasing cobalt content. This results in a decrease of the hardness of the WC-Co alloy with increasing cobalt content. The reduction in hardness of the binder phase is believed to be caused by the reduced plastic constraint associated with increasing mean free path (Heathcock, 1980).

The hardness of the WC-Co alloy was observed to increase with a decrease in grain size. As mentioned previously (Section 6.1), an increase in grain size results in an increased mean free path. This results in a decrease in plastic constraint, and thus, a reduction in hardness.

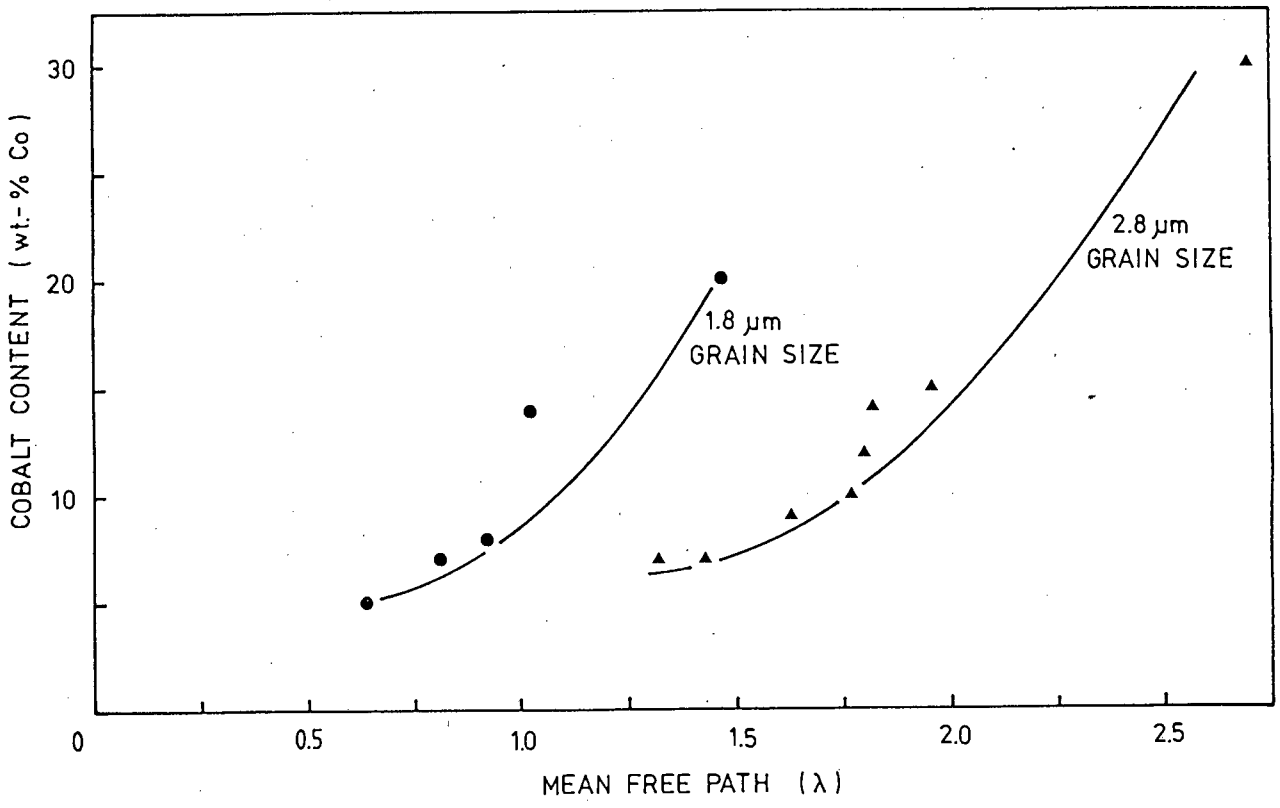


FIGURE 6.1 : Mean free path as a function of experimental binder content and grain size with trends indicated

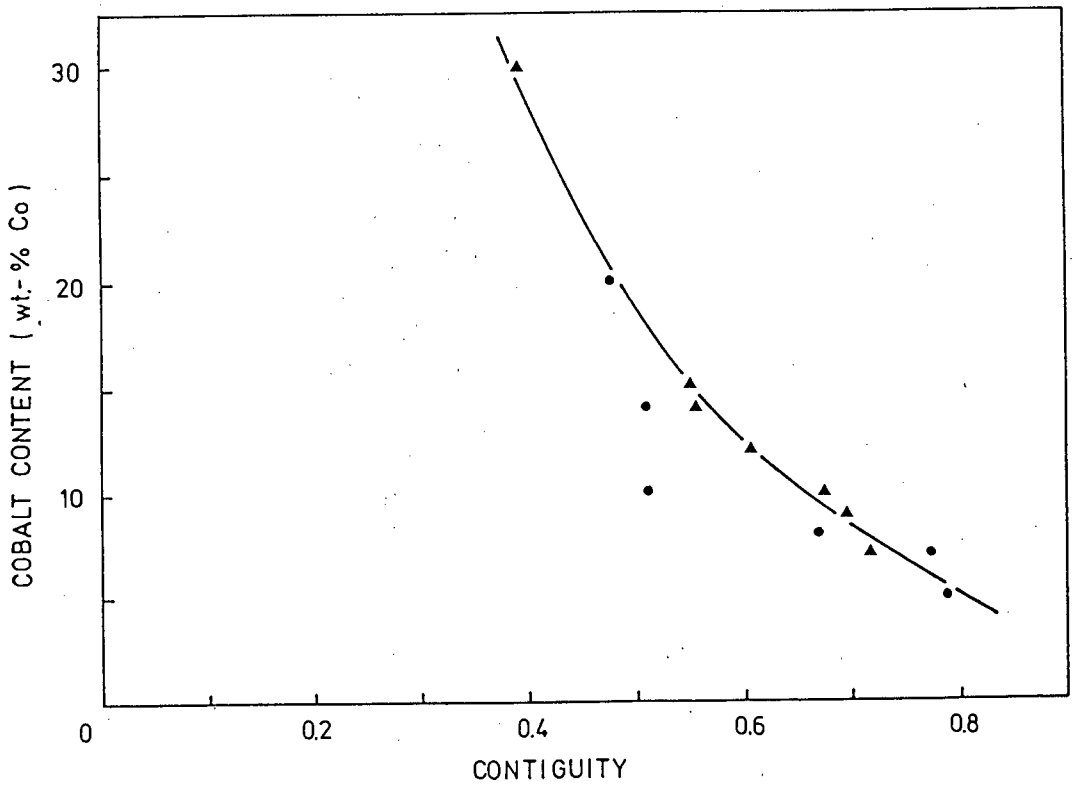


FIGURE 6.2 : Contiguity as a function of experimental binder content and grain size with the apparent trend indicated

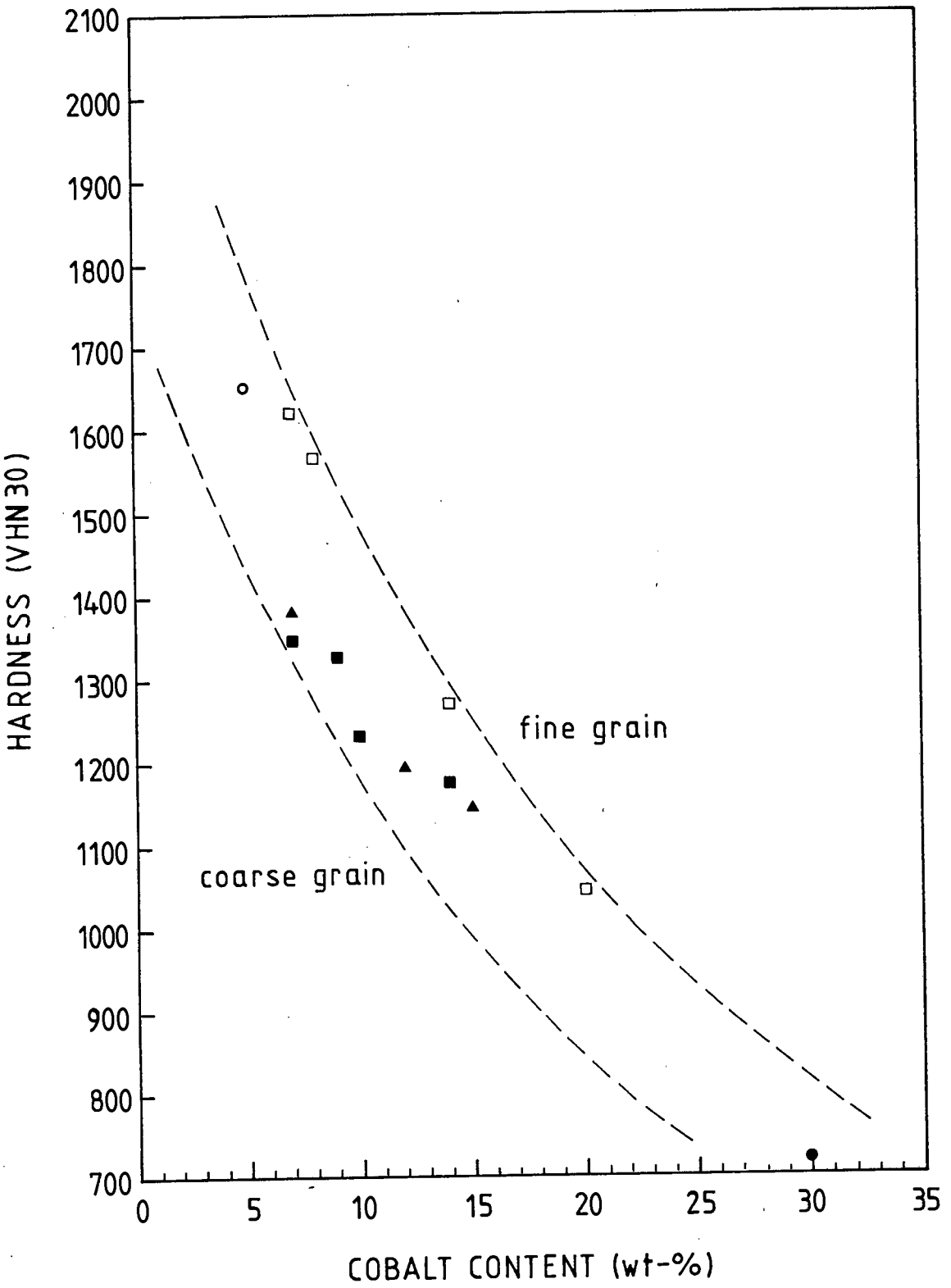


FIGURE 6.3 : The effect of binder content on hardness, for the nominal 1,8 μm and 2,8 μm grain sizes. The symbol ○ = A series and □ = B series refer to the 1,8 μm grain sized materials. The symbols ▲ = F series, ■ = G series and ● = I series refer to the 2,8 μm grain sized samples

### 6.2.2 Fracture Toughness

The Palmqvist indentation method of measuring fracture toughness is very sensitive to surface residual stresses. Hence, careful and often time-consuming preparation of the sample is necessary.

Exner (1979) observed that the compressive stresses introduced to the surface region can be removed by polishing away the deformed layer. The stresses eventually reach a constant level corresponding to the equlibrium thermal stresses. A test was carried out on five samples to determine the optimal polishing time, x, required before a state of thermal stress equivalent to that occurring after sintering is obtained. The polishing method used is:-

i) x hours on an automatic polisher with 15μ m diamond paste.
ii) 15 minutes polishing with 6 μm diamond paste.
iii) 15 minutes polishing with 3 μm diamond paste.
iv) 5 minutes polishing with 1 μm diamond paste.

The effect of polishing time on crack length is illustrated in Figure 6.4.

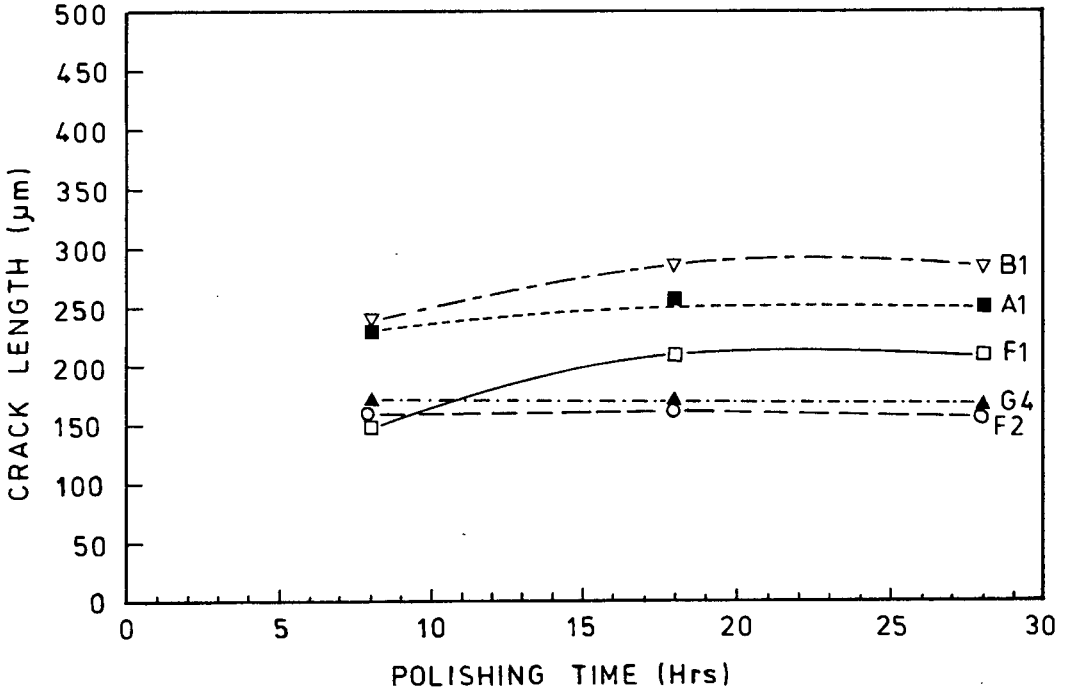


FIGURE 6.4 : Crack length as a function of polishing time for five grades

For the higher cobalt content materials (G4 and F2), the optimal polishing time appears to be approximately 8 hours on the automatic polisher with 15 $\mu$m diamond paste. For polishing times of less than 8 hours surface defects were still present. The lower cobalt content grades, however, required approximately 18 hours before stresses introduced by grinding and eroding are removed. The lower cobalt content grades are harder than the high cobalt content grades. It would therefore be expected that more time would be required for the removal of a given amount of material from the surface of a lower cobalt content grade.

The fracture toughness values obtained by the Palmqvist method were then plotted against cobalt content, as illustrated in Figure 6.5. Fracture toughness was found to increase with increasing binder content. This is to be expected as the cobalt binder toughness value is much greater than that of tungsten carbide.

An increase in grain size resulted in an increase in toughness. Chermant and Osterstock (1979) observed a similar result. This was explained in terms of the larger grains being more susceptible to transgranular fracture. In the case of WC-Co alloys transgranular fracture is a higher energy fracture process than intergranular fracture.

As previously observed (Section 2.4.3) fracture toughness is generally influenced by mean free path. The variation of fracture toughness with mean free path for experimental values along with a selection of published data is plotted in Figure 6.6.

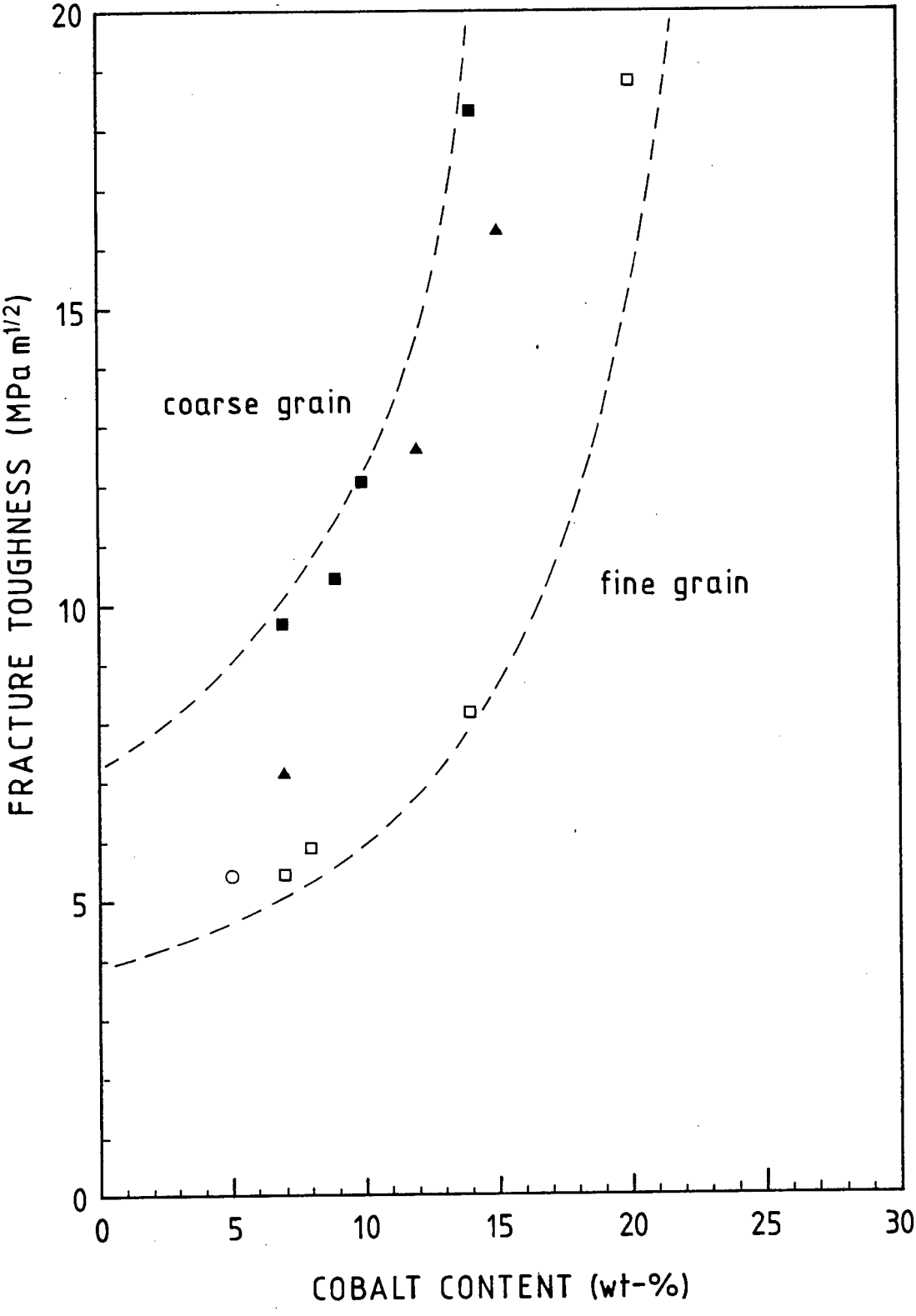


FIGURE 6.5 : The effect of the binder content on fracture toughness. The symbols ○ = A series and □ = B series, both of which have a 1,8 μm grain size. The symbols ■ and ▲ refer to the 2,8 μm grain sized G and F series respectively

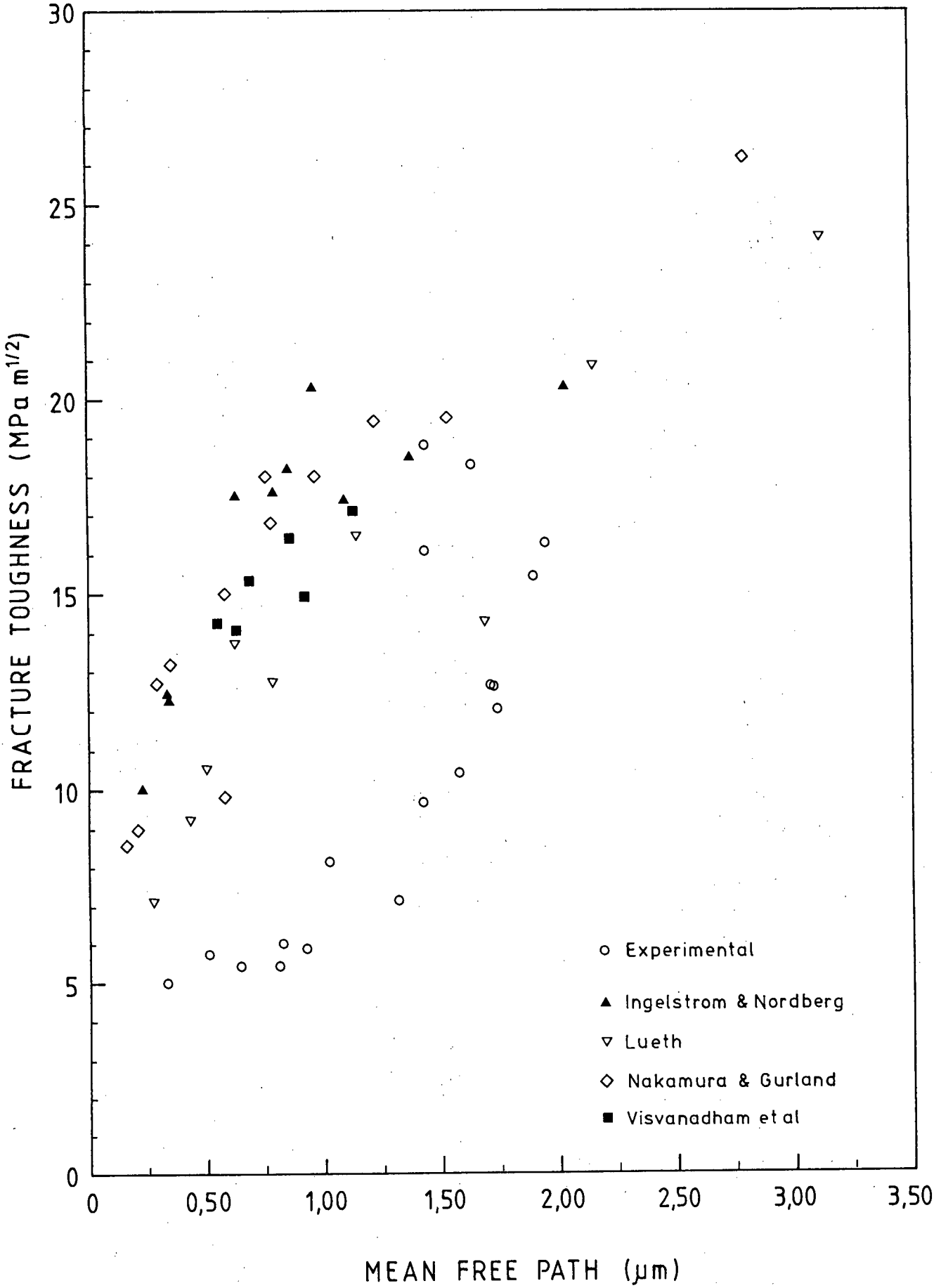


FIGURE 6.6 : Fracture toughness as a function of mean free path for various published results and experimental values

The published mean free path values, were quoted, did not take contiguity into account. Fry (1982), however, calculated the true mean free path by first extrapolating the contiguity values from the Lee and Gurland (1978) graphs, relating contiguity to volume fraction of the binder phase. These mean free path values were used to plot fracture toughness. As can be seen from Figure 6.6, although the experimentally determined fracture toughness values where lower, they did appear to follow a similar trend to the published results. The lower experimental values may be due to the technique used to determine the fracture toughness values. The published values were determined by a variety of techniques (see Table 2.1), none of which employed the Palmqvist method. As mentioned previously (Section 2.4.3.1), this method is only accepted as a comparative method and not as a quantitative method.

# CHAPTER 7

## THE EROSION OF WC-Co ALLOYS

Due to the small size of the sample (14 mm), the gas-solid particle erosive stream diameter was larger than the specimen surface. This resulted in not all the erodent striking the sample. The area eroded was angle dependent; for large angles the area of particle stream sampled is smaller. Consequently no comparison between erosion rates could be made for tests conducted at different angles of incidence, without the erosion rate data being standardized.

### 7.1 STANDARIZATION OF EROSION RATE VALUES

Glass slides, having a surface area larger than the erosive stream diameter, were employed to determine the spread of erosion. Both optical microscopy, where the impact densities were determined at given distances from the centre of erosion, and Talysurf surface profilometer techniques showed that the erosive distribution gave a reasonable fit to a Gaussian relationships as illustrated in Figure 7.1.

The general expression for a Gaussian distribution is given by:

$$f(x) = \frac{1}{\sqrt{2\pi\sigma^2}} \exp - \frac{1}{2}\left(\frac{x - \mu}{\sigma}\right)^2 \qquad (7.1)$$

where $\mu$ is the mean and $\sigma$ is the standard deviations.

The parameters in the equation varied according to the erodent size as shown in Table 7.1.

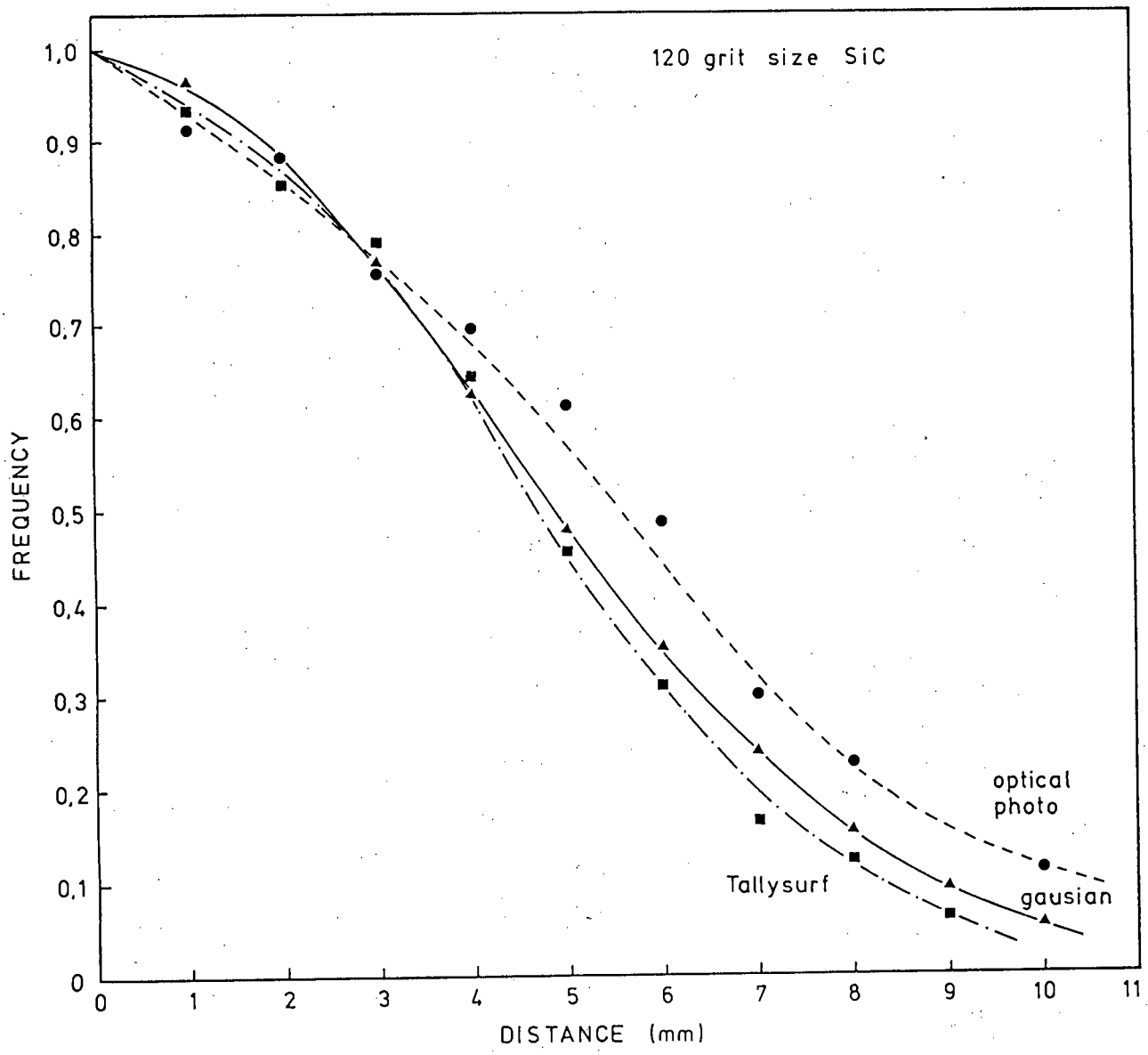


FIGURE 7.1 : Comparison between optical and Talysurf measurements and a Gaussian curve for the distribution of impacts using 100 $\mu$m SiC erodent

TABLE 7.1 : The Gaussian curve parameters for the three different erodent sizes

| SiC ERODENT SIZE ($\mu$m) | $\mu$ | $\sigma$ |
|---|---|---|
| 100 | 0 | 4,15 |
| 50 | 0 | 4,43 |
| 30 | 0 | 4,98 |

The amount of erosion occurring is governed by the portion of the Gaussian distribution which is sampled by the specimen. This active portion may be determined from the volume under the relevant region of the Gaussian distribution. The erosion amount is angle dependent: a decrease in the incident angle, caused by an increase in the tilt angle, results in a decrease in the apparent erosion rate as illustrated in Figure 7.2.

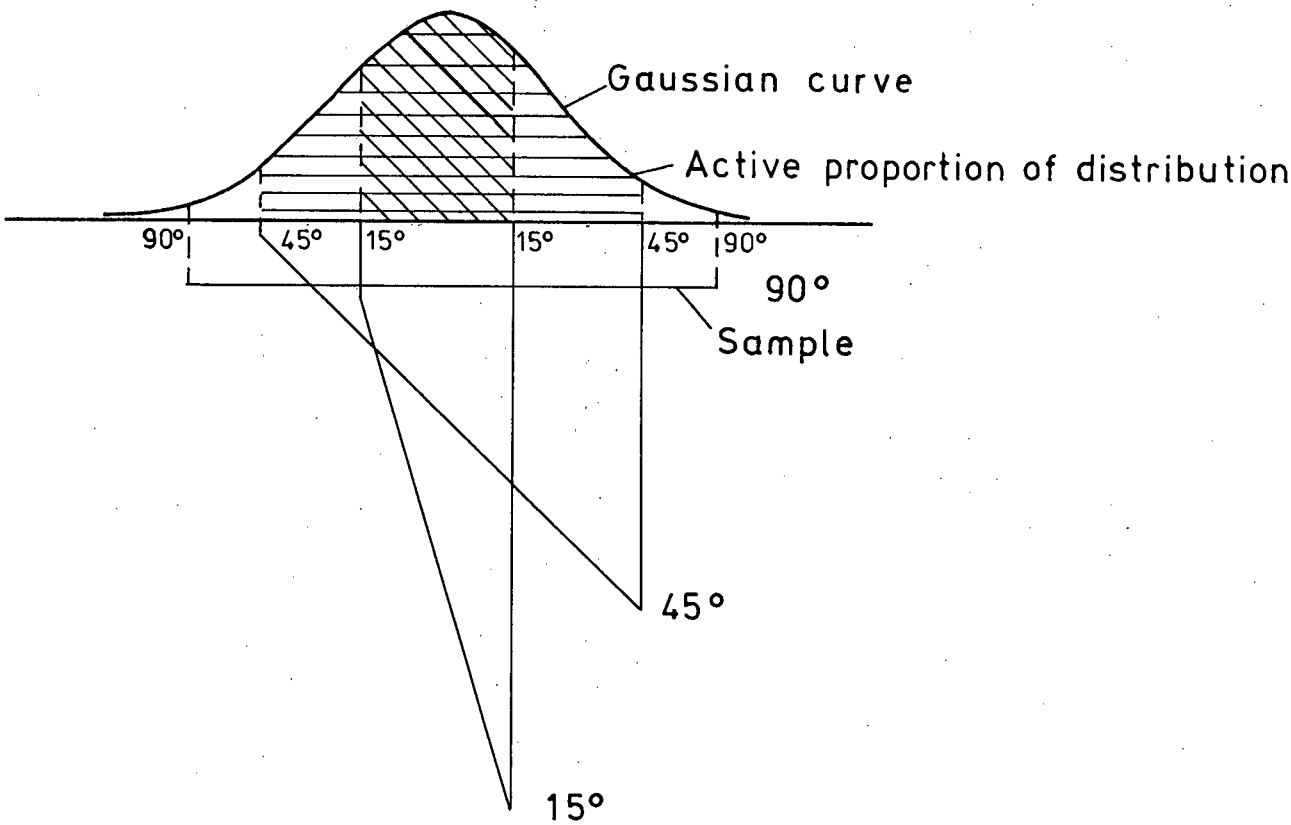


FIGURE 7.2 : A schematic representation of the decrease of erosion with decreasing angle of incidence

The calculation is complicated by the fact that this fore-shortening occurs only in the direction perpendicular to the axis of tilt and not along the tilt axis itself. Therefore a computer programme was written to calculate the area under the curve for the different angles, and hence the normalised erosion rate (see Appendix C for a listing of the computer programme).

Tests were then conducted to verify these calculations. At every angle two tests were performed on glass slides. For the first test a thin foil cover containing a hole the size of the WC-Co alloy samples, was placed over the slide. For the second test no cover was used. The percentage difference in erosion for the two tests was then determined. This difference was then compared with the values calculated theoretically. Figure 7.3 shows that a good agreement existed between the two curves. It was therefore felt that this method for standardising the erosion rate was acceptable. No experimental data was obtained for low angles as the foil cover was found to act as a shield to the incoming particles. The difference between the experimental and theoretical data at 30° may be explained by the occurrance of partial shielding due to the foil cover, whilst at 90° the difference is considered to be due to the incomplete collection of erodent on the glass slick due to tailing. A good functional relationship, however, is still considered to exist.

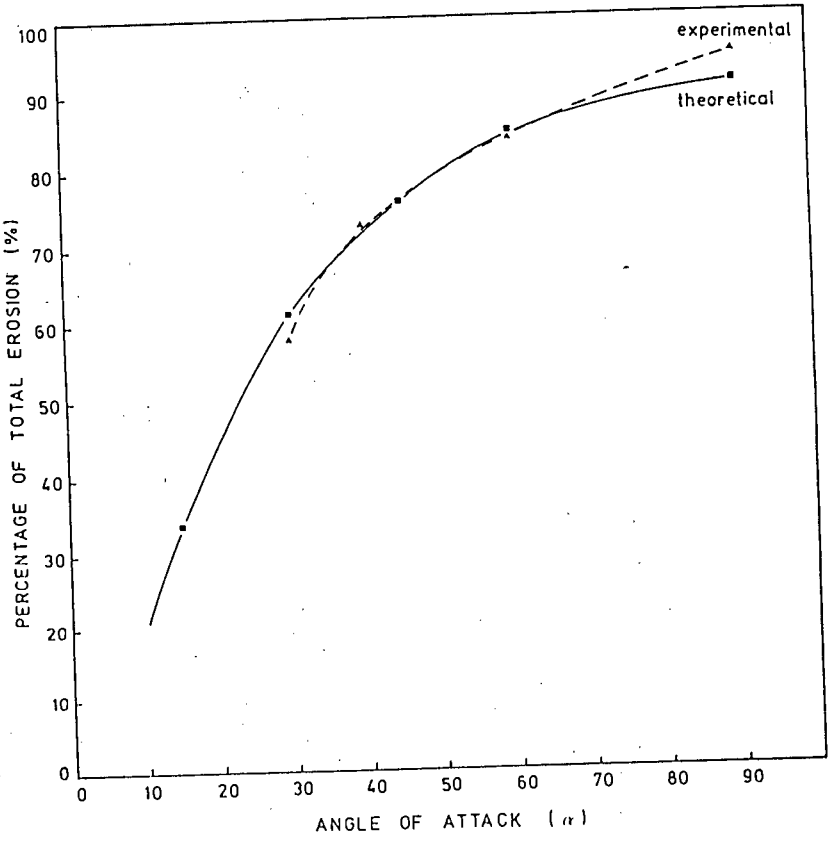


FIGURE 7.3 : Comparison between theoretical and experimental calculations and of percentage difference in erosion for samples greater and smaller than the erosive stream diameter

## 7.2 EFFECT OF TARGET MATERIAL PROPERTIES ON EROSION

The erosion results for all the tests were corrected using the above standardization method. (The results of which are given in Appendix D). Ranking the specific materials according to these results revealed very little information, as the order changed with changing test conditions. It did, however, show that for all three erodent sizes, material I1 (30 wt-%, 2,17 μm) was the most erosion resistant grade at high angles, namely 60° and 90° attack angles. For all the other tests, the low cobalt content alloys were found to be the more erosion resistant alloys.

### 7.2.1 Microstructural Effect

Due to the large variation in the microstructure of the WC-Co alloys, only the grades containing a nominal grain size of 1.8 μm and 2.8 μm were considered when studying the effect of mirostructure. Figures 7.4, 7.5 and 7.6 illustrate the dependence of erosion rate on binder content and grain size for the 100 μm, 50 μm and 30 μm SiC erodent respectively.

#### 7.2.1.1 Binder Content

For the low angle tests, namely 15° and 30°, the observed trend was in agreement with the more common finding of erosion rate increasing with increasing binder content (see Section 4.1.1). At higher angles, the effect of binder content on erosion rate was found to be similar to that reported by Ball and Paterson (1985). It should be noted that the work carried out by Ball and Paterson (1985) and the present work were performed under the same test conditions. Conrad et al (1982) only studied WC-Co alloys having a binder content of or less than 11.3 wt-%. Consequently, there is agreement between the results of Conrad et al (1982) and the present work, if only low cobalt content alloys are considered. Uuēmyis et al (1974) performed erosion tests at higher velocities, and with much larger impacting particles. Both these factors may have contributed to the different relationship being observed.

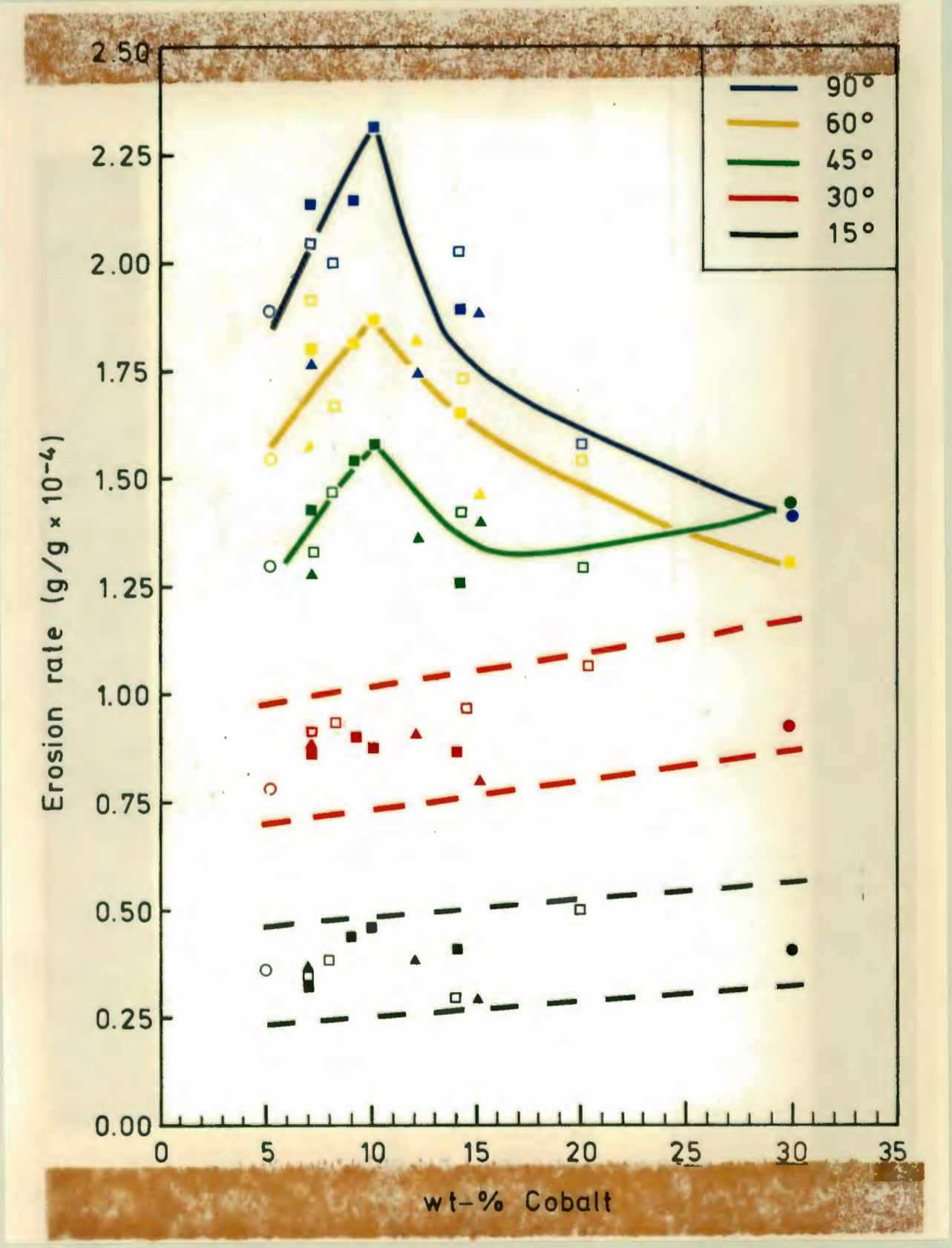


FIGURE 7.4 : The effect of binder content on erosion rate for the 1,8 µm (open symbols) and the 2,8 µm (closed symbols) grain sized samples using 100 µm SiC erodent. The symbols ○ , □ , ▲ , ■ and ● refer to A, B, F, G and I series respectively

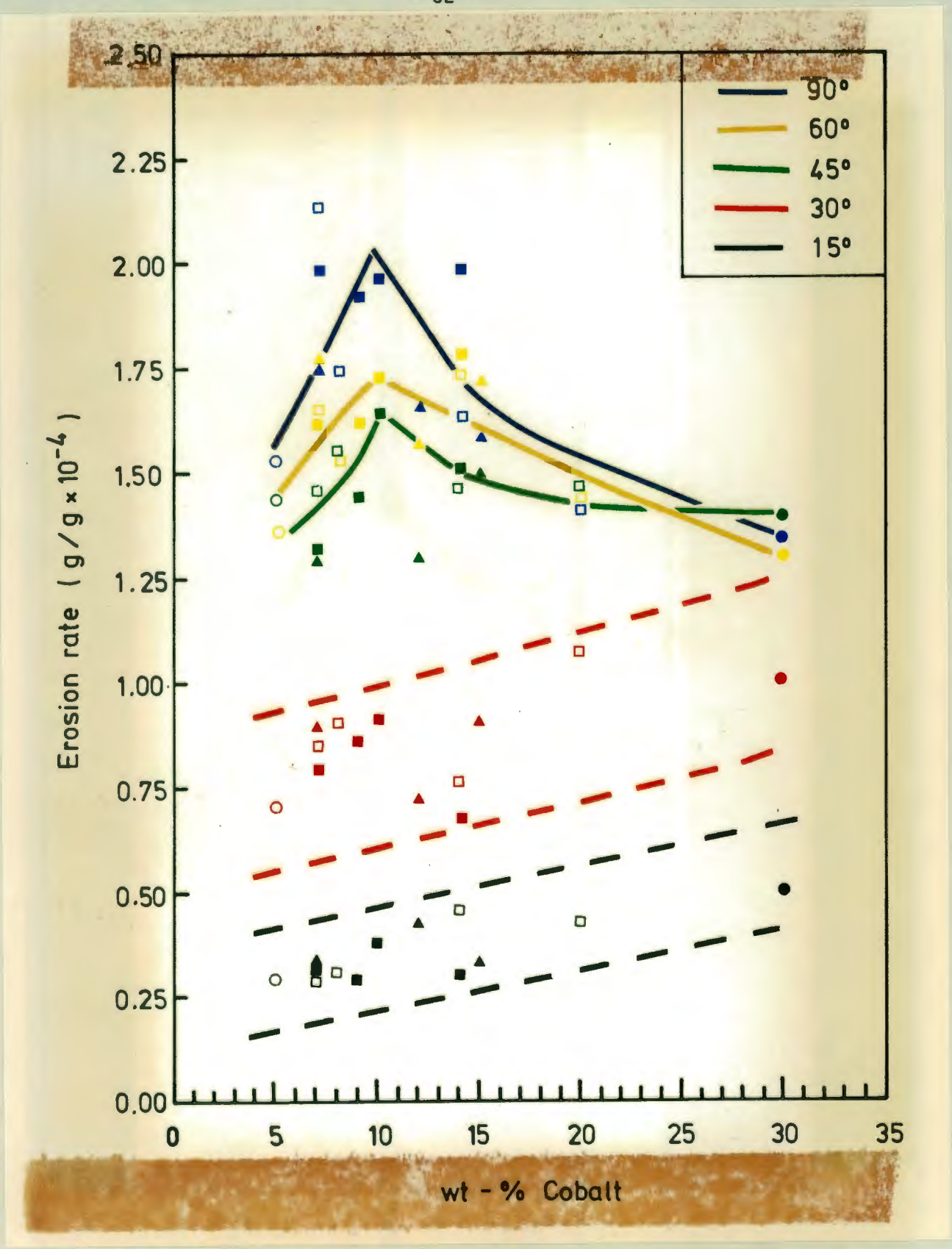


FIGURE 7.5 : The effect of binder content on erosion rate for the 1,8 μm (open symbols) and the 2,8 μm (closed symbols) grain sized samples using 50 μm SiC erodent. The symbols ○, □, ■, ▲ and ● refer to the A, B, G, F and I grades respectively

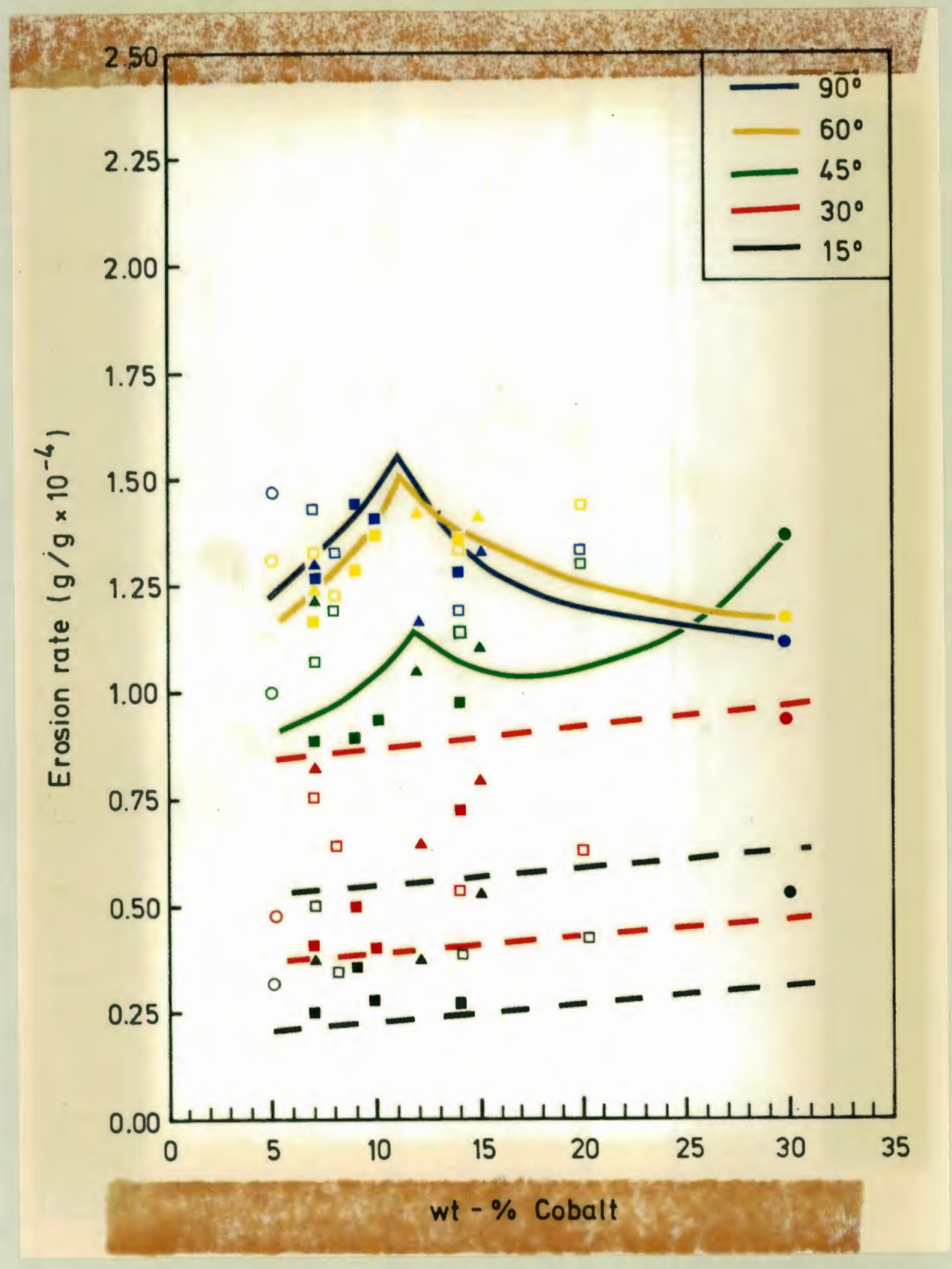


FIGURE 7.6 : The effect of binder content on erosion rate for the 1,8 µm (open symbols) and the 2,8 µm (closed symbols) grain sized samples using 30 µm SiC erodent. The symbols ○, □, ■, ▲ and ● refer to the A, B, G, F and I series respectively

7.2.1.2 Grain Size

As illustrated by Figures 7.4, 7.5 and 7.6, the low angle tests showed no grain size effect. For the larger angle tests, above 30°, the smaller grain sized alloys, however, eroded at a higher rate. This was more evident for erosion tests conducted with 100 μm SiC erodent. As only two grain sizes were considered, it is not reasonable to draw any quantitative conclusions on the grain size effect.

The results for the higher angles are, however, in agreement with Ball and Paterson (1985) and Conrad et al (1982). As mentioned previously (Section 4.1.1), the latter noted that erosion rate passed through a maximum at a grain size of 1.5 μm.

7.2.1.3 Mean Free Path

The effect of mean free path on erosion rate for the 100 μm particle size erodent is illustrated in Figure 7.7. Similar, but less well defined trends, due to the smaller spread in erosion, were observed for the smaller impacting particles.

No simple relationship was observed for the effect of mean free path on erosion rate. For an angle of incidence greater than 30°, both grain sizes pass through a maximum, but not at a constant mean free path.

7.2.1.4 Contiguity

Figure 7.8 shows the dependence of erosion rate on contiguity for the 100 μm SiC erodent. As for mean free path, similar trends were observed for the other two erodent sizes. For the low incident angles, namely 15° and 30°, contiguity had no effect on the erosion rate.

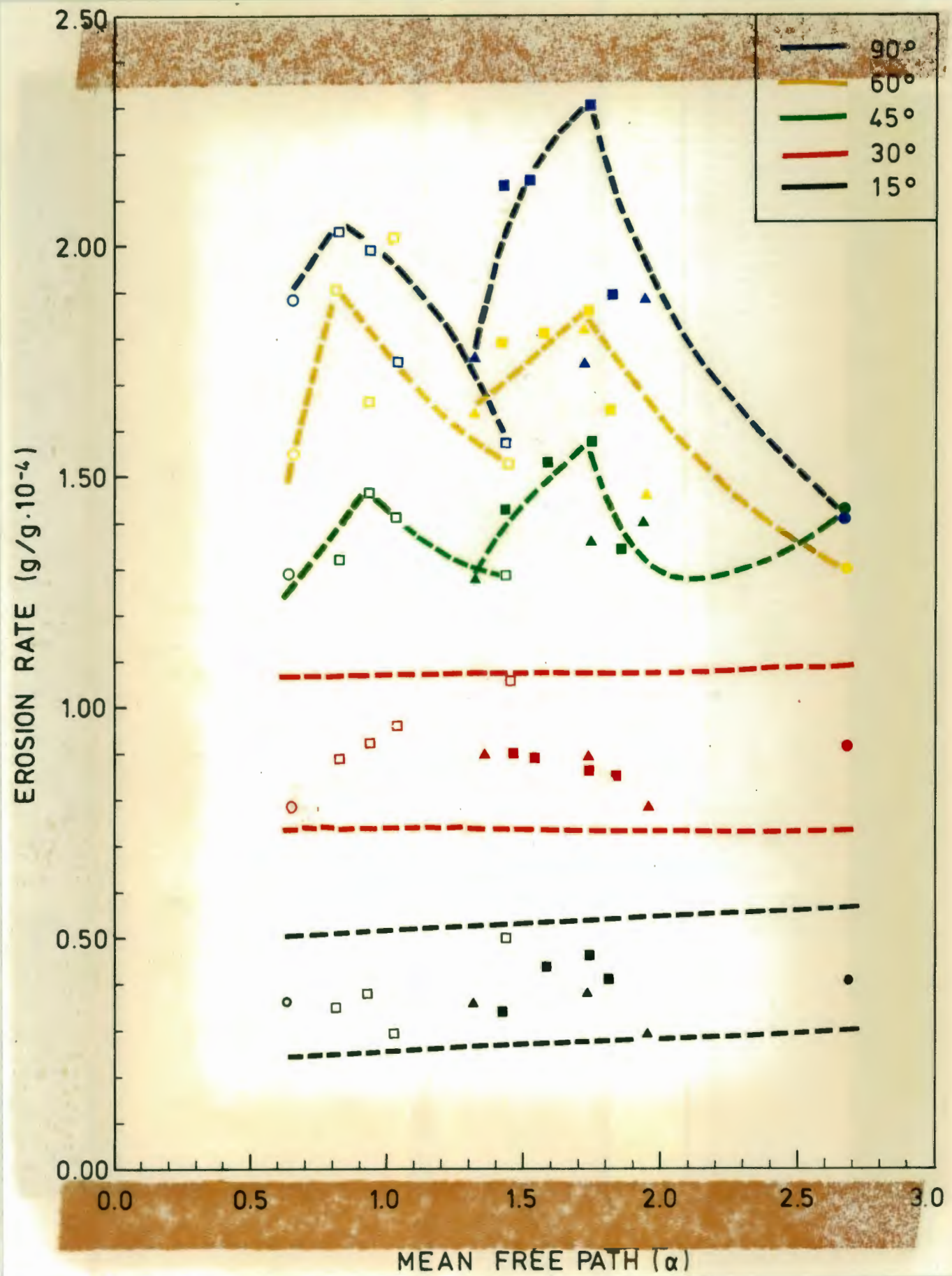


FIGURE 7.7 : Erosion rate versus mean free path for the 1,8 μm (open symbols) and the 2,8 μm (closed symbols) grain sized samples using 100 μm SiC erodent. The symbols ○, □, ■, ▲ and ● refer to the A, B, G, F and I series respectively

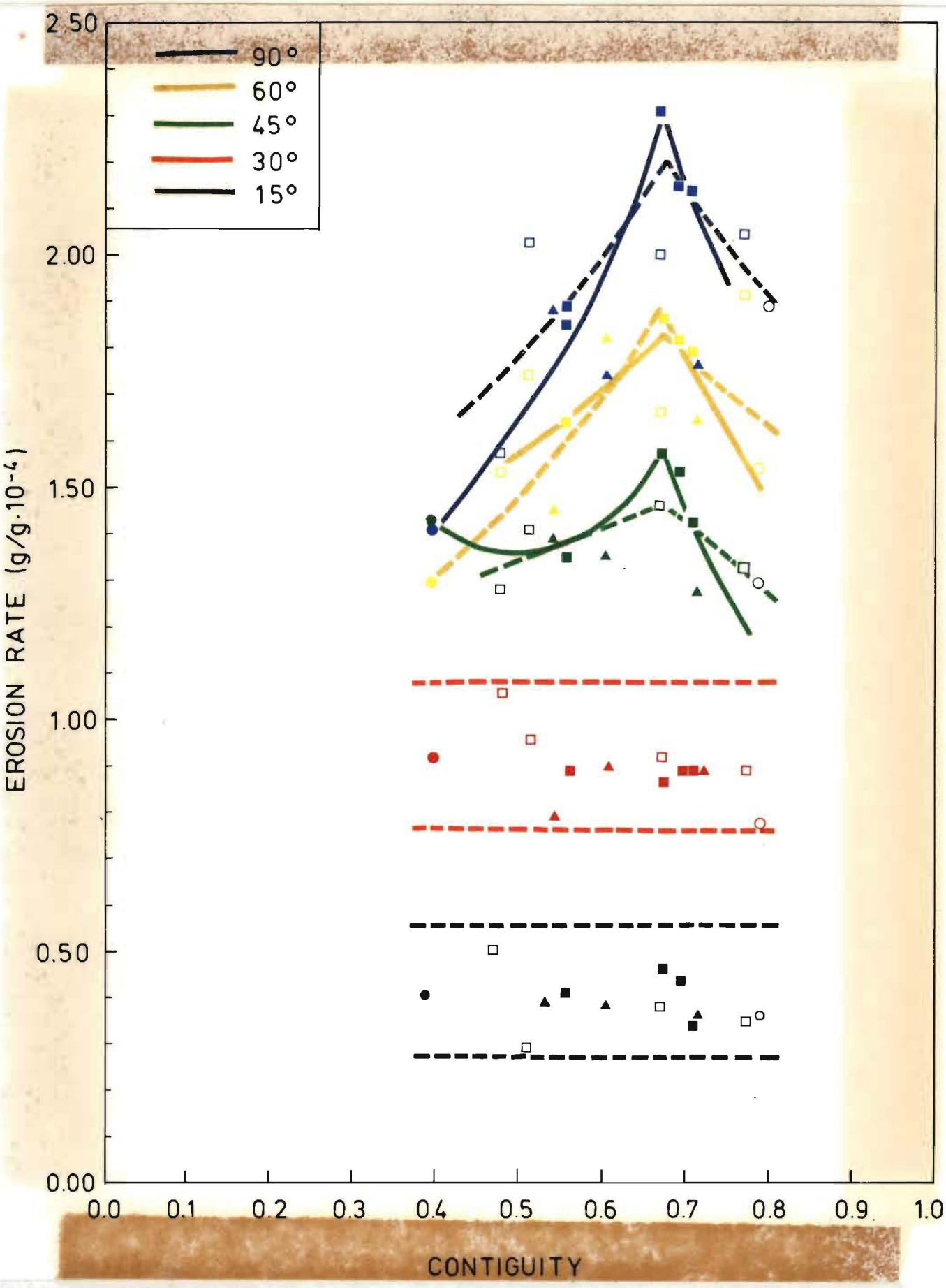


FIGURE 7.8 : Erosion rate as a function of contiguity for the 1,8 μm (open symbols) and the 2,8 μm (closed symbols) grain sized samples using 100 μm SiC erodent. The symbols ○, □, ■, ▲ and ● refer to the A, B, G, F and I series respectively

Above an incident angle of 30°, however, the erosion rate appears to pass through a maximum at a contiguity value of 0,65 for both grain sizes. This contiguity value corresponds to a cobalt binder content of approximately 10 wt-%. As previously mentioned (Section 2.2), many researchers assume a change in structure to occur at this binder level. Below a binder level of 10 wt-%, a continuous 'skeleton' structure is present. Above this value the continuous structure is believed to begin to break down and the WC grains become 'embedded' in the cobalt matrix. In slurry erosion tests Shetty et al (1984) noted this structural change resulted in a change in the erosion mechanism. The maximum at 10 wt-% cobalt, for high angles of incidence, is therefore most probably due to a change in the material removal mechanism, as will be discussed further in Section 8.2.

### 7.2.2 Effect of Mechanical Properties

#### 7.2.2.1 Hardness

The general trend observed for all erosion tests was one of increasing erosion rate with decreasing hardness. For the glancing angles of 15° and 30°, the microstructural effect disappeared, causing the dependence upon hardness to be more marked. At these low angles, the dependence of erosion rate on hardness appeared to be broadly linear as illustrated in Figure 7.9.

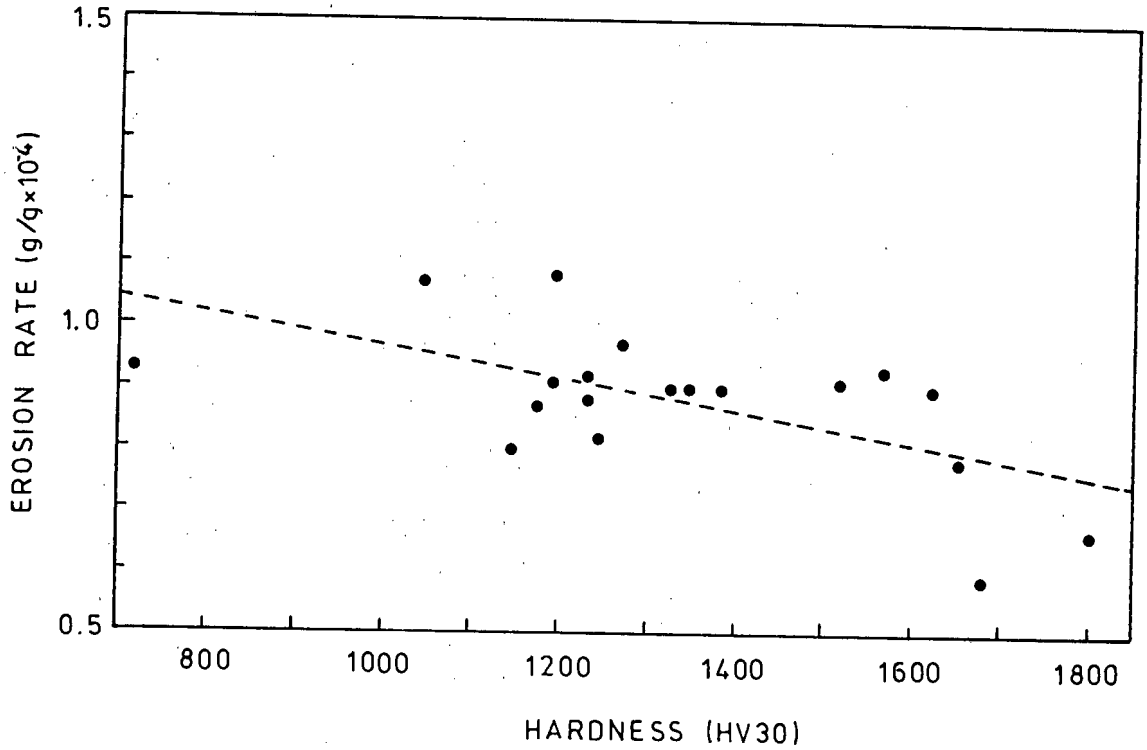


FIGURE 7.9 : The dependence of erosion rate on hardness for an angle of incidence of 30° using 100 μm SiC erodent

7.2.2.2 Fracture Toughness

Erosion rate showed no dependence on fracture toughness. The fracture toughness values measured were macroscopic values. The Palmqvist cracks were found to extend over a distance much greater than a grain whilst the cracks produced by an impacting particle were generally confined to a single grain. This implies that a microscopic measure of fracture toughness would be the appropriate value affecting erosion rate. No such technique is yet available for the determination of this microscopic value.

## 7.3 EFFECT OF PARTICLE PROPERTIES ON EROSION

The only property of the impacting particle studied in this work was size. A limit in erosion rate occurred with an increase in particle size, as is the case with ductile materials. This is illustrated in Figure 7.10.

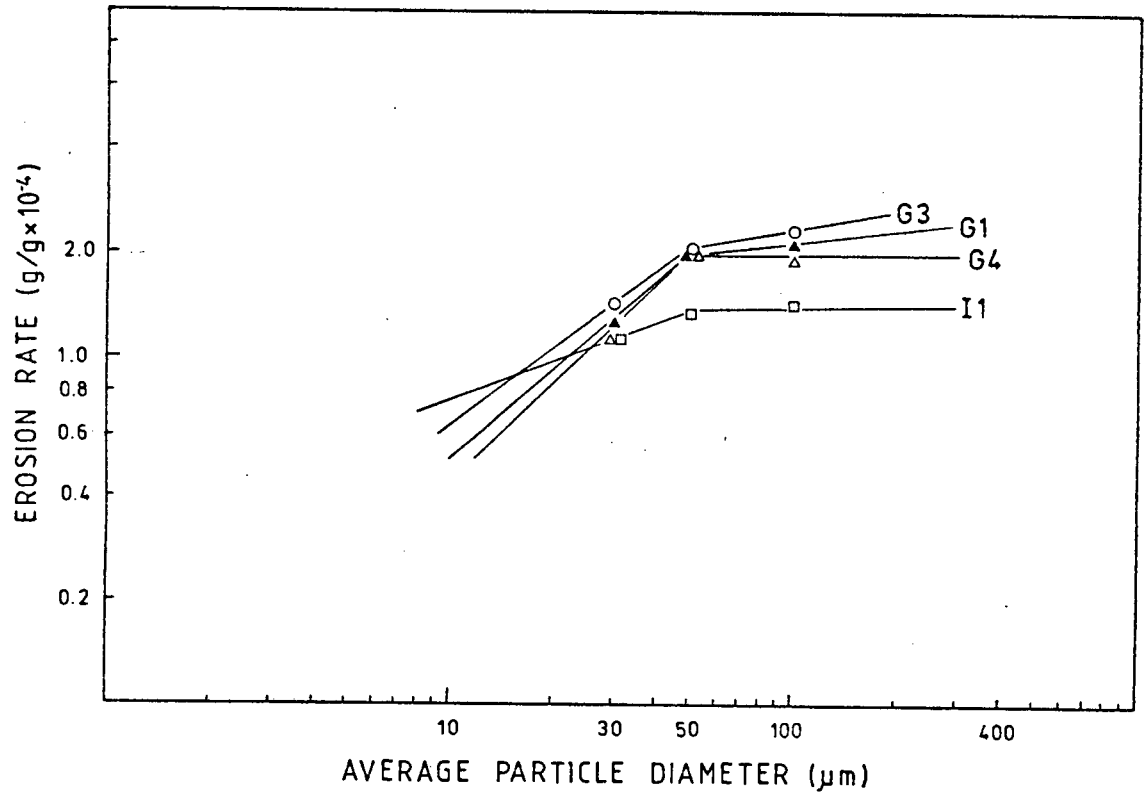


FIGURE 7.10 : Erosion rate versus average particle size. The angle of incidence is 90°. The symbol □ refers to I1 (30 wt-%; 2,17 µm), △ to G4 (14 wt-%; 2,58 µm), ○ to G3 (10 wt-%; 2,82 µm) and ▲ to G1 (7 wt-%; 2,8 µm)

## 7.4 THE EFFECT OF IMPACTING PARAMETERS ON EROSION

The influence of the angle of impact on erosion rate was the only parameter studied. Previous research conducted by Conrad et al (1982) has found maximum erosion to occur at 90° for all cobalt contents investigated. Thus suggesting the WC-Co alloys erode in a brittle fashion.

The effect of angle on the erosion of the WC-Co alloys was investigated for all three erodents. Five angles, 15° 30°, 45°, 60° amd 90° were employed. The particle velocity was kept constant at 40 $ms^{-1}$. In Figure 7.11 the erosion rates are plotted as a function of angle for three grades eroded with the 100 m SiC particle type.

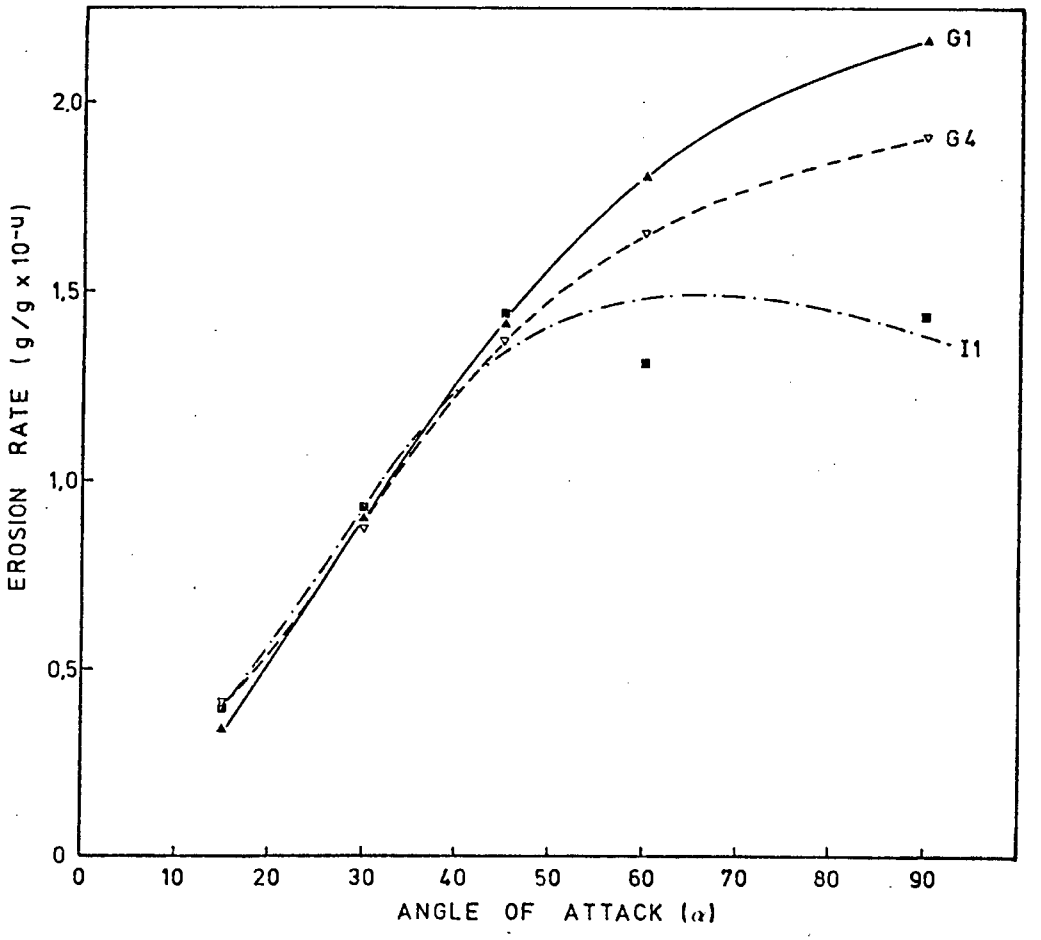


FIGURE 7.11 : The effect of angle of incidence on the erosion rate for I1 (30 wt-%, 2.17 μm), G1 ( 8 wt-%, 2.80 μm) and G4 (14 wt-%, 2.58 μm)

The response of the low cobalt alloys was typical of the behaviour of brittle material with maximum material removal occurring at 90°, as found by Conrad et al (1982), for similar cobalt content alloys. For the higher cobalt content alloys, in particular I1 (30 wt-%, 2.17 $\mu$m) and B4 (20 wt-%, 1.76 $\mu$m), maximum erosion occurred in the region of 50°. This is indicative of materials which exhibit a combination of brittle and ductile erosion.

A brief summary of the points which emerged from this study is given below:

i) Ranking of the WC-Co alloys by erosion revealed material I1 (30 wt-%, 2.17 $\mu$m) to be the most erosion resistant grade at high angles of incidence, namely 60° and 90°. For angles less than 60°, the lowest cobalt content alloys were the most erosion resistant grades.

ii) All microstructural parameters studied were found to influence erosion, but mean free path showed no simple relationship.

iii) Hardness was found to inversely effect erosion. For high angles, however, this influence was masked by other microstructurally based effects.

iv) Macroscopic fracture toughness values were found to be irrelevant. A microscopic measure of fracture toughness would be more useful.

v) A limit in erosion rate occurred with increasing particle size, which is associated with ductile erosion.

vi) The variation of erosion rate with the angle of impact indicated that the high cobalt content grades erode by a combination of brittle and ductile modes.

vii) The above points all suggest that a change in the erosion mechanism occurs in the region of 10 wt-% cobalt.

# CHAPTER 8

## THE MECHANISM OF EROSION OF WC-Co ALLOYS

In Chapter 7 it is clearly shown that the erosion rate of WC-Co alloys is influenced by microstructural parameters. Prominant features have included a local maximum in erosion rate in the region of 10 wt-% cobalt. For the grain sizes considered, this binder level corresponds to a contiguity of approximately 0,65. Above a binder level of 20 wt-% cobalt, ductile erosion is more apparent, as indicated by the angle dependence of the high cobalt alloys on erosion rate. The results of scanning electron microscopy work will now be presented, and used to elucidate mechanisms for observed effects, and hence formulate a model.

### 8.1 MODES OF MATERIAL REMOVAL

#### 8.1.1 Tungsten Carbide Grains

Scanning electron micrographs of the eroded surface of the WC-Co alloy revealed little useful information. The presence of cobalt smearing resulted in the masking of WC grains. Thus it was impossible to detect the manner in which the WC grains were eroded. A technique of leaching away the cobalt was consequently employed. This involved the boiling of the alloy in concentrated HCl for half an hour, the results of which are shown in Figure 8.1 and 8.2.

Figure 8.1 illustrates the leached, uneroded surface alongside the leached, eroded surface of the three grades eroded at an impact angle of 90° by 30 g of 100 $\mu$m SiC erodent.

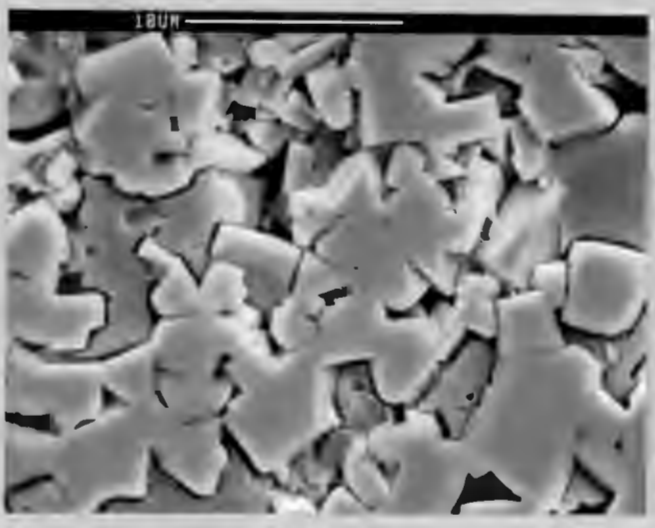

(a) : Uneroded I1 (30 wt-%, 2.17 μm)

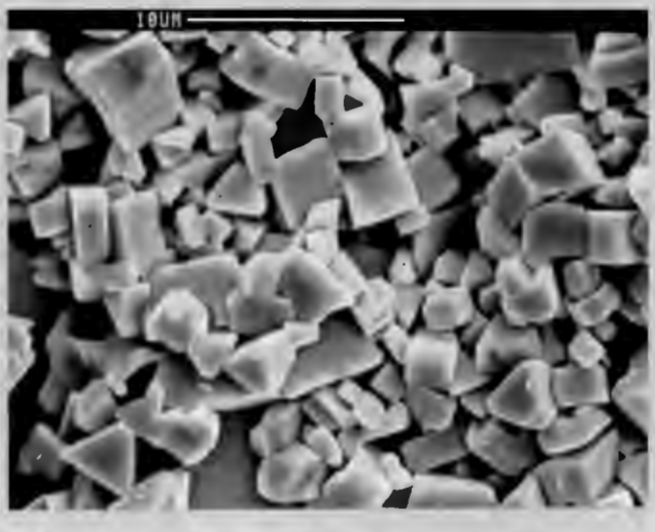

(b) : Eroded I1 (30 wt-%, 2.17 μm)

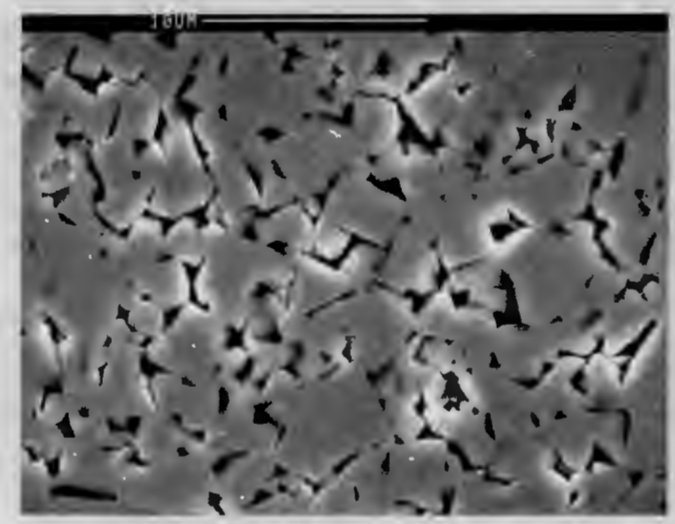

(c) : Uneroded G3 (10 wt-%, 2.82 μm)

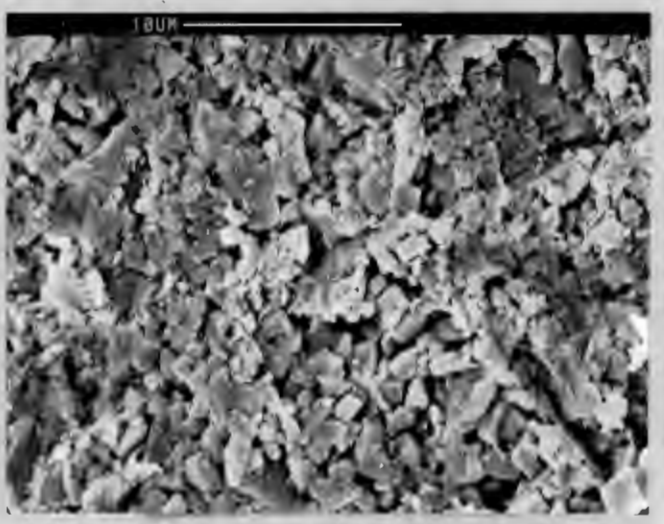

(d) : Eroded G3 (10 wt-%, 2.82 μm)

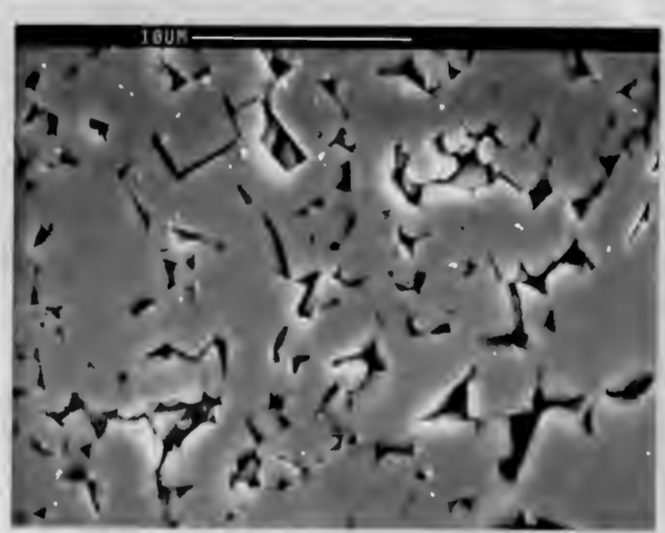

(e) : Uneroded G1 (7 wt-%, 2.80 μm)

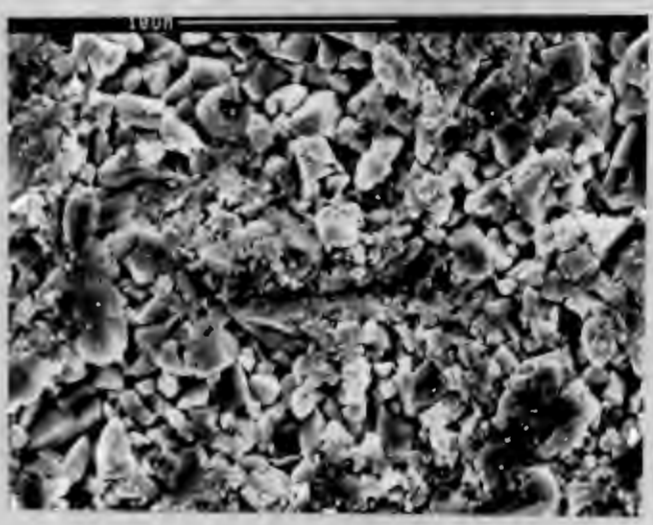

(f) : Eroded G1 (7 wt-%, 2.82 μm)

FIGURE 8.1 : Micrographs of HCl leached WC-Co alloys. The steady state eroded samples were eroded by 30 g of 100 μm SiC erodent at an incident angle of 90°

Little or no fracture is apparent for the high cobalt content I1 (30 wt-%, 2.17 $\mu$m), thus indicating that a ductile mode of removal predominates.

The occurrence of grains undergoing brittle fracture increases with decreasing cobalt content. This is indicative of the increasing importance of brittle fracture as a mode of material removal. For the low cobalt content G1 (7 wt-%, 2.80 $\mu$m), all the carbide grains appear to be fractured, suggesting that brittle erosion is the predominant mode of erosion at low cobalt contents.

The same three grades were eroded under the same conditions at an angle of impact of 30°. The micrographs of these leached, eroded surfaces are given in Figure 8.2. Due to the similarity of the micrographs, binder content appears to have no influence on the mechanism of material removal.

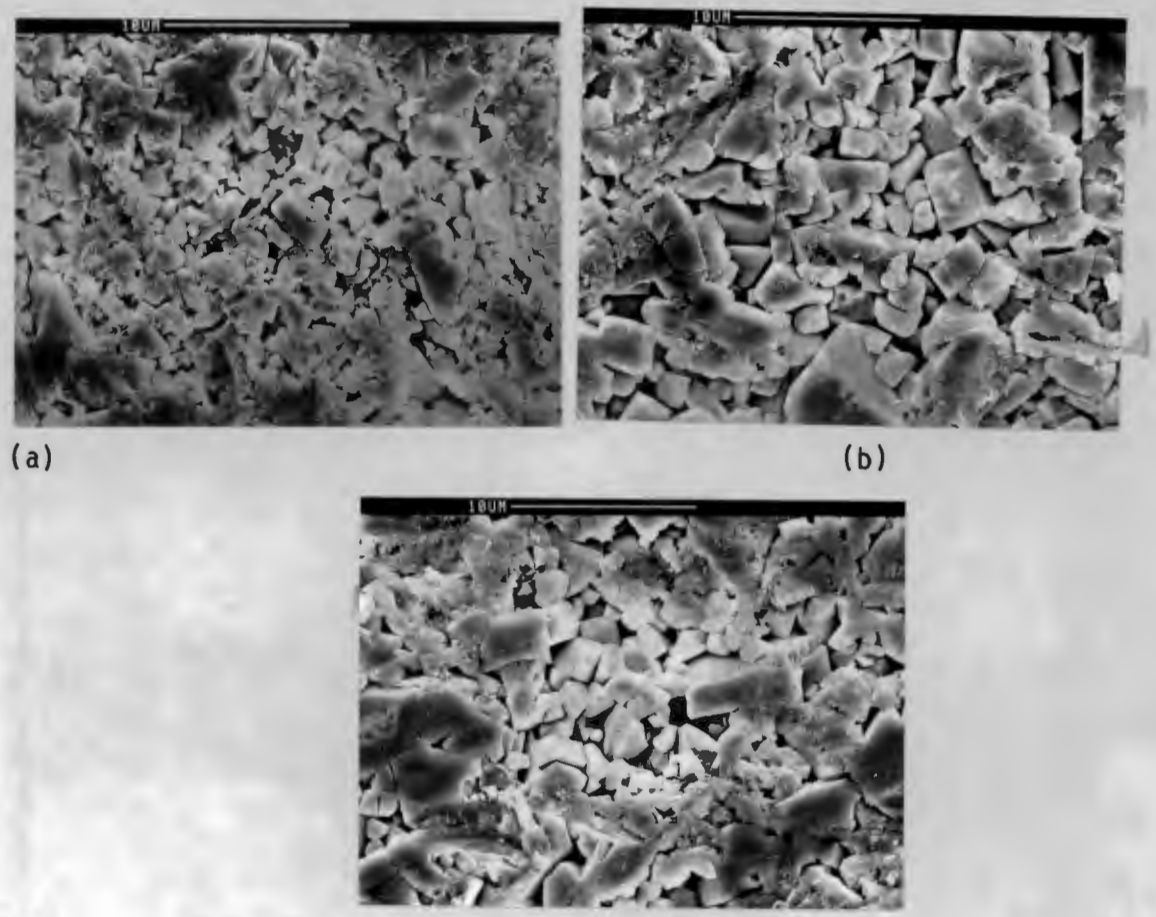


(a) (b)

(c)

FIGURE 8.2 : Scanning electron micrographs of (a) I1 (Wt-%, 2.17 $\mu$m) (b) G3 (10 wt-%, 2.82 $\mu$m) and (c) G1 (7 wt-%, 2.80 $\mu$m). The erodent used is 100 $\mu$m SiC and the angle of incidence is 30°

When compared to the micrographs in Figure 8.1, far less cobalt leaching is apparant in the Figure 8.2 micrographs.

### 8.1.2 Cobalt Binder

To determine the mechanisms by which cobalt is removed, low concentration impact tests were performed. A nominal amount of 0.1 g of erodent was used, making it possible to observe single impacts. A common feature of these impacts was the evidence of cobalt extrusion as illustrated in Figure 8.3.

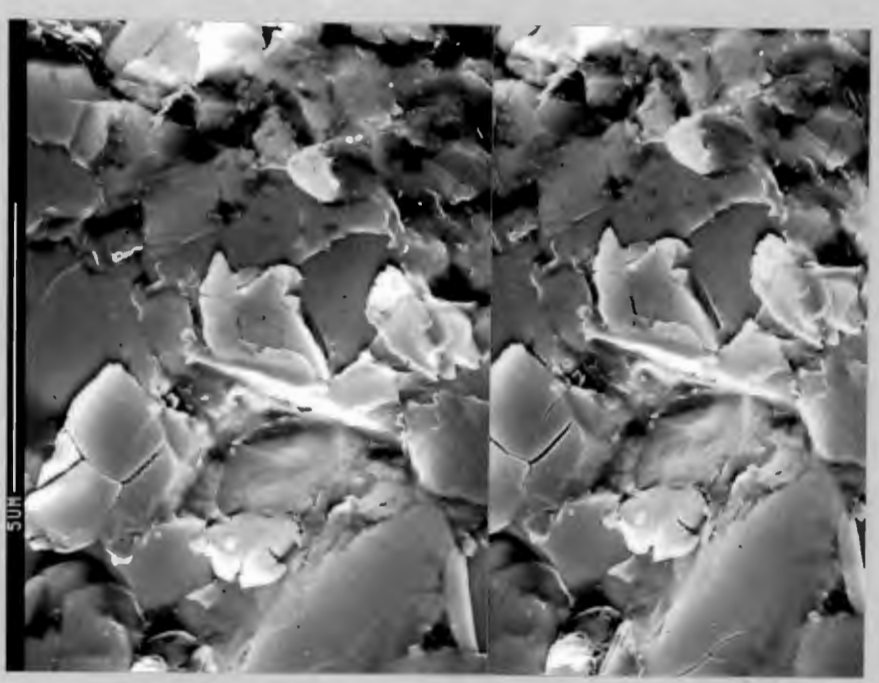

FIGURE 8.3 : A stereo micrograph pair of an impact region produced by 50 $\mu$m SiC erodent impacting at an impact angle of 90° on a G3 (10 wt-%, 2.82 $\mu$m) specimen. Note the uplifting of the WC grains as well as the extruded cobalt from the binder region, which is associated with the vertical displacement of the WC grains

Stereo micrograph pairs were taken of individual impact sites, in which evidence of cobalt extrusion could be clearly observed. The loading force due to the incoming particle is considered to have resulted in the movement of the carbide grains. The displacement of the WC grains occurs in both a vertical and a horizontal direction. The vertical component of displacement causes the cobalt to be extruded from the binder region. Similar observations have been reported by Larsen-Basse (1985) when studying the sliding wear of WC-Co alloys.

## 8.2 MODEL OF THE EROSION MECHANISM

Figure 8.3 is a schematic summary of the model used to describe the mechanism of erosion for WC-Co alloys eroded at, or above, a 45° angle of incidence.

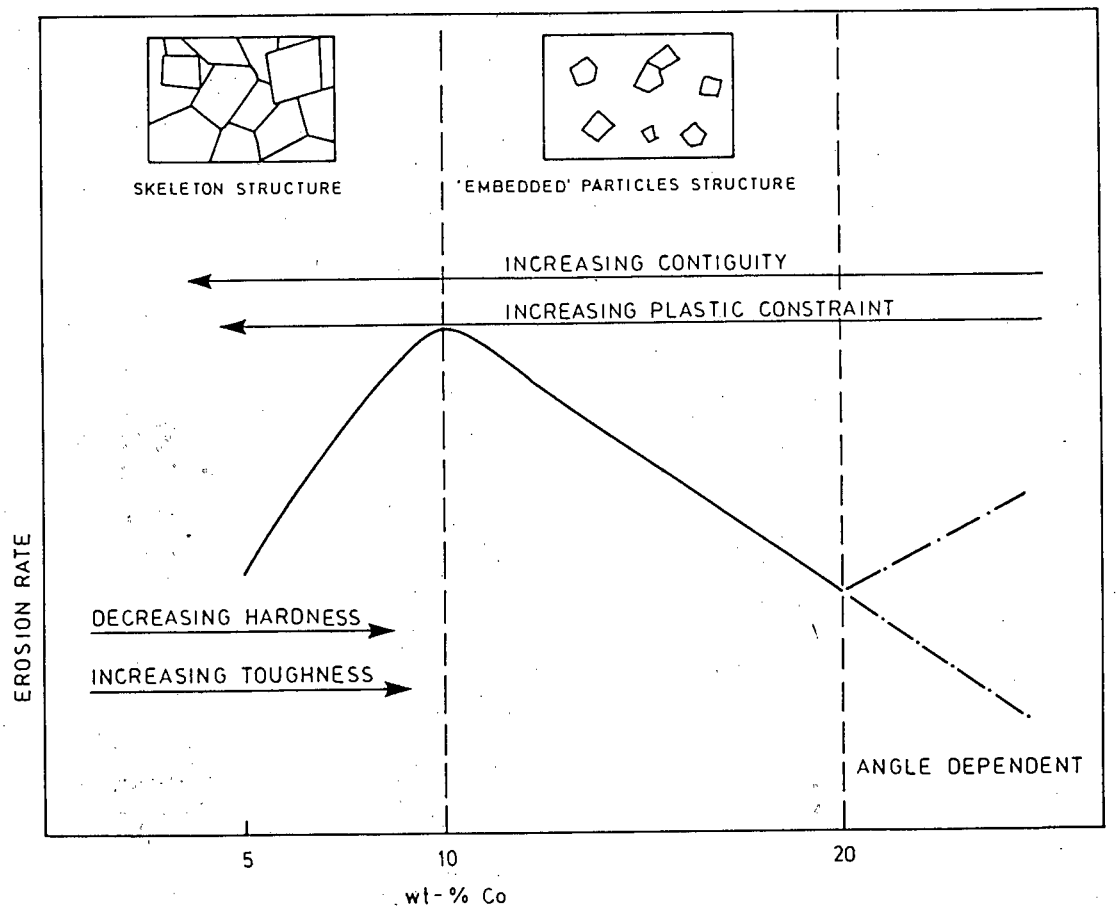


FIGURE 8.3 : A schematic summary of erosion processes in WC-Co alloy. The parameters believed to affect erosion rate are indicated

The model can be divided into three sections according to mechanism of material removal. This is dependent on the binder level. These are:

i) Alloys containing less than 10 wt-% cobalt
ii) Alloys containing between 10 and 20 wt-% cobalt
iii) Alloys containing more than 20 wt-% cobalt

### 8.2.1 WC-Co Alloys Containing less than 10 wt-% Cobalt

For low cobalt content alloys, a reduction in binder content results in the development of a more rigid 'skeleton' structure.

Proportionally more grains overlap, thus causing the event illustrated in Figure 8.4(a) to predominate.

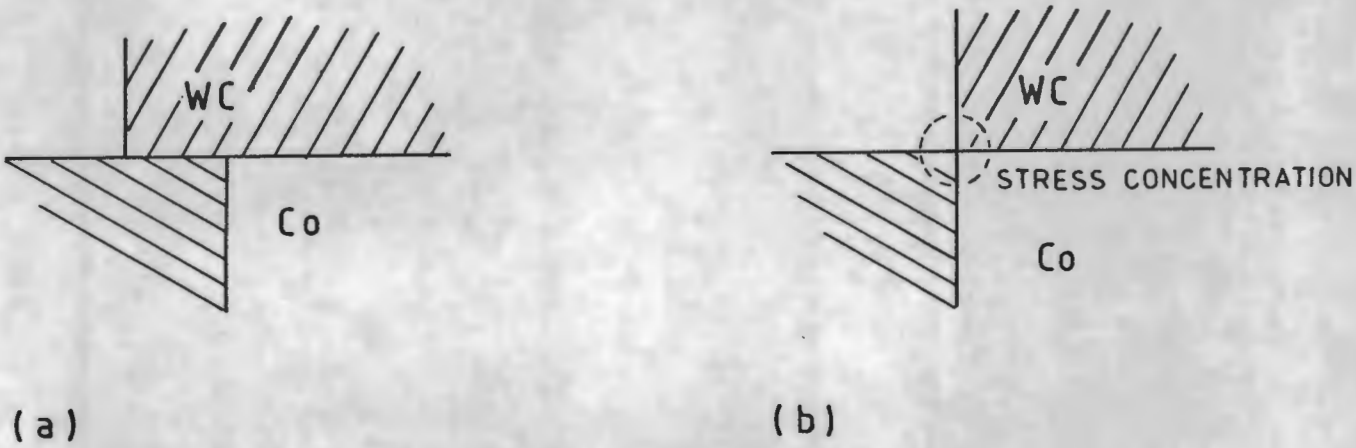


FIGURE 8.4 : Schematic representation of (a) grains overlapping and (b) grains touching, with the region where stress build up will occur when an impacting particle strikes

When an impacting particle strikes the surface, load is transferred across the rigid 'skeleton' structure, resulting in little grain fracture. The formation of the impact site is due mainly to the extrusion of cobalt and the displacement of the WC grains, as illustrated in Figure 8.5.

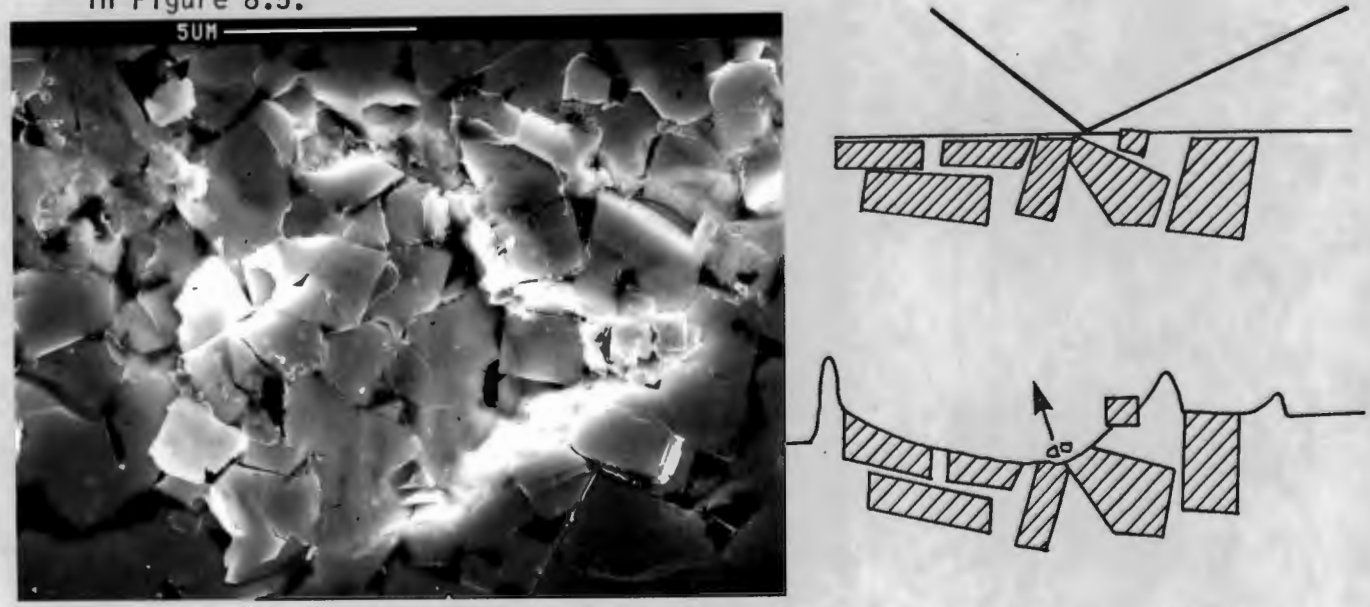


FIGURE 8.5 : a) A SEM micrograph of an impact site formed by an 100 $\mu$m SiC particle travelling at 40 $ms^{-1}$ and impacting a G1 (7 wt-%, 2.8 $\mu$m) specimen at 90°; b) Schematic representation of the modes considered to occur in material removal

Associated with an increase in binder level is a reduction in contiguity. A weaker structure is thus formed, due to fewer grains overlapping and more grains only touching, as is the case illustrated in Figure 8.4(b). When an impacting particle strikes the surface where grains are just touching, stress results in fracture occurring in the grain touching region. A cobalt content of approximately 10 wt-% appears to have the highest percentage of carbide grains touching. Consequently, it is expected that most carbide grain fracture would occur at this binder level. Figure 8.6 illustrates an impact event for a G3 (10 wt-%, 2.82 $\mu$m) specimen, where evidence of carbide grain fracture is readily observed.

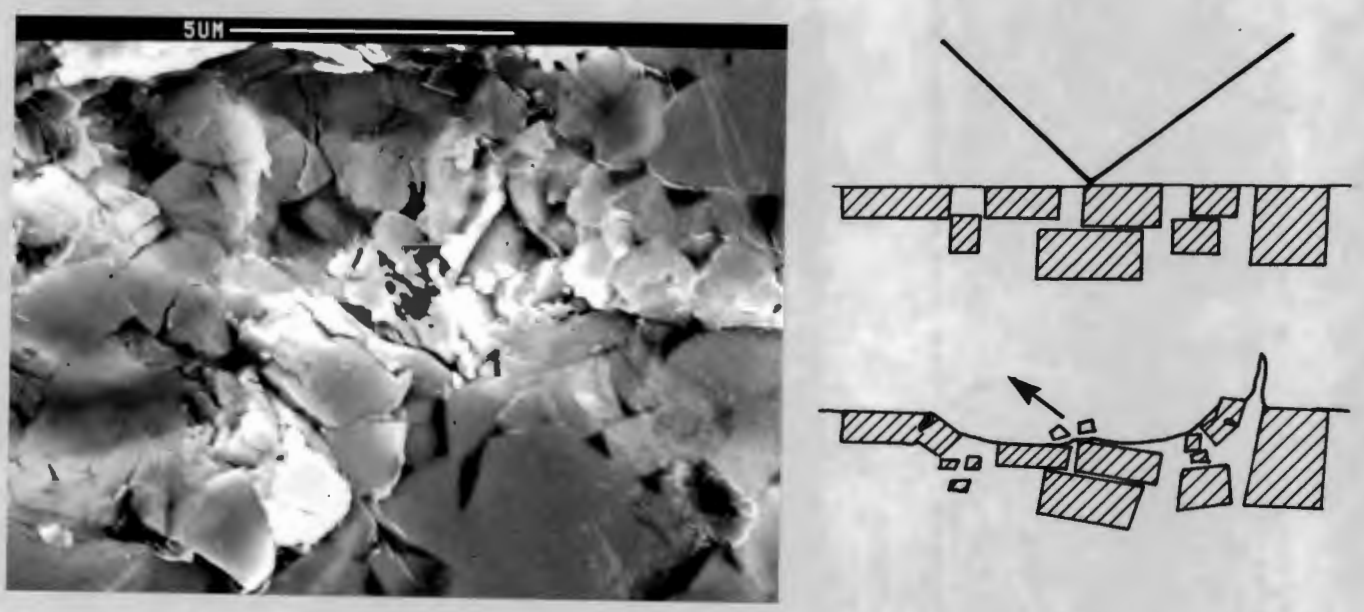


FIGURE 8.6 : a) SEM micrograph of an impact site formed be an 100 $\mu$m SiC particle travelling at 40 $ms^{-1}$ and impacting a G3 (10 wt-%, 2.82 $\mu$m) specimen at 90°; b) Schematic representation of the modes considered to occur in material removal

### 8.2.2 WC-Co Alloys Containing Between 10 and 20 wt-% Cobalt

In this region a change in structure is considered to gradually take place (see Section 2.2). More carbide grains become embedded in the cobalt matrix, resulting in fewer carbide grains touching. Thus the event of impacting particles striking touching carbide grains decreases, causing less carbide grain fracture to occur. Hence, the erosion rate is found to decrease.

### 8.2.3 WC-Co Alloys Containing More Than 20 wt-% Cobalt

At high binder levels an 'embedded' structure is considered to predominate. In Chapter 7 it was found that the parametric effects on the erosion of these alloys was indicative of ductile predominated erosion. Maximum erosion was found to occur in the 50˚ impact angle region (see Section 7.4), thus explaining the increase in erosion rate occurring above 20 wt-% cobalt for tests conducted at a 45° impact angle, while for tests conducted at the higher impact angles, a decrease in erosion rate was observed, as indicated in Figure 8.3. The ductile cutting action illustrated in Figure 8.7(a) is representative of the deformation observed for high binder level alloys. Some brittle fracture of the carbide grains still occurs, but the amount is reduced by the decrease in contiguity. Figure 8.7(b) is a schematic representation of the manner is which high binder level alloys are considered to erode.

Stereo micrographs of impact sites were used to compare the amounts of material removed in specimens of G3 (10 wt-%, 2.82 $\mu$m) and I1 (30 wt-%, 2.17 $\mu$m), under the same erosion conditions. The volume of material removed from the impact site was measured with the aid of a parallax bar. The lowest point of the impact was found, and depending on the shape of the impact, various surface heights were measured enabling the volume of the impact to be calculated. Cobalt extrusion and grain uplift account for some of the material removed from the impact, as illustrated in Figure 8.8, and hence these volumes were also determined. Calculations, using an average of four impacts, showed the G3 (10 wt-%, 2.82 $\mu$m) grade alloy lost 72% of the material from the impact, compared to 55% for the I1 (30 wt-%, 2.17 $\mu$m) grade alloy. These results confirm the findings that the high cobalt content alloys lose material by a more ductile manner than the low cobalt content alloys.

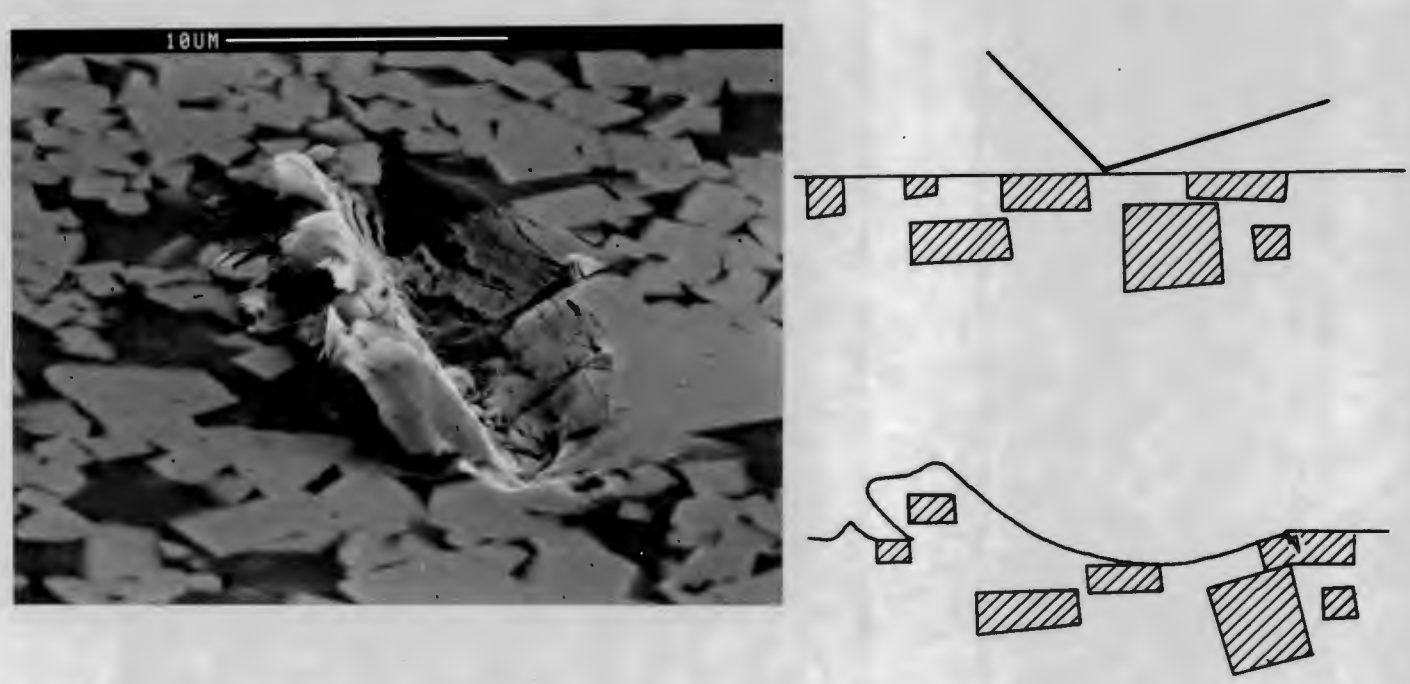


FIGURE 8.7 : a) SEM micrograph of an impact site formed by an 100 $\mu$m SiC particle travelling at 40 $ms^{-1}$ and impacting a I1 (30 wt-%, 2.17 $\mu$m) specimen at 90°; b) Schematic representation of the modes by which material is considered to be removed.

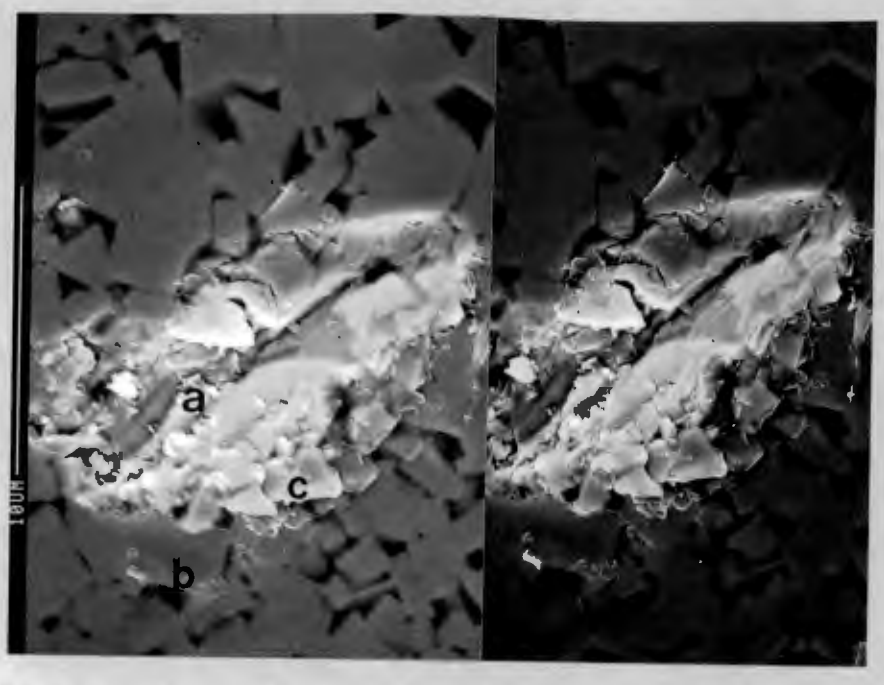


FIGURE 8.8 : Stereo micrographs of an impact site formed by 100 $\mu$m SiC particle travelling at 40 $ms^{-1}$ and impacting a G3 (10 wt-%, 2.82 $\mu$m) specimen at 90°. Where (a) refers to the impact site, (b) extruded cobalt and (c) uplifted grains

## 8.3 SUMMARY OF MODEL

The erosion of WC-Co alloys can be considered as a combination of ductile and brittle modes of material removal. The ductile mode is limited by hardness, hence the importance of this mode increases with binder level, as illustrated in Figure 8.9(a). The brittle erosion observed in WC-Co alloys is not the classical interpretation which is limited by the toughness of the material. Instead, as has been noted in Section 7.2.2.2, the brittle erosion is microtoughness limited as illustrated in Figure 8.9(b).

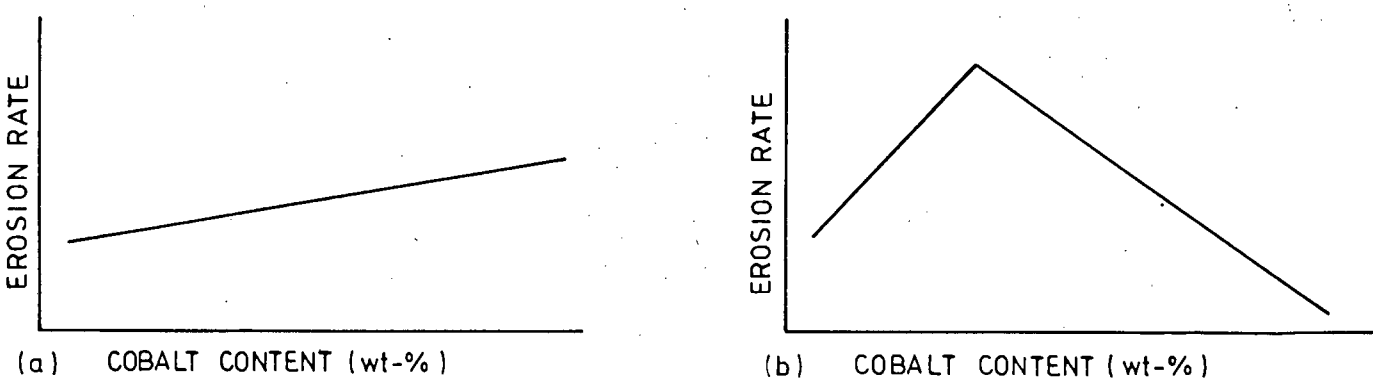


FIGURE 8.9 : The effect of (a) the ductile component and (b) the brittle component of erosion on the erosion rate of WC-Co alloys as a function of binder content

The importance of each mode of erosion is dependent on the angle of impact and particle size. For low and intermediate angles of impact, the ductile mode of erosion predominates, as illustrated in Figure 8.10(a) and (b). At high angles of impact the brittle mode of erosion was found to predominate, as shown in Figure 8.10(c). As the particle size of the SiC erodent was increased, so the brittle mode of erosion became more important.

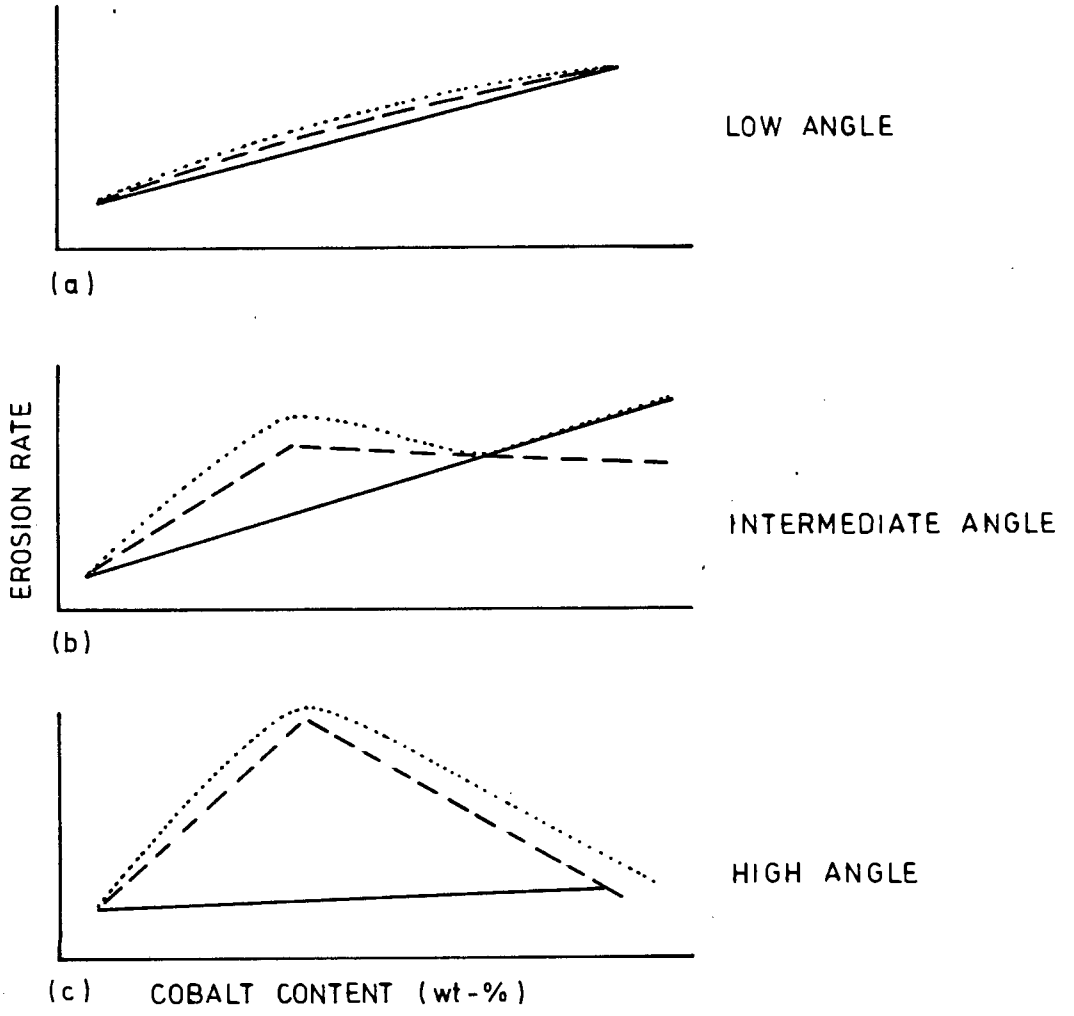


FIGURE 8.10 : Schematic summary of the importance of the ductile and brittle modes of erosion with impact angle. —— refers to ductile erosion, --- refers to brittle erosion and ····· represents the combination of ductile and brittle erosion

# CHAPTER 9

## CONCLUSIONS

From microstructural characterization of the nineteen WC-Co alloys by lineal analysis, it was established that the majority of alloys could be divided into two groups according to grain size. Since microstructure was observed to be an important parameter influencing the erosion by solid particle impact of WC-Co alloys, attention was focussed on these alloys. The following conclusions were drawn from the investigation:

i) The microstructural parameters contiguity grain size and binder content were found to influence the erosion of the WC-Co alloys for impact angles of 45° and greater. Mean free path was less clearly defined. For high impact angles maximum erosion was observed at a binder content of 10 wt-% cobalt, which corresponded to a contiguity value of 0.65. Erosion rate was found to increase with increasing grain size, but no quantitative relationship could be made as only two grain sizes were investigated.

ii) Generally, erosion rate was found to increase with decreasing hardness, but this effect was masked at high angles by microstructural influences.

iii) Erosion was found to have no dependence on macroscopic fracture toughness as determined by the Palmqvist method. Microscopic toughness is considered to be the more relevant parameter.

iv) The WC-Co alloys were found to erode by a combination of ductile and brittle modes. The ductile mode was observed to be hardness limited, whilst the brittle mode was considered to be microtoughness limited. The importance of each mode is determined by erodent particle size and impact angle. The ductile erosion mode was found to predominate at low or intermediate impact angles and for small SiC erodent particles. At high impact angles and for large SiC erodent particles the brittle mode of erosion predominates.

v) Three modes of material removal were observed : cobalt extrusion, brittle fracture of the carbide grains and ductile cutting of the cobalt matrix. For grades of the WC-Co alloy containing less than 10 wt-% cobalt, cobalt extrusion was found to predominate. At 10 wt-% cobalt, cracking of the carbide grains was observed. With increasing cobalt content the ductile cutting of the matrix became more prevalent. At 30 wt-% cobalt, the highest cobalt content tested, the cutting mode of material removal predominated. It should, however, be noted that all three modes occur simultaneously at any binder level. The predominant mode is, however, dependent on the cobalt content of the WC-Co alloy.

# CHAPTER 10

## RECOMMENDATIONS FOR FUTURE WORK

During the course of this study a few interesting points developed which warrant further investigation. It was also outside the scope of this work to study all the aspects affecting the solid particle impact erosion of WC-Co. Future work in this field should therefore include:

i) A scratch test or a similar technique should be developed to determine the microtoughness of the WC-Co alloys.

ii) A further controlled range of WC-Co alloys should be studied so the effect of grain size can be ascertained.

iii) A re-application of the WC-Co alloys studied to an extended range of erosion parameters known to influence impact erosion, namely velocity and particle type should be investigated.

iv) The amount of grain overlapping was found to affect the amount of material removed. A small area of contact results in easy fracture but a small volume loss, while a large area of contact is difficult to fracture but a large volume of material is lost. Extensive study and modelling of the optimum microstructure, as regards material loss, should be undertaken.

## REFERENCES

A.S.T.M. (1977) ANSI/ASTM G40 - 77 : "Standard Terminology Relating to Erosion and Wear", American Society of Testing and Materials.

ALMOND E.A. and ROEBUCK B. (1982) : "The Origin of WC substructure and the Effect of Processing on the Microstructure of WC-Co Hardmetals", High Temperature - High Pressure, Vol. 14, pp. 143-154.

BALL A. (1985) : "On the Mechanisms of Wear and the Performance of Engineering Metals", Colloquim on Wear, Mintek, South Africa.

BALL A. and PATERSON A.W. (1985) : "Microstructure Design of Erosion Resistant Hard Metals", Proceedings of the International Conference on Recent Developments in Special Steels and Hard Metals, Rhodes Island, pp. 377-391.

BELLMAN R. and LEVY A. (1981) : "Erosion Mechanisms in Ductile Metals", Wear, Vol. 70, pp. 1-27.

BITTER J.G.A. (1963) : "A Study of Erosion Phenomena - Part I", Wear, Vol. 6, pp. 5-21.

BLOMBERY R.I., PERROT C.M. and ROBINSON P.M. (1974) : "Similarities in the Mechanism of Wear of WC-Co Tools in Rock and Metal Cutting", Wear, Vol. 27, pp. 383-390.

BROOKES K.A. (1982) : "World directory and handbook of hard metals", 3rd edition, Engineer's Digest and International Carbide Data, U.K. (publishers).

BUDINSKI K.G. and CHIN H. (1983) : "Surface Alterations in Abrasive Blasting", Wear on Materials, pp. 311-318.

CHERMANT J.L. and OSTERSTOCK F. (1979) : "Elastic and Plastic Characteristics of WC-Co Composite Materials", Powder Metallurgy International, Vol. 11, No. 3, pp. 106-109.

CHERMANT J.L., IOST A. and OSTERSTOCK F. (1975) : "Mechanical Characteristics of Carbide-Metal Composites and the Correlation with Microstructural Parameters", Proceedings of the British Ceramic Society, pp. 197-209.

CONRAD H., SHIN Y. and SARGENT G.A. (1982) : "Erosion of Sintered WC-Co Alloys", Proceedings of the International Conference on Recent Developments in Special Steels and Hard Metals, Pretoria, South Africa, pp. 423-429.

CUTLER R. and VIRKAR A.V. (1985) : "The Effect of Binder Thickness and Residual Stresses on the Fracture Toughness of Cemented Carbides", Journal of Materials Science, Vol. 20, pp. 3557-3573.

DAWIHL W. and FRISCH B. (1964) : "The Mechanical Characteristics of the Cobalt Phase in WC-Co Hard Metals", Cobalt, Vol. 22, pp. 22-26.

EVANS A.G. and CHARLES E.A. (1976) : "Fracture Toughness Determined by Indentation", Journal of the American Ceramic Society, Vol. 59, pp. 371-372.

EVANS A.G., GULDEN M.E. and ROSENBLATT M. (1978) : "Impact Damage in Brittle Materials in the Elastic-Plastic Response Regime", Proceedings of the Royal Society, London, A361, pp. 343-365.

EXNER H.E. (1979) : "Physical and Chemical Nature of Cemented Carbides", International Metals Reviews, Review No. 243, No. 4, pp. 149-173.

EXNER E.L., PICKENS J.R. and GURLAND J. (1978) : "A Comparison of Indentation Crack Resistance and Fracture Toughness of Five WC-Co Alloys", Metallurgica Transactions, Vol. 9A, pp. 736-738.

FINNIE I. (1960) : "Erosion of the Surface by Solid Particles", Wear, Vol. 19, pp. 81-90.

FINNIE I., WOLAK J. and KABIL Y. (1967) : "Erosion of Metals by Solid Particles ", Journal of Materials, Vol. 2, No. 3, pp. 682-700.

FRENCH D.N. and THOMAS D.A. ((1965) : "Hardness Anisotropy and Slip in WC Crystals", Transactions of the AIME, Vol. 233, pp. 950-952.

FRITH, V. and HECKROODT R.O. (1984) : "The Reliability of a Digitizer System for Image Analysis", Practical Metallography, Vol. 21, pp. 593-601.

FRY P.R. (1982) : "Fatigue Crack Growth Behaviour of Tungsten Carbide-Cobalt Hardmetal Alloys", M.Sc Thesis, Faculty of Engineering, University of Witwatersrand.

GOODWIN J.E., SAGE E. and TILLY G.P. (1969) : "Study of Erosion by Solid Particles", Proceedings of the Institute of Mechanical Engineers, Vol. 184, No. 15, pp. 279-292.

GREENWOOD R.M., LORETTO M.H. and SMALLMAN R.E. (1982) : "The Defect Structure of Tungsten Carbide in Deformed Tungsten Carbide-Cobalt Composites", Acta Metallurgica, Vol. 33, pp. 1193-1196.

GURLAND J. and EXNER H.E. (1970) : "A Review of Parameters Influencing Some Mechanical Properties of Tungsten Carbide-Cobalt Alloys", Powder Metallurgy, Vol. 13, No. 25, pp. 12-31.

GURLAND J. and PARIKH N.M. (1972) : "Microstructure Aspect of the Fracture of Two Phase Alloys", Fracture, Vol. 2, Ed H. Lebowitz, pp. 841-878.

HANKEY S.E. (1986) : Dept. of Materials Eng, University of Cape Town. Private communication.

HANSEN J.S., KELLEY J.E. and WOOD F.W. (1979) : "Erosion Testing of Potential Valve Materials for Coal Gasification Systems", Bureau of Mines Report of Investigation Bumines, R.I. 8335.

HEATHCOCK C.J. (1980) : "Cavitation Erosion of Materials", Ph.D. Thesis, University of Cape Town.

HOCKEY B.J. and WIEDERHORN S.M. (1979) : "Erosion of Ceramic Materials : The Role of Plastic Flow", Proceedings of the 5th International Confrence on Erosion by Solid and Liquid Impact, pp. 41.1-41.7.

HOCKEY B.J., WIEDERHORN S.M. and JOHNSON H. (1977) : "Erosion of Brittle Materials by Solid Particle Impact", Fracture Mechanics of Ceramics, Vol. 3, Flaws and Testing, Eds. Bradt, Hasselman and Lange, pp. 379-401.

HOVIS S.K., TALIA J.E. and SCATTERGOOD R.O. (1986) : "Erosion in Multiphase Systems", Wear, Vol. 108, pp. 139-155.

INGELSTROM N. and NORDBERG H. 1974) : "The Fracture Toughness of Cemented Tungsten Carbides", Engineering Fracture Mechanics, Vol. 6, pp. 597-607.

KARLSEN T.M. (1985) : "The Erosive Characteristics of South African Pulverised Coals", M.Sc. Thesis, Faculty of Engineering, University of Cape Town.

KENNY P. (1971) : "The Application of Fracture Mechanics to Cemented Tungsten Carbides", Powder Metallurgy, Vol. 14, No. 27, pp. 22-38.

LANKFORD J. (1982) : "Indentation Microfracture in Palmqvist Crack Regime : Implications for Fracture Toughness Evaluation by the Indentation Method", Journal of Material Science Letters, Vol. 1, pp. 493-495.

LARSEN-BASSE J. (1985) : "Binder Extrusion in Sliding Wear of WC-Co Alloys", Wear, Vol. 105, pp. 247-256.

LARSEN-BASSE J., PERROT C.N. and ROBINSON P.M. (1974) : "Abrasive Wear of WC-Co Composites : 1. Rotary Drilling Tests", Materials Science of Engineering, Vol. 13, pp. 83-91.

LAUGIER M.T. (1985 a) : "Palmqvist Cracking in WC-Co Composites", Journal of Materials Science Letters, Vol. 4, pp. 207-210.

LAUGIER M.T. (1985 b) : "A Note on Contiguity in Sintered WC-Co Composites", Journal of Materials Science Letters, Vol. 4, pp. 263-264.

LEE H.C. and GURLAND J. (1978) : "Hardness and Deformation of Cemented WC", Materials Science and Engineering, Vol. 33, pp. 125-139.

LEVY A.V. (1986) : "The Platelet Mechanism of Erosion of Ductile Metals", Wear, Vol. 108, pp. 1-21.

LUETH R. (1974) : "Determination of Fracture Toughness Parametes for WC-Co Alloys", Fracture Mechanics of Ceramics, Vol. 2, pp. 365-377.

LUYCKX S.B. (1968) : "Microscopic Aspects of Fracture in WC-Co Alloys", Acta Metallurgica, Vol. 16, pp. 535-544.

LUYCKX S.B. (1970) : "Slip System of Tungsten Carbide Crystals at Room Temperture", Acta Metallurgica, Vol. 16, pp. 535-544.

MARSHALL D.B., EVANS A.G., GULDEN M.E., ROUTBORT J.L. and SCATTERGOOD R.O. (1981) : "Particle Distribution Effects of the Solid Particle Erosion of Brittle Materials", Wear, Vol. 71, pp. 363-373.

MURRAY M.J. (1977) : "Fracture of WC-Co Alloys : An Example of Spatially Constrained Crack Tip Opening Displacement", Proceedings of the Royal Society, London, A356, pp. 483-508.

NAKAMURA M. and GURLAND J. (1980) : "The Fracture Toughness of WC-Co 2-Phase Alloys : A Preliminary Model", Metallurgica Transactions, Vol. 11A, pp. 141-146.

NEILSON J.H. and GULCHRIST A. (1968) : "Erosion of a Stream of Solid Particles", Wear, Vol. 11, pp. 111-122.

NIDIKOM B. and DAVIES T.J. (1980) : "Fracture Toughness of Some WC-Co Alloys", Vol. 28, No. 1-2, pp. 29-38.

NIIHARA K., MORENA R. and HASSELMAN D.P.H. (1982) : "Evaluation of $K_{IC}$ of Brittle Solids by the Indentation Method with Low Crack-to-Indent Ratios", Journal of Materials Science Letters, Vol. 1, pp. 13-16.

OGILVY I.M., PERROT C.M. and SUITER J.W. (1977) : "On the Indentation Fracture of Cemented Carbide : Part 1 - Survey of Operative Fracture Modes", Wear, Vol. 43, pp. 239-252.

PERROT C.M. (1977) : "Elastic-Plastic Indentation : Hardness and Fracture", Wear, Vol. 45, pp. 293-309.

PETERS C.T. (1979) : "The Relationship Between Palmqvist Indentation Toughness and Bulk Fracture for Some WC-Co Cemented Carbides", Journal of Materials Science, Vol. 14, pp. 1619-1623.

PETERS C.T. and COOPER R. (1978) : "Effects of Eta Phase Precipitation on the Structure and Mechanical Properties of WC-5% Co Hardmetal", Planseeberichte for Pulvermetallurgie, Vol. 26, pp. 181-190.

PICKENS J.R. and GURLAND J. (1978) : "The Fracture Toughness of WC-Co Alloys Measured on Single-Edge Notched Beam Specimens Precracked by Electron Discharge Machining", Materials Science and Engineering, Vol. 33, pp. 135-142.

ROEBUCK E., ALMOND E.A. and COTTENDON A.M. (1984) : "The Influence of Composition, Phase Transformation and Varying the Relative F.C.C. and H.C.P. Phase Contents on the Properties of Dilute Co-W-C Alloys", Materials Science and Engineering, Vol. 66, pp. 179-194.

ROUTBORT J.L., SCATTERGOOD R.O. and TURNER A.P.L. (1980) : "Erosion of Reaction Bonded SiC", Wear, Vol. 59, pp. 363-375.

RUFF A.W. and IVES L.K. (1975) : "Measurement of Solid Particle Velocity in Erosive Wear", Wear, Vol. 35, pp. 195-199.

RUFF A.W. and WIEDERHORN S.M. (1979) : "Erosion by Solid Particle Impact", Treatise on Materials Science and Technology, Vol. 16, pp. 69-126.

SHELDON G.L. (1970) : "Similarities and Differences in the Erosion Behaviour of Materials", Journal of Basic Engineering, Transactions of the ASME, pp. 619-626.

SHELDON G.L. and FINNIE I. (1966) : "On the Ductile Behaviour of Nominally Brittle Materials During Erosive Cutting", Journal of Engineering for Industry, Transactions of the ASME, pp. 387-392.

SHETTY D.K., WRIGHT I.G., MINCER A.H. and CLAUER A.H. (1985) : "Indentation Fracture of WC-Co Cermets", Journal of Materials Science, Vol. 20, pp. 1873-1882.

SHETTY D.K., WRIGHT I.G. and STROPKI J.T. (1984) : "Slurry Erosion of WC-Co Cermets and Ceramics", A.S.L.E. Transactions, Vol. 28, pp. 123-133.

SHEWMON P.G. (1981) : "Particle Size Threshold in the Erosion of Metals", Wear, Vol. 68, pp. 253-258.

SHEWMON P. and SUNDARARAJAN G. (1983) : "The Erosion of Metals", Annual Review of Materials Science, Vol. 13, pp. 301-318.

SMELTZER C.F., GULDEN M.E. and COMPTON W.A. (1970) : "Mechanisms of Metal Removal by Impacting Dust Particles", Journal of Basic Engineering, Vol. 92, pp. 636-654.

TABAKOFF W., HAMED A. and BEACHER B. (1983) : "Investigation of Gas Particle Flow in an Erosion Wind Tunnel", Wear, Vol. 86, pp. 73-88.

TILLY G.P. (1979) : "Erosion Caused by Imact of Solid Particles", Treatise on Materials Science and Technology, Vol. 13, pp. 287-318.

UUEMÔIS H. and KLEIS I. (1975) : "A Critical Analysis of Erosion Problems Which Have Been Little Studied", Wear, Vol. 31, pp. 359-371.

UUÉMYIS K.H., KLEIS I., TUMANOV V. and TIIDEMANN T. (1974) : "Abrasive Erosion of Sintered Tungsten Carbide Base Hard Metals", Soviet Powder Metallurgy and Metal Ceramics", pp. 248-250.

VISVANADHAM R.K., SUN T.S., DRAKE E.F. and PECK J.A. (1981) : "Quantitave Fractography of WC-Co Cermets by Auger Spectroscopy", Journal of Materials Science and Engineering, Vol. 16, pp. 1029-1038.

WIEDERHORN S.M. and LAWN B.R. (1979) : "Strength Degradation of Glass impacted with Sharp Particles : 1. Annealed Surfaces", Journal of the American Ceramic Society, Vol. 62, No. 1-2, pp. 66-70.

WINTER R.E. and HUTCHINGS I.M. (1974) : "Solid Particle Erosion Studies Using Single Angular Particles", Wear, Vol. 29, pp. 181-194.

WRIGHT I.G., SHETTY D.K. and CLAUER A.H. (1983) : "Slurry Erosion of WC-Co Cermets and its Relationship to Materials Properties", Proceedings of the 6th International Conference on Erosion by Liquid and Solid Impact, pp. 63.1-63.8.

## APPENDIX A

### DETERMINATION OF FRACTURE TOUGHNESS USING THE PALMQVIST METHOD

This method establishes a relationship between the indentation load P and the sum of the lengths of the cracks formed at the corners of the indentation (see Figure 1).

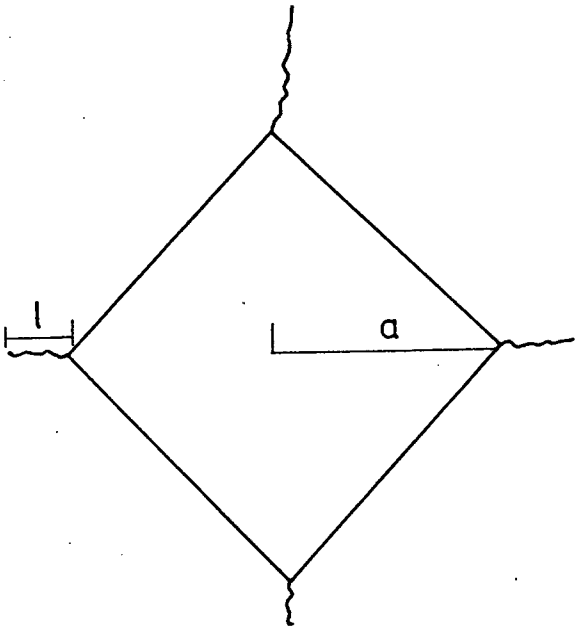


FIGURE 1 : Typical indentation crack pattern

The relationship is then used in the following equation to calculate the fracture toughness ($K_{IC}$) in MPa $m^{\frac{1}{2}}$:

$$K_{IC} = 0{,}0084\ (E/H)^{0{,}4}\left(\frac{P}{a\ l^{\frac{1}{2}}}\right)$$

where E is the Young's modulus, H the hardness and l and a are defined in Figure 1. Loads varying from 30 kg to 120 kg were used.

To obtain H in GPa for the equation, the formula

$$H = 0{,}4636\left(\frac{P}{a^2}\right)$$

was used. The values for E were taken from Brookes (1982).

## APPENDIX B

### THE RUFF AND IVES TECHNIQUE OF MEASURING PARTICLE VELOCITY

The velocity of a particle is determined over a controlled path length between two rotating discs. The apparatus is illustrated in Figure 1.

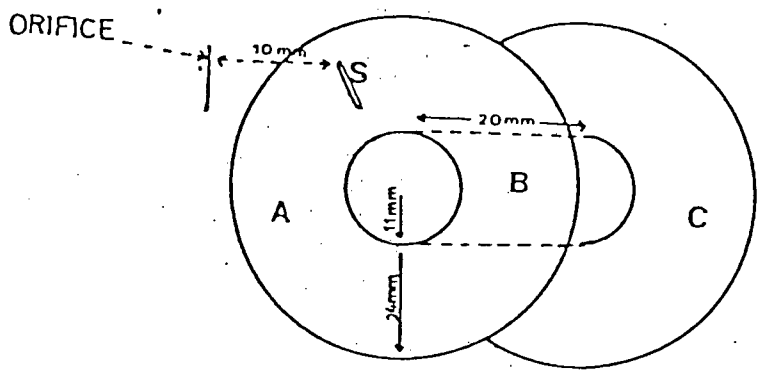


FIGURE 1 : Schematic representation of the double disc apparatus

B is a common shaft, onto which discs A and C are mounted. S is a single radial slit in disc A.

During rotation, the slit S acts as a shutter which allows a packet of particles to pass through. Once through the shutter, the flux packet of particles travel until impacting the second disc, producing a line of erosion.

Two erosion exposures are made, one with the disc rotating clockwise, the other with the disc rotating anticlockwise. The motor speed is kept constant and is measured by a digital tachometer. The measurement of the angular displacement, $\theta$, between the marks gives the time-of-flight of the particles as they cross the space between the discs. The average particle velocity, V, is calculated using the following equation:

$$V = 4\pi r\ U\ L/\theta$$

where L is the distance separating the two discs, U is the rotational frequency of the disc (35 $s^{-1}$), r is the radius from disc centre (20 mm) and $\theta$ is the linear separation of the two marks.

A linear relationship was observed when the average particle velocity was plotted against air pressure, as illustrated in Figure 2. As noted by Ruff and Ives (1975), a large positive y-intercept was obtained, indicating that the particle velocities of pressures below 100 KPa must be determined by extrapolation.

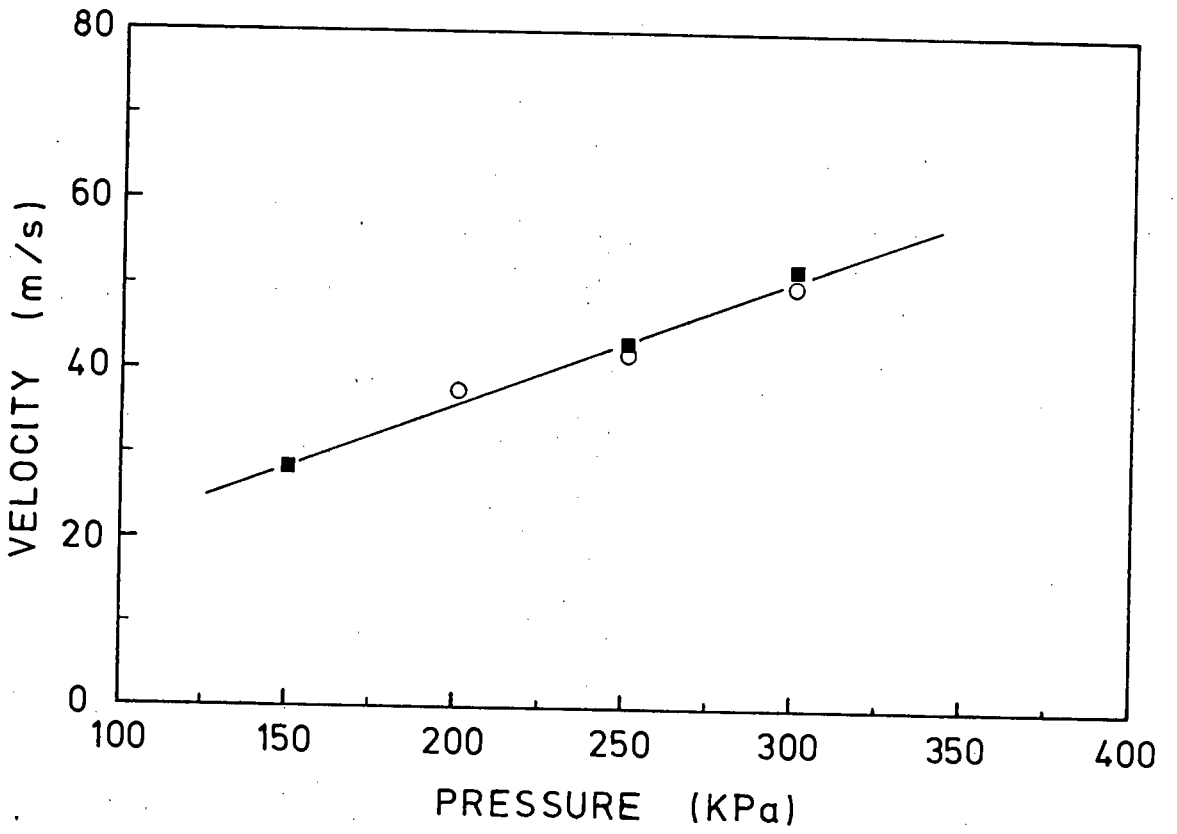


FIGURE 2 : The variation of particle velocity with air pressure for the 100 $\mu$m SiC erodent

# APPENDIX C

## THE COMPUTER PROGRAMME USED TO STANDARDIZE THE EROSION RATE

```
10 REM *STD ANGLE*
20 CLEAR
30 DEG
40 PEN -1
50 GCLEAR
60 SCALE 0,100,0,100
70 MOVE 40,80 @ CSIZE 6 @ LORG 5 @ LABEL "ANGLE"
80 MOVE 50,60 @ LABEL "STANDARDISATION"
90 MOVE 30,40 @ CSIZE 4 @ LORG 5 @ LABEL "By R.P."
100 WAIT 1000 @ BEEP 30,1000
110 Y=0 @ S=0 @ F=0 @ T=0
120 DISP "ENTER ANGLE:ENTER 0 TO END"
130 INPUT A
140 IF A=0 THEN GOTO 360
150 X=7*SIN(A)
160 Z=X*2.15/7
170 DISP "ENTER INCREMENTAL INCREASE IN D"
180 INPUT D@ CLEAR
190 DIM A(1000)
200 FOR I=1 TO 1000
210 LET S=S+D
220 ! PRINT S
230 IF S>Z THEN GOTO 270
240 A(I)=1/SQR(2*3.14)*EXP(-(S^2/2))
250 ! PRINT "Y=";A(I)
260 NEXT I
270 FOR N=1 TO N=I-1
280 F=A(N+1)-A(N)
290 ON ERROR GOTO 300
300 ! PRINT "dY=";F
310 V=2.15*3.14*Z*A(N)+3.14*Z*F
320 T=T+V
330 NEXT N
340 PRINT "VOLUME IS =";T
350 GOTO 110
360 END
```

## APPENDIX D

Erosion values for the three different erodents used in g/g x $10^{-4}$

### CORRECTED EROSION RATES FOR 120 SiC

| GRADE | % Co | 15° | 30° | 45° | 60° | 90° |
|---|---|---|---|---|---|---|
| A1 | 5 | 0.36 | 0.78 | 1.31 | 1.56 | 1.91 |
| B1 | 7 | 0.35 | 0.90 | 1.34 | 1.93 | 2.06 |
| C1 | 5 | 0.34 | 0.91 | 1.38 | 1.67 | 2.19 |
| D1 | 6 | 0.35 | 0.59 | 1.19 | 1.54 | 1.77 |
| E1 | 6 | 0.29 | 0.66 | 1.15 | 1.32 | 1.60 |
| F1 | 7 | 0.36 | 0.90 | 1.29 | 1.66 | 1.78 |
| B2 | 8 | 0.38 | 0.93 | 1.48 | 1.68 | 2.02 |
| G1 | 7 | 0.34 | 0.90 | 1.44 | 1.81 | 2.16 |
| G2 | 9 | 0.43 | 0.90 | 1.55 | 1.83 | 2.17 |
| H1 | 9 | 0.29 | 0.82 | 1.38 | 1.6 | 2.02 |
| G3 | 10 | 0.46 | 0.88 | 1.59 | 1.88 | 2.33 |
| F2 | 12 | 0.38 | 0.91 | 1.37 | 1.84 | 1.76 |
| B3 | 14 | 0.29 | 0.97 | 1.43 | 1.76 | 2.05 |
| H2 | 12 | 0.32 | 1.08 | 1.43 | 1.61 | 1.91 |
| G4 | 14 | 0.41 | 0.87 | 1.37 | 1.66 | 1.91 |
| C2 | 13 | 0.50 | 0.92 | 1.34 | 1.65 | 1.98 |
| F3 | 15 | 0.29 | 0.80 | 1.41 | 1.47 | 1.90 |
| B4 | 20 | 0.50 | 1.07 | 1.30 | 1.55 | 1.59 |
| I1 | 30 | 0.40 | 0.93 | 1.44 | 1.31 | 1.43 |

## CORRECTED EROSION RATES FOR 240 SiC

| GRADE | % Co | 15° | 30° | 45° | 60° | 90° |
|---|---|---|---|---|---|---|
| A1 | 5 | 0.29 | 0.71 | 1.45 | 1.37 | 1.54 |
| B1 | 7 | 0.29 | 0.86 | 1.47 | 1.67 | 2.15 |
| C1 | 5 | 0.27 | 0.86 | 1.49 | 1.83 | 2.56 |
| D1 | 6 | 0.30 | 0.79 | 0.98 | 1.58 | 1.68 |
| E1 | 6 | 0.39 | 0.65 | 1.33 | 1.59 | 1.77 |
| F1 | 7 | 0.34 | 0.90 | 1.32 | 1.78 | 1.76 |
| B2 | 8 | 0.31 | 0.91 | 1.57 | 1.55 | 1.76 |
| G1 | 7 | 0.31 | 0.80 | 1.32 | 1.63 | 2.00 |
| G2 | 9 | 0.29 | 0.87 | 1.46 | 1.63 | 1.94 |
| H1 | 9 | 0.30 | 0.73 | 1.28 | 1.54 | 1.64 |
| G3 | 10 | 0.37 | 0.92 | 1.66 | 1.74 | 1.98 |
| F2 | 12 | 0.42 | 0.73 | 1.31 | 1.58 | 1.67 |
| B3 | 14 | 0.45 | 0.77 | 1.48 | 1.75 | 1.65 |
| H2 | 12 | 0.42 | 0.84 | 1.54 | 1.57 | 1.69 |
| G4 | 14 | 0.30 | 0.68 | 1.53 | 1.80 | 2.00 |
| C2 | 13 | 0.28 | 0.82 | 1.56 | 1.48 | 1.77 |
| F3 | 15 | 0.33 | 0.91 | 1.51 | 1.73 | 1.60 |
| B4 | 20 | 0.42 | 1.08 | 1.48 | 1.44 | 1.43 |
| I1 | 30 | 0.50 | 1.01 | 1.41 | 1.31 | 1.35 |

## CORRECTED EROSION RATES FOR 320 SiC

| GRADE | % Co | 15° | 30° | 45° | 60° | 90° |
|---|---|---|---|---|---|---|
| A1 | 5 | 0.32 | 0.48 | 1.01 | 1.32 | 1.48 |
| B1 | 7 | 0.50 | 0.76 | 1.08 | 1.32 | 1.44 |
| C1 | 5 | 0.27 | 0.55 | 1.07 | 1.24 | 1.37 |
| D1 | 6 | 0.35 | 0.53 | 0.99 | 1.19 | 1.42 |
| E1 | 6 | 0.24 | 0.40 | 1.09 | 1.30 | 1.39 |
| F1 | 7 | 0.38 | 0.83 | 1.23 | 1.65 | 1.32 |
| B2 | 8 | 0.35 | 0.65 | 1.20 | 1.24 | 1.34 |
| G1 | 7 | 0.25 | 0.40 | 0.89 | 1.18 | 1.27 |
| G2 | 9 | 0.36 | 0.50 | 0.90 | 1.30 | 1.45 |
| H1 | 9 | 0.38 | 0.44 | 1.13 | 1.24 | 1.25 |
| G3 | 10 | 0.28 | 0.40 | 0.94 | 1.38 | 1.42 |
| F2 | 12 | 0.38 | 0.65 | 1.06 | 1.43 | 1.17 |
| B3 | 14 | 0.38 | 0.54 | 1.15 | 1.35 | 1.20 |
| H2 | 12 | 0.29 | 0.73 | 1.01 | 1.48 | 1.13 |
| G4 | 14 | 0.27 | 0.73 | 0.98 | 1.36 | 1.29 |
| C2 | 13 | 0.38 | 0.64 | 0.83 | 1.26 | 1.34 |
| F3 | 15 | 0.53 | 0.80 | 1.11 | 1.42 | 1.34 |
| B4 | 20 | 0.42 | 0.63 | 1.31 | 1.45 | 1.34 |
| I1 | 30 | 0.52 | 0.94 | 1.37 | 1.18 | 1.12 |